

Mag.rer.nat. Josef Clemens Hödl

Coordination polymers with 2,2'-bisimidazole-carboxylate containing ligands

MASTER'S THESIS

to achieve the university degree of
Diplom-Ingenieur

Master's degree programme:
Technical Chemistry

submitted to

Graz University of Technology

Supervisor

Assoc.Prof. Dipl.-Ing. Dr.techn. Christian Slugovc
Institute for Chemistry and Technology of Materials

Graz, October 2020

AFFIDAVIT

I declare that I have authored this thesis independently, that I have not used other than the declared sources/resources, and that I have explicitly indicated all material which has been quoted either literally or by content from the sources used. The text document uploaded to TUGRAZonline is identical to the present master's thesis.

Date, Signature

DANKSAGUNG

An dieser Stelle möchte ich mich gerne meinen besonderen Dank den nachstehenden Personen aussprechen, ohne deren Mithilfe die Erstellung meiner Masterarbeit niemals zustande gekommen wäre:

Besonderer Dank gilt zunächst meinem Masterarbeitsbetreuer Herrn Prof. Dr. Christian Slugovc, der mir stets Verständnis für meine Fragestellungen entgegenbrachte und mit der richtigen Hilfestellung immer wieder auf den richtigen Weg führte. Zudem bin ich äußerst dankbar für die Gewährung der freien Zeiteinteilung aufgrund meines Berufs. Herzlichen Dank dafür!

Ein großer Dank gilt auch der gesamten Arbeitsgruppe und den Institutsmitgliedern des ICTM. Ohne eure anregenden und zahlreichen Hilfestellungen bei den Synthesen, Auswertungen und Interpretationen wäre diese Arbeit für mich nicht durchführbar gewesen.

Einen weiteren wichtigen Beitrag leisteten auch meine Freunde die mich am Weg durchs Studium oftmals mit außergewöhnlichen Methoden aufgemuntert und sogar in anstrengenden Lebensphasen motivierend hinter mir gestanden sind.

At last but not least möchte ich mich auch bei meinen Eltern, Familienmitgliedern und meiner Freundin Anna, die mir stets mit Rat und Tat bei Seite standen und mir all ihre Unterstützung in den vielen unerlässlichen Dingen des Alltags gegeben haben, erwähnen. Danke für eure Hilfe!

ABSTRACT

Metal-organic frameworks and coordination polymers have earned a lot of attention in recent years because of the intriguing structural diversities and potential applications in a wide range.

In this Master's thesis a variety of metal-organic compounds have been prepared and analysed. The preparation focused the use of 3,3'-(1H,1'H-[2,2'-biimidazole]-1,1'-diyl)dipropionic acid (Pra₂biim) as a nitrogen and carboxylate containing multifunctional ligand and different metal ions like Mn²⁺, Co²⁺ and Ni²⁺. The ligand precursor 2,2-bisimidazole has been synthesised out of ammonium acetate and aqueous glyoxal. In further step the preparation of the ligands was done by base-catalysed aza-Michael addition reactions. The ethyl acrylate product was then saponified and used to build coordination polymers from aqueous salt solutions of the metal ions Mn²⁺, Co²⁺ and Ni²⁺.

The metal-organic coordination polymers were characterized with different methods like Powder X-ray Diffraction, attenuated total reflection infrared spectroscopy and Thermogravimetric Analysis. The manganese containing coordination polymer was further analysed by Single Crystal X-ray Diffraction revealing the presence of 2D coordination polymer sheets featuring almost no porosity.

KURZFASSUNG

Metallorganische Gerüste und Koordinationspolymere haben in den letzten Jahren aufgrund ihrer faszinierenden strukturellen Vielfalt und potenziellen Anwendungen in einem breiten Spektrum viel Aufmerksamkeit auf sich gezogen.

In dieser Masterarbeit wurden verschiedene metallorganische Verbindungen hergestellt und analysiert. Die Herstellung konzentrierte sich auf die Verwendung von 3,3'- $(1H, 1'H$ - [2,2'-Biimidazol]-1,1'-diyl) dipropionsäure (Pra_2biim) als multifunktionalen Stickstoff und Carboxylat Liganden, mit verschiedenen Metallionen wie beispielsweise Mn^{2+} , Co^{2+} und Ni^{2+} . Der Ausgangssubstanz für den Liganden, 2,2-Bisimidazol, wurde aus Ammoniumacetat und wässrigem Glyoxal synthetisiert. In einem weiteren Schritt erfolgte die Herstellung der Liganden durch eine basenkatalysierte Aza-Michael-Additionsreaktion. Das Ethylacrylatprodukt wurde anschließend verseift und verwendet, um Koordinationspolymere aus wässrigen Salzlösungen der Metallionen Mn^{2+} , Co^{2+} und Ni^{2+} aufzubauen.

Die metallorganischen Koordinationspolymere wurden mit verschiedenen Methoden wie Pulverröntgenbeugung, abgeschwächter Totalreflexions-Infrarotspektroskopie und thermogravimetrischer Analyse charakterisiert. Das manganhaltige Koordinationspolymer wurde weiters durch Einkristall-Röntgenbeugung analysiert, wobei das Vorhandensein von 2D-Koordinationspolymerschichten mit nahezu keiner Porosität festgestellt wurde.

TABLE OF CONTENT

1. Introduction	1
2. Theoretical	2
2.1. 2,2'-bisimidazole-carboxylate containing ligands	2
2.2. Glyoxal-ammonia interaction and diimine synthesis	2
2.3. The Reaction of glyoxal with ammonia – Synthesis of heterocyclic products	7
2.4. A variety of reactions with 2,2'-bisimidazole	10
2.4.1. Synthesis of 1,1'-diethyl-2,2'-biimidazole	10
2.4.2. Synthesis of a complex structure $[\text{Rh}_2(\text{R}_2\text{bim})\text{Cl}_2(\text{CO})_4]$ (R = Et, Pr)	11
2.4.3. Synthesis of disubstituted 2,2'-bi-1H-biimidazoles	11
2.4.4. Formation of two-dimensional hydrogen bonded supramolecular networks in the compounds of benzene-1,2,4,5,-tetracarboxylic acid with 2,2'-biimidazole	13
2.4.5. Hydrogen-bonded self-assemblies based upon $[\text{M}(\text{H}_2\text{biim})_2(\text{H}_2\text{O})_n]^{2+}$ (M=Cd ²⁺ , Co ²⁺ , Zn ²⁺ ; n= 1,2) building units and carboxylates	15
2.4.6. Aza-Michael addition reaction of N-heterocycles	18
2.5. Zeolitic imidazolate frameworks (ZIFs)	20
2.6. Metal-organic frameworks and coordination polymers with different dimensionalities	23
2.7. Coordination polymers and MOFs based on 1,1'-Bis(propionic acid)-2,2'-biimidazole	27
3. Results and Discussion	33
3.1. The synthesis of 2,2'-Biimidazole	33
3.2. The aza-Michael addition	35
3.3. Saponification reaction	42
3.4. Metal-organic frameworks and coordination polymers	45
3.4.1. Manganese-organic coordination polymer (Compound C1)	45
3.4.1.1. $\text{Na}_2\text{Pra}_2\text{biim} + \text{MnSO}_4 \cdot \text{H}_2\text{O}$	45
3.4.2. Synthesis of a cobalt-organic (C2) and a nickel-organic coordination polymer (C3)	54
3.4.2.1. $\text{Na}_2\text{Pra}_2\text{biim} + \text{Co}(\text{NO}_3)_2 \cdot 6\text{H}_2\text{O}$	54
3.4.2.2. $\text{Na}_2\text{Pra}_2\text{biim} + \text{Ni}(\text{NO}_3)_2 \cdot 6\text{H}_2\text{O}$	55
4. Conclusion and Outlook	60
5. Experimental	61
5.1. Reagents	61
5.1.1. Chemical reaction products	61

5.2.	Instruments	61
5.2.1.	NMR-spectroscopy	61
5.2.2.	Single Crystal – X-ray diffraction (SC-XRD)	61
5.2.3.	X-ray diffraction (XRD)	61
5.2.4.	Infrared-spectroscopy (IR)	62
5.2.5.	Thermogravimetric analysis (TGA)	62
5.3.	Synthesis reactions	63
5.3.1.	Synthesis of 2,2'-Biimidazole	63
5.3.1.1.	2,2'-Biimidazole	63
5.3.2.	Aza-Michael reaction	64
5.3.2.1.	4,4'-(1H,1'H-[2,2'-biimidazole]-1,1'-diyl)bis(butan-2-one)	64
5.3.2.2.	1,1'-bis(2-(methylsulfonyl)-1H,1'H-2,2'-biimidazole	65
5.3.2.3.	3,3'-(1H,1'H-[2,2'-biimidazole]-1,1'-diyl)dipropanenitrile	66
5.3.2.4.	Diethyl 3,3-(1H,1'H-[2,2'-biimidazole]-1,1'-diyl)dipropionate	67
5.3.2.5.	3,3-(1H,1'H-[2,2'-biimidazole]-1,1'-diyl)dipropanamide	68
5.3.2.6.	Dimethyl 3,3-(1H,1'H-[2,2'-biimidazole]-1,1'-diyl)dibutyrate	69
5.3.3.	Saponification reaction	70
5.3.3.1.	Na ₂ Pra ₂ biim = 1,1'-di(propionic acid)-2,2'-biimidazole disodium salt	70
5.3.4.	Metal-organic frameworks and coordination polymers	71
5.3.4.1.	Zink-organic coordination polymer	71
5.3.4.2.	Copper-organic coordination polymer	71
5.3.4.3.	Cobalt-organic coordination polymer (C2)	72
5.3.4.4.	Nickel-organic coordination polymer (C3)	72
5.3.4.5.	Iron-organic coordination polymer	73
5.3.4.6.	Manganese-organic coordination polymer (C1)	73
6.	List of Abbreviations	74
7.	List of Figures	75
8.	List of Tables	77
9.	Appendix	77

1. Introduction

The design and preparation of functional coordination polymers made up of metal ions and organic linkers have earned a lot of attention in recent years because of the intriguing structural diversities and potential application in a wide range. Single-linker-based coordination polymers show for instance benefits like stability and greater expectedness. But how does an ideal single organic linker look like? At first it should contain a pair of donor atoms bridging metal ions together and additional arms habile of interconnecting the resulting metal cluster units into extended structures.¹ 2,2'-Biimidazole (H₂biim) has already been utilized as a biomimetic ligand in bioorganic chemistry^{2,3}, a bridging ligand in organometallic chemistry for catalysis^{4,5} and antitumor medicaments^{6,7}, and of course as a main building unit in supramolecular frameworks¹. Moreover, polycarboxylic functionalities have been demonstrated to be one of the most successful linkers in the construction of metal-organic frameworks (MOFs), due to their structural rigidity, chemical stability and immense coordinating ability. MOFs are built up of metal ions and bridging ligands that extend to either two- or three-dimensional networks which may exhibit porosity.⁸ For the reasons above a multifunctional ligand called Pra₂biim²⁻ [1,1'-bis(propionic acid)-2,2'-biimidazole] was generated.

The focus of this master thesis lies on the assemblies and metal-organic structures formed by metal ions like (Mn²⁺, Co²⁺, Ni²⁺) and of the N and O donor ligand Pra₂biim²⁻. In a preliminary step the H₂biim compound was synthesized out of an ammonium acetate and aqueous glyoxal and in the second step the ligand was generated via aza-Michael addition. There are some aza-Michael addition examples done, but only the product with ethyl acrylate was studied deeper. The obtained product out of ethyl acrylate was further saponified and used as linker in the metal-organic coordination polymers.

¹ R.-L. Sang, L. Xu, Construction of a Series of 1D and 2D Inorganic-Organic Hybrid Coordination Polymers Based on 1,1'-(Bis(propionic acid)-2,2'-biimidazole, *Eur. J. Inorg. Chem.*, 2010, 4962-4968.

² Y. Cui, H.-J. Mo, J.-C. Chen, Y.-L. Niu, Y.-R. Zhang, K.-C. Zheng, B.-H. Ye, *Inorg. Chem.* 2007, 46, 6427-6436.

³ S. Fortin, A. L. Beauchamp, *Inorg. Chem.* 2000, 39, 4886-4893.

⁴ S. W. Kaiser, R. B. Saillant, P. G. Rasmussen, *J. Am. Chem. Soc.* 1975, 97, 425-426.

⁵ M. P. Garcia, A. M. López, M. A. Esteruelas, F. J. Lahoz, L. A. Oro, *J. Chem. Soc., Chem. Commun.* 1988, 793-809.

⁶ B. J. Holliday, Ch. A. Mirkin, *Angew. Chem. Int. Ed.* 2001, 40, 2023-2043.

⁷ J.-S. Casas, A. Castineiras, Y. Parajo, M.-L. Perez-Paralle, A. Sanchez, A. Sanchez-Gonzalez, J. Sordo, *Polyhedron* 2003, 22, 1113-1121.

⁸ S. Horike, S. Kitagawa, *Unveiling liquid MOFs*, *Nature Materials*, 16, 2017.

2. Theoretical

2.1. 2,2'-bisimidazole-carboxylate containing ligands

To produce these 2,2'-bisimidazole-carboxylate containing ligands the synthesis of 2,2'-bisimidazole out of glyoxal and an ammonium salt called ammonium acetate was done. But first the main theoretical aspects of the 2,2'-bisimidazole synthesis reaction should be mentioned.

The condensation reaction of carbonyl compounds with ammonia, amines, and their derivatives is a broad and widely used group of processes, which are important for the synthesis of most nitrogen-containing heterocycles like pyridines, azoles, etc. The application range includes for example the production of new-generation of drugs, insecticides, various dyes, and polymers. So, it is perspicuously that this is an interesting field of modern science.

Another aspect of prevailing studies is the investigation and determination of the composition of secondary organic aerosols (SOA) in the atmosphere. Some results show that there is a connection with the condensation of dicarbonyl compounds (mainly glyoxal) with ammonia and/or its derivatives for the production of imidazole containing oligomeric compounds to the so called "brown carbon".⁹ This "brown carbon" is also a relevant topic because of the possibility, that these aerosols have a negative effect on climate, air pollution and in consequence human health.¹⁰

2.2. Glyoxal-ammonia interaction and diimine synthesis

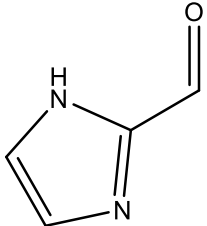
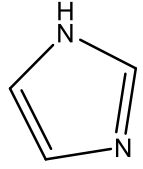
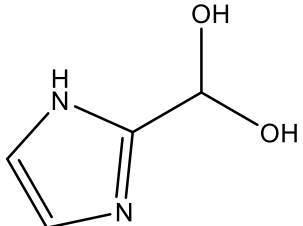
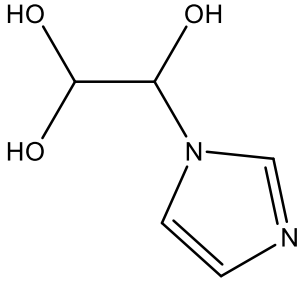
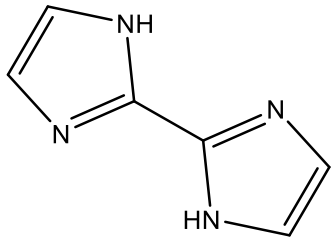
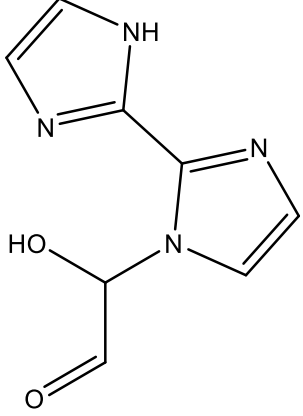
The reaction of glyoxal with ammonium salts in an aqueous solution exhibited various compounds as products. These possible products were shown in Table 2.2.1.:

Table 2.2.1. Possible products of the reaction of glyoxal with ammonium salts in an aqueous solution⁹

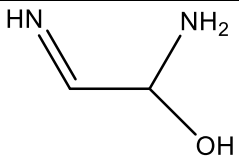
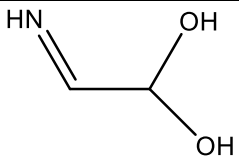
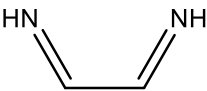
Compound	Structure	Position on the PES, kcal/mol	Identification
----------	-----------	-------------------------------	----------------

⁹ V. Tuguldurova, A. Fateev, O. Poleshchuk, O. Vodyankina, Theoretical Analysis of Glyoxal Condensation with Ammonia in Aqueous Solution, *Phys. Chem. Chem. Phys.*, 2019,21, 9326-9334.

¹⁰ J. Seinfeld, S. Pandis, *Atmospheric Chemistry and Physics: from Air Pollution to Climate Change*, 2nd edition, John Wiley & Sons, New York, USA, 2006.

Products			
1H-imidazole-2-carboxaldehyde (IC)		-37,3	Verified by MS, NMR
Imidazole (I)		-43,3	Verified by MS, NMR
Hydrated imidazole-2-carboxaldehyde (HIC)		-33,0	Verified by MS, NMR
Hydrated N-glyoxal substituted imidazole (HGI)		-52,6	Verified by MS, NMR
2,2'-bisimidazole (BI)		-63,5	Verified by MS
N-glyoxal substituted 2,2'-bisimidazole (GBI)		-68,3	Verified by MS

N-glyoxal substituted hydrated 1H-imidazole-2-carbaldehyde (GHIC)		-37,0	Verified by MS
Hydrated N-glyoxal substituted hydrated 1 H-imidazole-2-carbaldehyde (HGHC)		-42,3	Verified by MS
Hydrated glyoxal dimer substituted imidazole (HGGI)		-62,7	Verified by MS
1,3-oxazole		-30,8	Verified by MS
Intermediates			
aminoethanetriol		-9,5	Verified by NMR
iminoacetaldehyde		+1,9/+0,5*	proposed by MS, verified by NMR

iminoaminoethanol		+1,4/-0,6*	proposed by MS, verified by NMR
iminoethanediol		-0,4	Proposed by NMR
diiminoethane		+3,8/+5,5*	Proposed by NMR

*The positions of structures are obtained from glyoxal conformers (trans- or cis-, respectively)

The intermediates of table like aminoethanetriol, iminoacetaldehyde, and imino-aminoethanol are suggested for the formation of the cyclic products, but iminoethanediol and ethanediimine (diamine) were not verified yet, because of their low concentrations in and short lifetime in the mixture. ¹¹

In Figure 2.2.1. the stepwise mechanisms of the condensation of glyoxal with ammonia in an aqueous solution for the formation of the diimine intermediate, which later on yield to the formation of the verified heterocyclic products. Also, the cis- and trans- isomers equilibrium is included. To find out which is the most favourable pathway of the diimine formation, the positions on the PES of each structure in the mechanism was determined. Again, the cis- and trans- isomers of the glyoxal molecule and its hydration equilibria is shown in the graph. Because of the two cis- and trans- conformation of the glyoxal the reaction with ammonia is possible in both cases. On the left side the pathway starting with trans-glyoxal and on the right side the pathway starting from cis-glyoxal is represented. ⁹

¹¹ G. Yu, A. Bayer, M. Galloway, K. Korshavn, C. Fry and F. Keutsch, Environ. Sci. Technol. 2011, 45, 6336–6342.

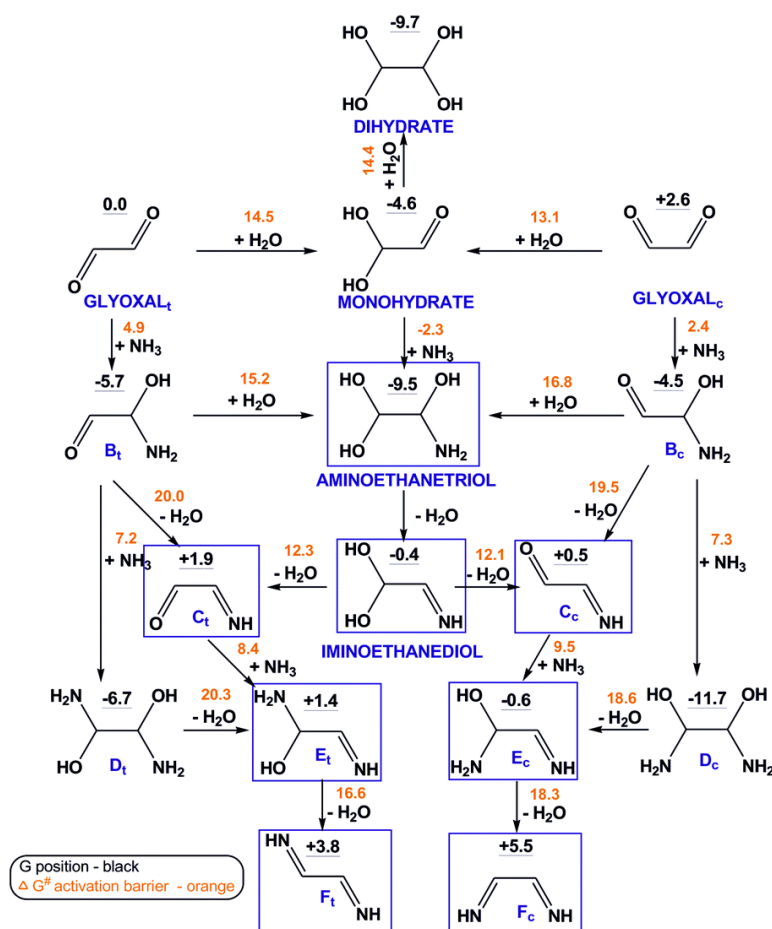


Fig. 2.2.1. The formation of ethanediimine ⁹

For the conformation of the trans-isomer of glyoxal to its cis-isomer in aqueous medium are two ways possible. On the one hand through a trivial rotation of the carbonyl group relative to the other, on the other hand through the generation of the glyoxal monohydrate. In aqueous solution the monohydrate and the dihydrate variation of glyoxal is possible. The PES measurements indicated -4,6 and -9,7 kcal/mol. As expected the G position of the cis-isomer is 2,6 kcal/mol higher than those of the trans-form. The Figure 2.2.1. exhibits also the most favourable pathways for the formation of glyoxal monohydrate and its following proposed intermediates like aminoethanetriol \rightarrow aminohydroxyacetaldehyde \rightarrow diaminoethanediol \rightarrow imino-aminoethanol \rightarrow ethanediimine.

The formation of aminoalcohols indicated in Figure 2.2.1. are specified by ΔG^\ddagger (-2,3)-(-9,5) kcal/mol. The Gibbs free energy of activation of the water addition to the carbonyl group is determined in the field of 13,1-16,8 kcal/mol, and the dehydration of aminoalcohols to form the imine derivatives lies in the range of 16,6 to 20,3 kcal/mol. These are high barriers for

the formation of the imine derivatives and so the equilibrium is shifted towards the formation of aminoalcohols.

The dehydration of intermediate aminoalcohols and gem-diols in the mechanism yield to an increase in the Gibbs free energy of the system by 2,4-11-1 kcal/mol and in the event of imine formation by 0,9-2,3 if the carbonyls are produced. So these are endergonic processes. An exergonic process for example is the addition of ammonia to the carbonyl groups yielding to the corresponding aminoalcohols. This decreases the Gibbs free energy by 0,5-7,2 kcal/mol. Subsequently the lowest positions on the PES are taken by the aminoethanetriol - 9,5 kcal/mol and two conformations of diaminoethanediol (-11,7 and -6,7 kcal/mol).

However, the Figure 2.2.1. shows that the key intermediate product diimine of the prior literature has the positions on the PES of +5,5 kcal/mol, which is in comparison to the other positions of the intermediates slightly higher. Furthermore, for the synthesis of the intermediate product two high-energy barriers have to be overcome. The formation of stable imines (Schiff bases) is also possible through the reaction of the primary amines with the carbonyl components in the presence of at least one aromatic reactant in acidic medium. Moreover, the formation of diimines was experimentally proven only by the formation of imidazole derivatives in the glyoxal interaction with amino acids. No evidence of the formation of diimine was given at the reaction of ammonia with the aldehyde group yet. So there is this basic question to answer.

Vera P. Tuguldurova did this by carrying out an analysis to specify the possibly participation of the amine intermediates in the formation of heterocyclic compounds. In the proposed mechanism the intermediates of aminoethanetriol, diaminoethanediol, glyoxal monohydrate and an aminohydroxyacetaldehyde are concerned.⁹

2.3. The Reaction of glyoxal with ammonia – Synthesis of heterocyclic products

Figure 2.3.1. shows a thermodynamic and kinetic analysis of the formation stages of hydrated imidazole-2-carboxaldehyde (HIC), as an example, out of glyoxal and ammonium salts.

- A) This mechanism is based on the interaction of cis-diimine and glyoxal monohydrate with the involvement of protons.¹¹

- B) The second mechanism is presented by the interaction between diaminoethanediol and glyoxal. This mechanism is proposed without preliminary dehydration and without the participation of a proton.
- C) The third variety analysis the mechanism between aminoethanetriol and aminohydroxyacetaldehyde. This mechanism is also proposed without preliminary dehydration and without the participation of a proton.⁹

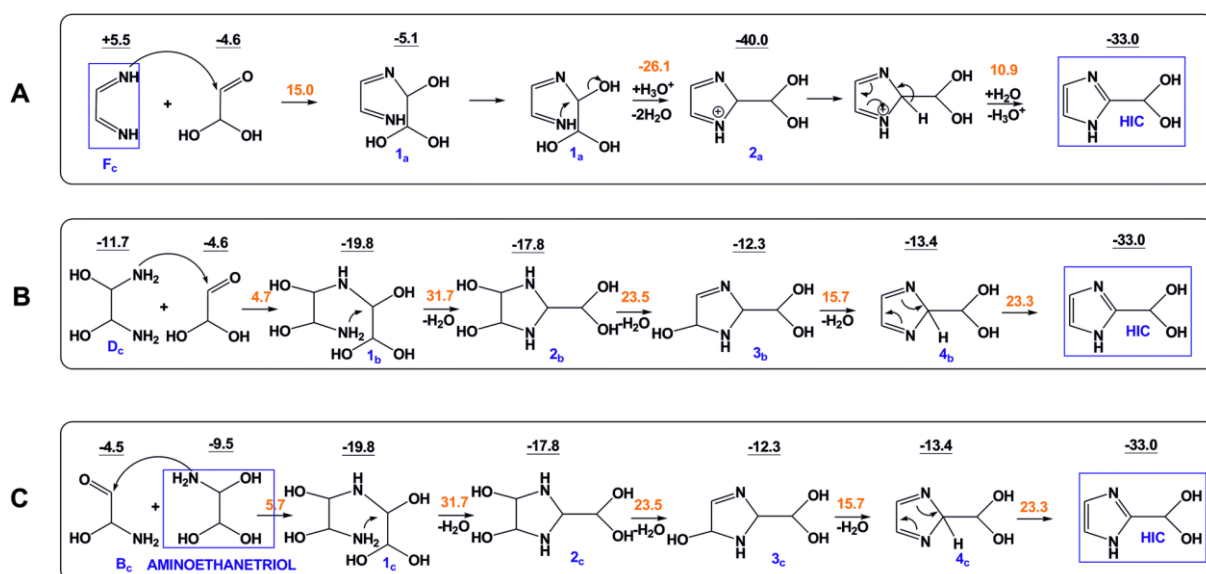


Fig. 2.3.1. Different synthesis mechanisms of hydrated imidazole-2-carboxaldehyde ⁹

The equilibrium in the reaction of ammonium salts in neutral and acidic media is shifted towards ammonium ions. Therefore, only a small amount of ammonia (NH_3) precedes to the rise of the formation of the diamines and diimines. This was one reason why pathway C was proposed and calculated. This mechanism presents the interaction of experimentally proven aminoethanetriol and aminohydroxyacetaldehyde yielding to the pericyclic and cyclic structures $1c$ and $2c$ coinciding with the intermediates $1b$ and $2b$ in pathway B. Mentionable is, that the probability of the reaction between two monosubstituted amines is much higher compared to the interaction between the disubstituted aminoalcohol and glyoxal monohydrate.

The lowest and the highest positions on the PES has the diaminoethanediol with $-11,7$ kcal/mol and the diimine with $+5,5$ kcal/mol. For the diimine formation, diaminoethanol has to be dehydrated twice, so this can be the reason for the high G position. The graph shows

different positions on the PES of the precyclic intermediates of the compared mechanisms A, B, and C. The analyses present with -19,8 kcal/mol a much lower G position of the amine pathways, compared to the diimine path with -5,1 kcal/mol. This results in a higher probability in the abundance of the amine schemes mechanism. Furthermore, Gibbs free energy of activation for the formation of the pericyclic stage is much higher in A (15,0 kcal/mol) than in B (4,7 kcal/mol) or C (5,7 kcal/mol).

The next step in the mechanism is the cyclization stage. There are significant differences in the Gibbs free energy of the mechanisms A, B and C observable. On the one hand in pathway A a ΔG of -34,9 kcal/mol is observable, meanwhile on the other hand in path B and C a ΔG of +2,0 kcal/mol is noticeable. This is the result of the participation of an external proton from the medium in case of pathway A. This proton transfer is not needed in the case of a nucleophilic attack of the amino group on the C atom in the precyclic structure 2b and 2c, because of the strong nucleophilic properties of the -NH_2 -group. This nucleophilic attack with the ring closure is characterized by a high energy barrier ΔG^\ddagger 31,7 kcal/mol and therefore this stage is rate-limiting.

The analyses point out that the mechanism of rout B and C happens along the dehydration states of the cyclic intermediates with moderate barriers and includes a final stage of proton transfer yielding to the HIC product. The final stage has a Gibbs free energy barrier of 23,3 kcal/mol and decreases the energy by 19,6 kcal/mol, which is a lot.

To sum up pathway A needs an additional protonation/deprotonation of the imine intermediates at the cyclization step ($1a \rightarrow 2a$) and is therefore energetically not that likely compared to the mechanisms B and C. The possible end-products which are mentioned in Fig. have positions on the PES in the range of -30,8 to -68,3 kcal/mol, which is quite low and verifies the high probability of their generation. However, a number of equivalent heterocyclic products are produced during the glyoxal condensation with ammonia. Which final products are synthesized depend on the molar ratio of glyoxal and ammonia in the aqueous solution, the pH, and of course the electrolytes, which affects the ratio of the mono- and dihydrate forms of glyoxal. ⁹

2.4. A variety of reactions with 2,2'-biimidazole

In one-dimensional metal atom chains are interesting properties like for example magnetism, conductivity, photo physical and catalytically behaviour noticeable. These properties are dependent by the metal–metal interactions, and of course by the ligands, which play an important role in the formation of chain compounds. For example, a multidentate ligand can coordinate the metal centres via covalent bonds, yielding coordination polymers.

2.4.1. Synthesis of 1,1'-diethyl-2,2'-biimidazole

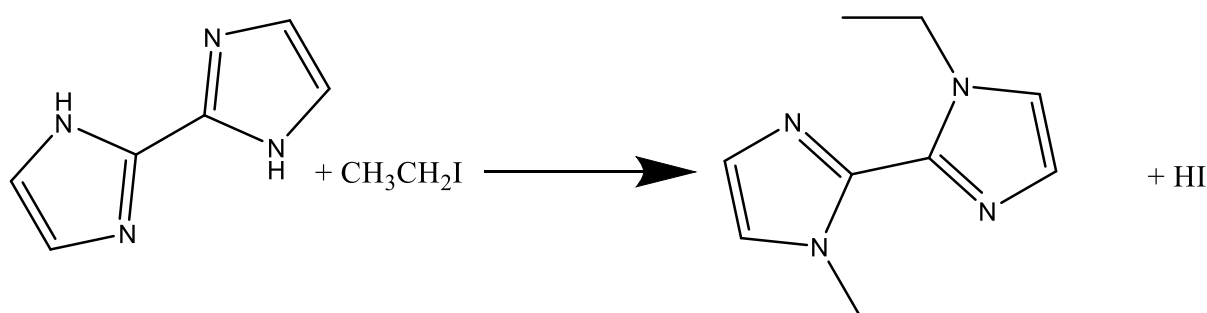


Fig. 2.4.1. Structure of 1,1'-diethyl-2,2'-biimidazole

To produce 1,1'-diethyl-2,2'-biimidazole a mixture of 2,2'-biimidazole (1,9 mmol), acetonitrile (8 mL) and an aqueous solution of sodium hydroxide NaOH (35 %) were stirred under nitrogen for one hour. In the next step ethyl iodide (4.0 mmol) and acetonitrile (1mL) were mixed together and added dropwise over the time of 20 min. Then the mixture was refluxed for 6 h and the two phases were disjoined. Before the reaction mixture was extracted by using dichloromethane, water was added to the acetonitrile phase. Then the organic phases were washed with water and dried over MgSO₄, filtered and evaporated.¹²

¹² R. Tatikonda, E. Laurilla, M. Haukka, Metallophilic interactions in stacked dinuclear rhodium 2, 2'-biimidazole carbonyl complexes, *CrystEngComm*, 2012,14, 8401-8408.

2.4.2. Synthesis of a complex structure $[\text{Rh}_2(\text{R}_2\text{bim})\text{Cl}_2(\text{CO})_4]$ (R = Et, Pr)

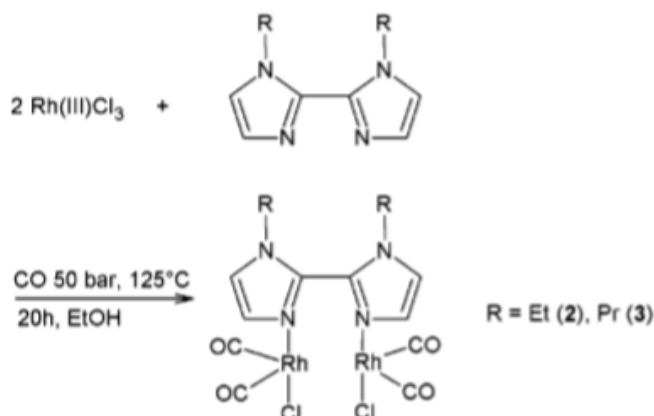


Fig. 2.4.2. Structure of $[\text{Rh}_2(\text{R}_2\text{bim})\text{Cl}_2(\text{CO})_4]$ (R = Et, Pr) ¹²

For the synthesis of $[\text{Rh}_2(\text{R}_2\text{bim})\text{Cl}_2(\text{CO})_4]$ (R = Et, Pr) the 1,1'-diethyl-2,2'-biimidazole (0,24 mmol) and the rhodium trichloride (0,48mmol) were put into a Berghof autoclave in a PTFE liner and dissolved in ethanol (4 mL). Then carbon monoxide was added to the autoclave with 50 bar. After the down cooling the purple with greenish metallic crystals were filtrated.¹²

2.4.3. Synthesis of disubstituted 2,2'-bi-1H-biimidazoles

2,2'-biimidazole has found lots of applications, for example in the pharmaceutical industry agriculture and natural products, so it is important to produce some derivatives. In the reaction below one pathway for the formation of these derivatives is represented. For this synthesis a protecting group is required. The [2-(trimethylsilyl)ethoxy]methyl group (SEM) fulfils the criteria, for example like the removability under compatible conditions for the other functional groups, of an ideal protecting group in this reaction. For the metalation of SEM-2,2'-bi-1H-imidazole the ratio of 2,5 equiv. of n-BuLi with 1 equiv. of tetramethylethylenediamine (TMEDA) is the most efficient. When the anion of SEM-2,2'-bi-1H-imidazole is processed with DMF or methyl disulphide, it leads to 21-23% of monosubstituted biimidazoles and 12-17% of disubstituted biimidazoles. These products

can be separated with flash chromatography. For the deprotection of the SEM-biimidazole derivatives dilute acid is used.¹³

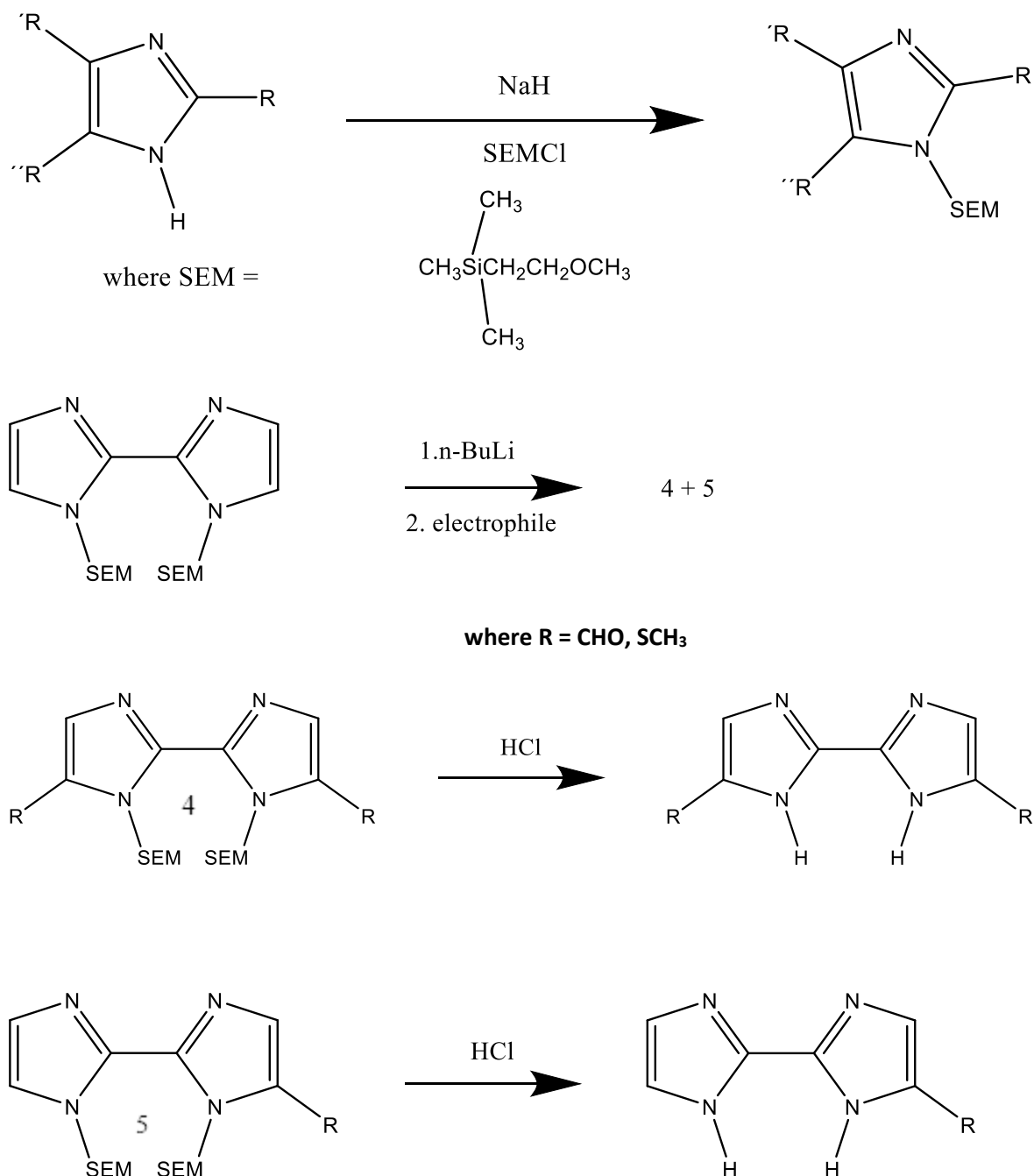


Fig. 2.4.3. Synthesis of disubstituted 2,2'-bi-1H-biimidazoles¹³

¹³ J. P. Whitten, D. P. Matthews, and J. R. McCarthy, [2-(Trimethylsilyl)ethoxy]methyl (SEM) as a novel and effective imidazole and fused aromatic imidazole protecting group, *The Journal of Organic Chemistry*, 1986, 51, (10), 1891-1894.

2.4.4. Formation of two-dimensional hydrogen bonded supramolecular networks in the compounds of benzene-1,2,4,5,-tetracarboxylic acid with 2,2'-biimidazole

Polycarboxylic acids, like benzene-1,2,4,5-tetracarboxylic acid, benzene-1,2,3,4-tetracarboxylic acid and benzene-1,3,5-tricarboxylic acid can build supramolecular networks because of their ability of a hydrogen-bond donor and hydrogen-bond-acceptor, depending upon the number of deprotonated carboxylic acid groups. In the literature many transition-metal complexes with benzene-1,2,4,5-tetracarboxylate have been synthesized and documented. PMA salts, like for example 2,2'-biimidazole-3,3'-dium 2,5-dicarboxybenzene-1,4-dicarboxylate, are formed during an attempt to synthesize mixed-ligand transition-metal complexes with PMA and N-containing ligands solvothermally. In this reaction 1 equiv. of 2,2'-biimidazole, 1 equiv. of benzene-1,2,4,5-tetracarboxylic acid and 1 equiv. of $\text{ZnSO}_4 \cdot 7\text{H}_2\text{O}$ in water were mixed together and heated to 383 K for 72 h. Then colourless block-shaped crystals were held. ¹⁴

In the reaction a proton transfer has occurred, which leads to product that crystallizes in space group P1. The produced asymmetric unit is made up of two halves of the 2,2'-biimidazole-3,3'-dium dication, each one protonated at two imidazole ring N atoms and two halves of the 2,5-dicarboxybenzene-1,4-dicarboxylate dianion, each one with two of the carboxylic acid groups deprotonated. The crystallographic centres of the two 2,5-dicarboxybenzene-1,4-dicarboxylate dianion anions are linked by an O1-H1...O7 hydrogen bond. The two 2,2'-biimidazole-3,3'-dium dications are connected by N3-H3A...O3, N4-H4B...O4, N1-H1B...O7 and N2-H2B...O8 hydrogen bonds with the neighbouring 2,5-dicarboxybenzene-1,4-dicarboxylate dianions. Because of these hydrogen-bond interactions a two-dimensional supramolecular sheet can be formed. ¹⁴

¹⁴ K. Zhong, Two-dimensional hydrogen-bonded supramolecular networks in the compounds of benzene-1,2,4,5-tetracarboxylic acid (pyromellitic acid) with 2,2'-biimidazole and 4,4'-dimethyl-2,2'-bipyridine. *Acta Cryst. C*, 2013, 69, 1537-1540.

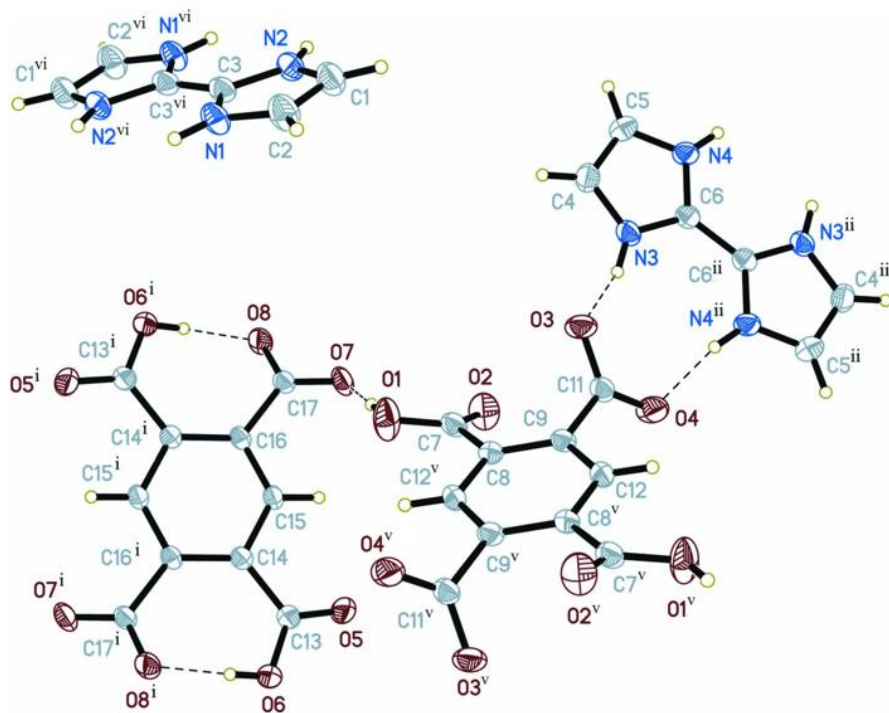


Fig. 2.4.4.1. "Basic unit" of the two-dimensional hydrogen-bonded network. The dashed lines show the intermolecular interactions.¹⁴

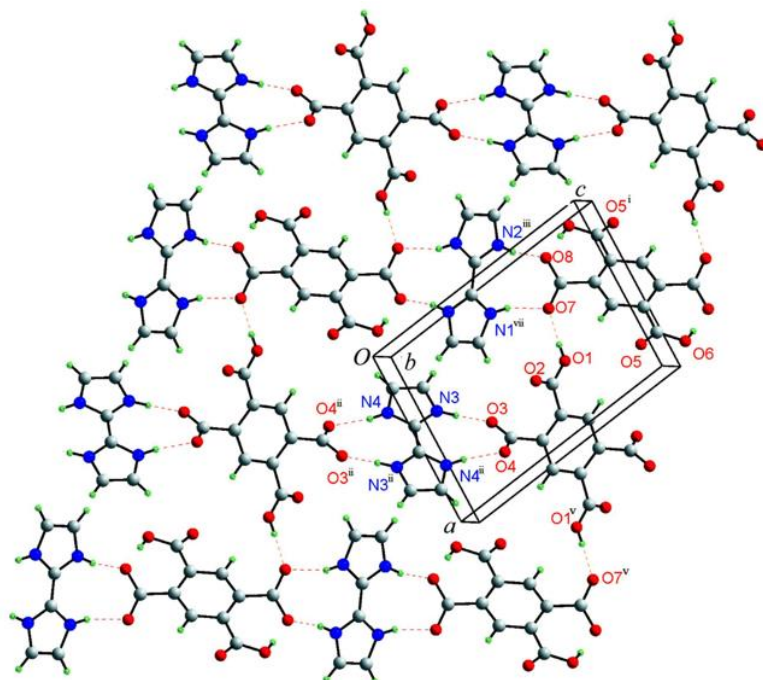


Fig. 2.4.4.2. Structure of the two-dimensional hydrogen-bonded network. The dashed lines show the O—H...O interactions.¹⁴

2.4.5. Hydrogen-bonded self-assemblies based upon $[M(H_2biim)_2(H_2O)_n]^{2+}$ ($M=Cd^{2+}$, Co^{2+} , Zn^{2+} ; $n=1,2$) building units and carboxylates

Because of the high variability in potential applications research in coordination polymers have become more and more focused in the last few years. To control the dimensionality, which is still a big challenge in this field, various factors like the medium, temperature, metal-ligand ratio, template and counter-ion are important. However, hydrogen-bonding is also a powerful force in building supramolecular structures. The intermolecular force of hydrogen bond is weaker than the coordination bond in the construction of hybrid inorganic-organic materials. To get over this disadvantage multiple hydrogen bonds were formed. For that application the neutral 2,2'-biimidazole (H_2biim) is an ideal molecule. It coordinates to metal ions and it provides two N-H hydrogen bond donating sites for multi-dimensional network assembly, as a second advantage. In addition, it is able to construct robust heteromeric hydrogen-bonded synthons such as the examples in Fig. 2.4.5.1.

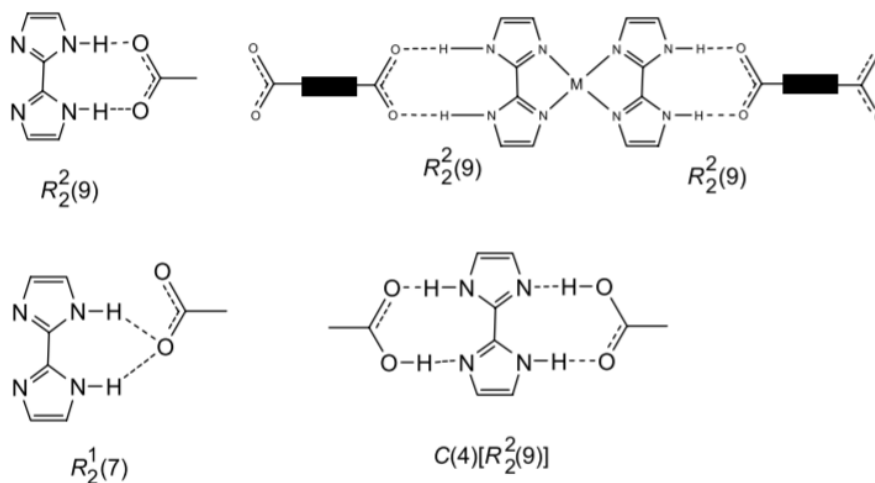


Fig. 2.4.5.1. Structure of the robust heteromeric hydrogen-bonded synthons¹⁵

Because of the almost linearity of the N-H...O unit and the N...O separation is near to the lower limit of the accepted domain, the interaction should be very stable and strong.

Furthermore, the H₂biim ligand and the carboxylate functional group form an almost coplanar arrangement.¹⁵

In literature the following molecules were synthesized and characterized by single crystal X-ray diffraction: [Zn(H₂biim)₂(H₂O)₂](Hbdc)₂*H₂biim*H₂O, [Zn(H₂biim)₂(H₂O)](bdc)*CH₃OH, [Co(H₂biim)₂(H₂O)₂](Hbtc)*4H₂O, [Cd(H₂biim)₂(H₂O)(bdc)]*H₂O (where btc = 1,3,5-benzenetricarboxylate and bdc = 1,3-benzenedicarboxylate)

Due to similarity, in this thesis only the first complex [Zn(H₂biim)₂(H₂O)₂](Hbdc)₂*H₂biim*H₂O is regarded closer.

For the synthesis of for instance [Zn(H₂biim)₂(H₂O)₂](Hbdc)₂*H₂biim*H₂O a Zn(NO₃)₂*6H₂O methanolic solution was added to a methanolic solution of H₂biim in a ratio of 1 equiv. to 3,5 equiv. To completely dissolve the ligand, the mixture had been refluxed. Afterwards an aqueous solution of 1 equiv. sodium 1,3-benzenedicarboxylate was applied into the solution. A pH-value of 5, to ensure that the H₂biim ligand was in neutral form to coordinate with the metal ions, was abandoned with dilute nitric acid, and then stirred at 60°C for 2h. To remove the solid by-products, the solution was filtrated. The filtrate was evaporated slowly for about one week to receive a colourless crystalline product.¹⁵

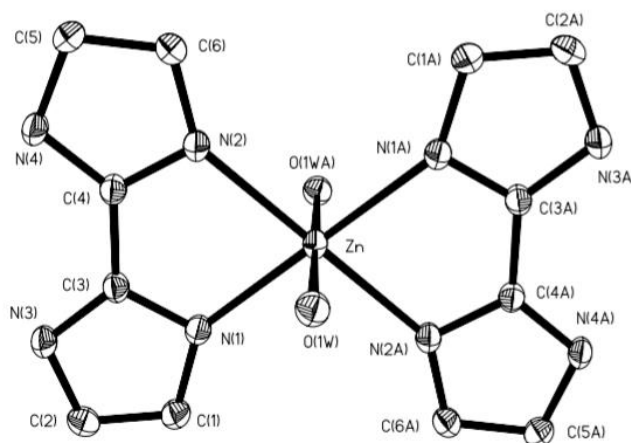


Fig. 2.4.5.2. The structure of [Zn(H₂biim)₂(H₂O)₂]²⁺¹⁵

The structure of [M(H₂biim)₂(H₂O)₂](X)₂ (M=Zn²⁺ and Co²⁺, X=acetate or isonicotinate) has two H₂biim ligands on the same equatorial plane and trans to each other. The

¹⁵ D. Bing-Bing, W. Yan-Qin, C. Ying, C. Xiao-Ming, Y. Bao-Hui, Robust Heteromeric Hydrogen-bonded Self-assemblies Based on [M(H₂biim)₂(H₂O)_n]²⁺ (M=Cd²⁺, Co²⁺, Zn²⁺; n=1, 2) Building Blocks and Carboxylates, *Supramolecular Chemistry*, 2005, 17:6, 475-483.

$[M(H_2biim)_2(H_2O)_2]^{2+}$ core is linked to the other two carboxylate anions with a strong N-H...O hydrogen bond interaction. A multi-dimensional structure can be received if dicarboxylate or tricarboxylate anions will be used. However, the $[M(H_2biim)_2(H_2O)_n]^{2+}$ building units are arranged with carboxylates by charge-assisted O-H...N and N-H...O (N...O = 2,607- 2,926 Å, $\angle N-H-O = 151-176^\circ$) hydrogen bonds into 3-dimensional networks and 1-dimensional ribbons. These 1-dimensional ribbons are assembled into 3 dimensional networks, based on hydrogen bonds between carboxylate, water molecules, methanol molecules and the free H_2biim molecule.¹⁵

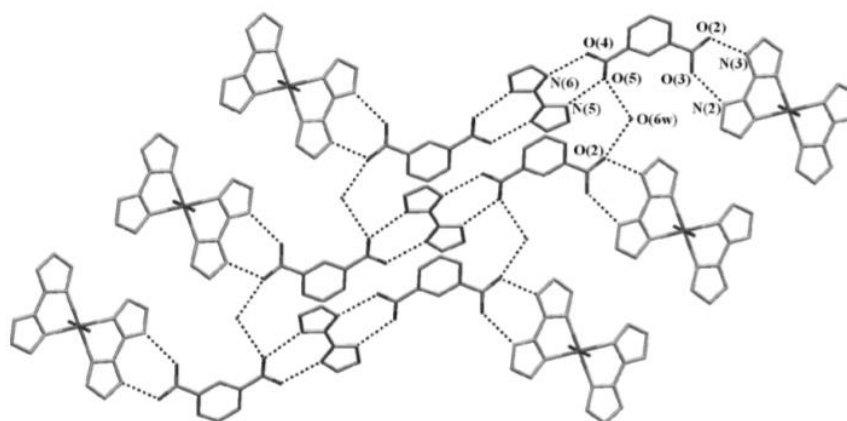


Fig. 2.4.5.3. 2-D network made by hydrogen bonds¹⁵

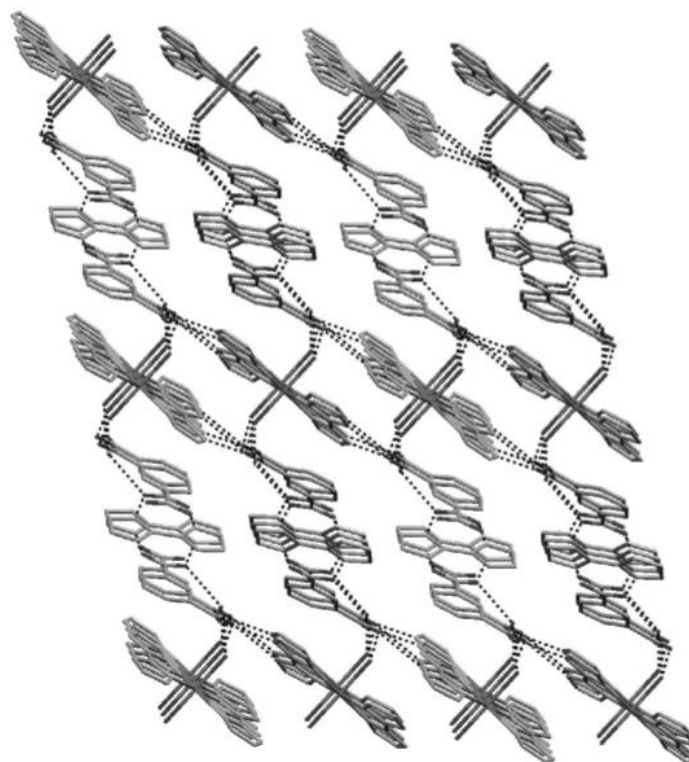


Fig. 2.4.5.4. 3-D network made by hydrogen bonds¹⁵

2.4.6. Aza-Michael addition reaction of N-heterocycles

The Michael addition reaction is because of its molecularly economic reaction and simple handling a widely used method for the synthesis of β -amino carbonyl compounds. In the early day's strong bases and acids, which are ecologically harmful, were used to carry out this reaction.¹⁶ Later lots of alternative reactants and catalysts, such as SmI_2 , CeCl_3 , InCl_3 , and heterogeneous solid acids, were developed to avoid such conditions. The disadvantage of this solution is the high price of the transition-metal complex catalysts. Therefore, organocatalysts like 1,8-diazabicyclo[5.4.0]undec-7-ene (DBU) were applied as mild promotor for the aza-Michael addition of amines with α,β -unsaturated carbonyl bonds.^{17,18}

Latest studies showed, that ionic liquids can also play an important role for the aza-Michael addition reaction. The cationic part of this ionic liquids has a structural similarity to N-methylimidazole. Therefore, this substance was used to promote the addition of N-heterocycles to α,β -unsaturated carbonyl educts yielding 1,4-adducts. The results were very good yields in short reaction times. Another conclusion was that the occurrence of an electron-withdrawing group raises the nucleophile power and leads to a higher reactivity of the N-heterocycles. Furthermore, this could be the reason for a bigger yield in those cases shown in Figure 2.4.6.1.¹⁹

¹⁶ M. Arend, B. Westermann, N. Risch, *Angew. Chem. Int. Ed.* 1998, 37, 1044.

¹⁷ (a) B.C. Ranu, S.S. Dey, *Tetrahedron* 2004, 60, 4183. (b) X.S. Fan, X.Y. Hu, X. Y. Zhang, J.J. Wang, J. Aust, *Chem.* 2004, 57, 1067. (c) B.C. Ranu, S. Banerjee, *Org. Lett.* 2005, 7, 3049. (d) V. Calo, A. Nacci, L. Lopez, V. L. Lerario, *Tetrahedron Lett.* 2000, 41, 8977.

¹⁸ C.E. Yeom, M.J. Kim, B.M. Kim, *Tetrahedron*, 2007, 63, 904.

¹⁹ B. K. Liu, Q. Wu, X. Q. Qian, D. S. Lv, X. F. Lin, N-Methylimidazole as a Promising Catalyst for the Aza-Michael Addition Reaction of N-Heterocycles, *Synthesis*, 2007,17, 2653-2659.

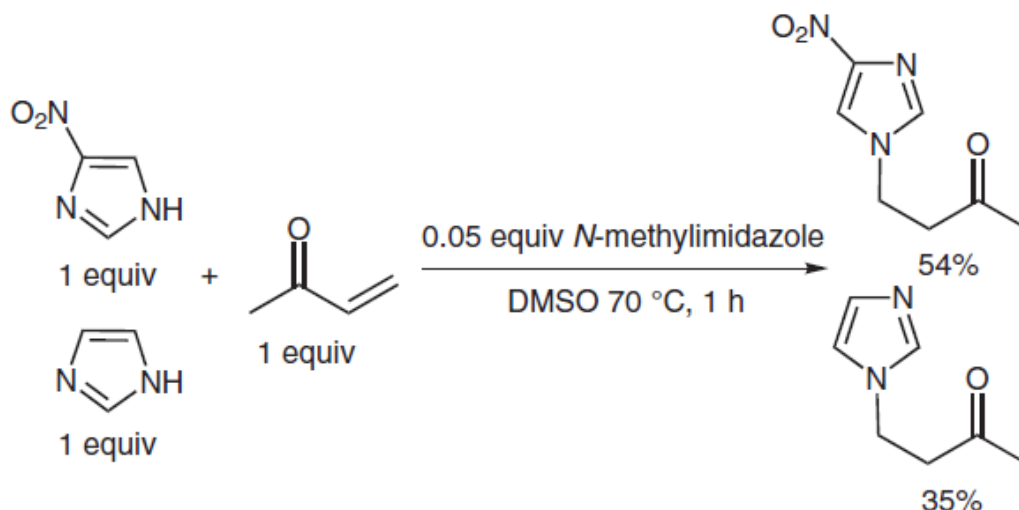


Figure 2.4.6.1. Reactivity of the *N*-heterocycles in the Aza-Michael reaction ¹¹

The proposed reaction mechanism for the nucleophile catalysed Michael-addition proceeds via abstraction of the N-H proton of the other *N*-heterocycle by the N¹ atom. This abstraction would increase the nucleophilic character of the *N*-heterocycle for addition to electron deficient alkenes. The possible corresponding mechanism of this scenario is shown in Figure 2.4.6.2. ¹⁹

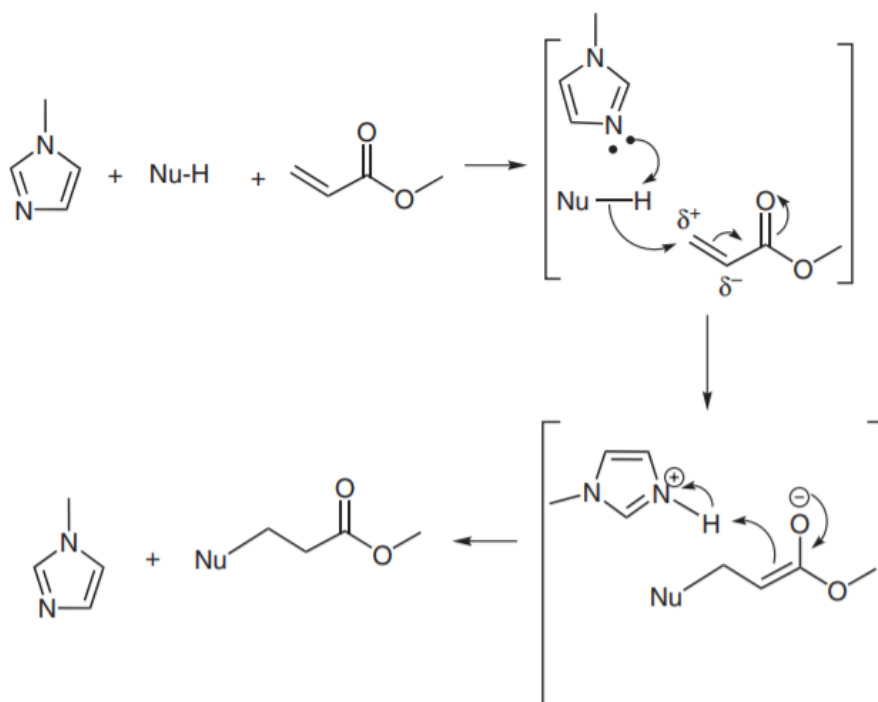


Figure 2.4.6.2. Nucleophile catalysed mechanism of the Aza-Michael addition ¹⁹

This conclusion was also an interesting fact for this master's-thesis. So, some of our realized reactions, for example like the addition of the acceptor ethyl acrylate with the donor 2,2'-biimidazole were based on these theoretical studies and on the assumption, that the imidazole components could auto-catalyse themselves.

2.5. Zeolitic imidazolate frameworks (ZIFs)

Zeolitic imidazolate frameworks (ZIFs) are a specific class of metal organic frameworks (MOFs) out of imidazolate linkers and metal ions.²⁰ These ultra-high surface crystal structures are very comparable to conventional aluminosilicate zeolites. The conventional aluminosilicate zeolites, which are composed of Si(Al)O_4 units, where covalently bonded oxygen is the so called linker for the formation of a framework, play already an important role in the segment of petrol engineering.²¹

Compared to the aluminosilicate zeolites the metal ions take the part of silicon and the imidazole anions build bridges, like the oxygen in zeolites. The metal-imidazole-metal angle is around 145° .^{22,23} In these frameworks, which are formed by a self-assembly approach, often Zn or Co metal-cations are used. Due to thermal and chemical stable intrinsic porous qualities of zeolitic imidazolate frameworks, these materials could have interesting properties in a wide range of potential applications. A few potential applications would be for example in gas separation, drug delivery, sensing and electronic devices, and catalysis.¹²

The imidazole containing compound is able to be a neutral and monodentate ligand or a negative bidentate ligand. The reason for this variation is two nitrogen atoms in the imidazole group and their substitution position. Frameworks are created by the coordination of deprotonated imidazolate ligands with metal centres.²⁴

²⁰ C. Binling, Y. Zhuxian, Z. Yanqiu, X. Yongde, Zeolitic imidazolate framework materials: Recent progress in synthesis and applications. *J. Mater. Chem. A.* 2.,2014,2,16811-16831.

²¹ K. Park, Z. Ni, A. Côté, et al. Exceptional Chemical and Thermal Stability of Zeolitic Imidazolate Frameworks. *Proceedings of the National Academy of Sciences of the United States of America* ,2006, 103 (27), 10186-91.

²² S. A. Moggach, T. D. Bennett and A. K. Cheetham, *Angew. Chem.*, 2009, 121, 7221-7223.

²³ D. Fairen-Jimenez, S. A. Moggach, M. T. Wharmby, P. A. Wright, S. Parsons and T. Düren, *J. Am. Chem. Soc.*, 2011, 133, 8900-8902.

²⁴ Y. Sun, W. Sun, Zinc and cadmium-organic frameworks with 1-imidazole-containing and 1-imidazole-carboxylate ligands, *CrystEngComm*, 2015, 17, 4045-4063.

In Figure 2.5.1. the representative crystal structures of ZIFs are shown. The structure code of the ZIF is constituted with the first three capital letters and the yellow sphere in the centre represents the maximum size of any absorbed particle.

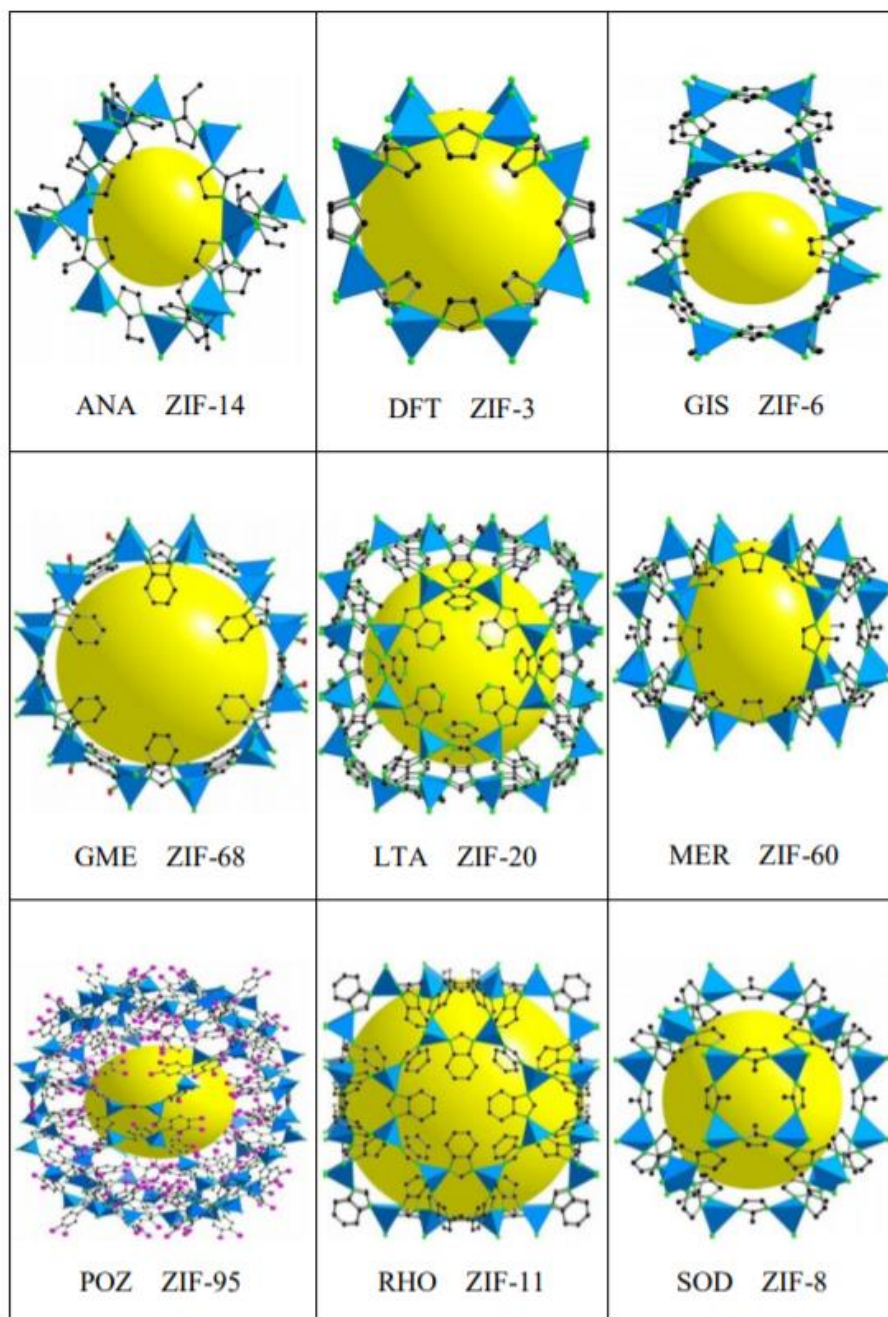


Figure 2.5.1. Crystal structures of ZIFs ²⁰

Today's most investigated ZIF structure is the so-called ZIF-8, which is built up of a 2-methylimidazole which is connected via the nitrogen to the zinc cations. The highly porous crystal structure is shown in Figure 2.5.2.

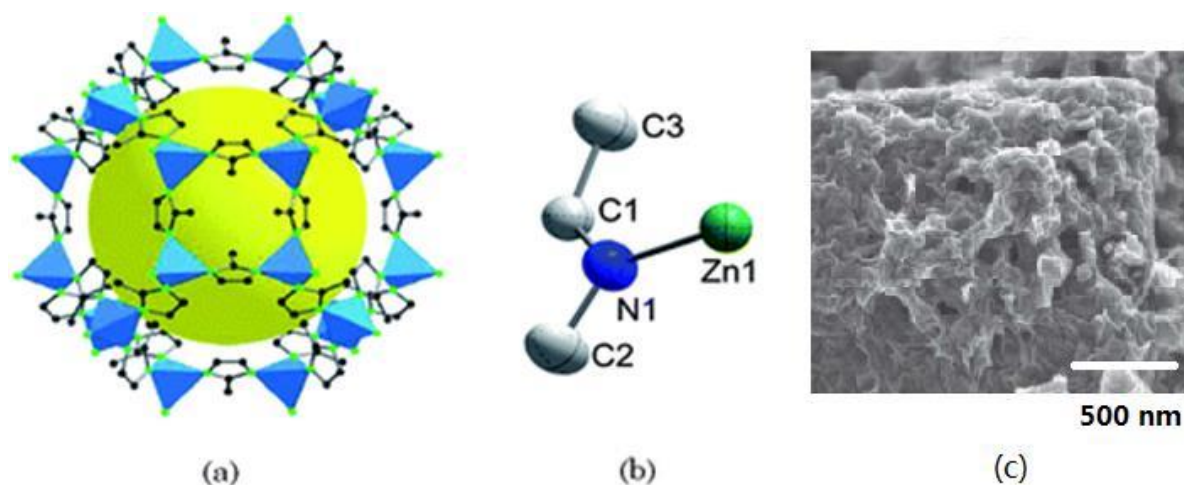


Figure 2.5.2. (a,b) Zeolitic imidazolate framework-8 (c) micrograph of the high surface structure of ZIF-8²⁵

The production of these structures is usually made hydrothermal or solvothermal with water or organic solvents. In literature the reaction temperature varies from room temperature to 200°C and the reaction duration from hours to days. Mostly these variations are depending on the different desired structures, like membrane/film, powder etc.²⁰

The porosity of these high-surface structures is measured by gas-sorption analysis. For the ZIF-8 structure the highest surface areas with 1,810m²/g with Langmuir model and 1,630m²/g with Brunauer-Emmett-Teller of all zeolites were obtained. In consequence of these large pores the diameter in ZIF-8 is determined with 11,6 Å and the pore aperture diameter is determined with 3,4 Å. Moreover, these ZIF-8 compounds are remarkable thermal stable, as shown in the TGA analysis. The thermal gravimetric analysis for ZIF-8 indicated a gradual weight-loss step of 28,3% in a range between 25 and 450°C, associated to some loss of guest species DMF and H₂O.²¹

²⁵ S. Zhuang, New Nitrogen-Doped Graphene/MOF-modified catalyst for Fuel Cell Systems, ECS Transactions, 2016, 72, (8), 149-154.

2.6. Metal-organic frameworks and coordination polymers with different dimensionalities

The preparation and of coordination polymers with lots of topological frameworks are getting more and more focused in modern science. One of the reasons might be the huge application potential, ranging from the areas of luminescence, catalysis until gas storage and so on. The structural features of coordination polymers strongly depend on the organic ligands and the metal ions. So, it is necessary to select the suitable multifunctional organic ligands and metal ions for the desired product and its properties. The bi-functional organic ligands, such as imidazole-based carboxy ligands, benzimidazole-based carboxylate ligands, triazole-based carboxylate ligands, pyrazole-based carboxylate ligands, offer more chances to build higher dimensional coordination polymers, than for instance monofunctional ligands. An interesting example for a bi-functional organic ligand would be benzimidazole-2-butanoic acid (H_2L). This ligand could make various coordination modes with the benzimidazole nitrogen atoms and the carboxylate oxygen atoms coordinating metal cations, like Cd^{2+} and Zn^{2+} .²⁶

In the Cd-complex, $[Cd(HL)_2]_n \cdot nH_2O$, each Cd^{2+} is coordinated by four carboxylate oxygen atoms, from two carboxylate groups and two nitrogen atoms, yielding to a distorted octahedral coordination system. The XRD measurements reveal that the Cd-O bond length are in the range of 2,303-2,471 Å, and the Cd-N bond length is 2,264 Å. The Cd^{2+} cations are linked by the HL-ligands into a two-dimensional layered structure with opened quadrilateral windows. The measurement of the open window is 8.502x8.502 Å. Because of the intermolecular hydrogen bonds between the lattice water molecules and the carboxylate oxygen atom and the nitrogen atoms a 3D supramolecular framework as shown in Figure 2.6.1.c. is generated.²⁶

²⁶ Y. Zhang, Z. Du, X. Luo, Coordination Polymers with Different Dimensionalities: from 2D Layer to 3D Framework, *Z. Anorg. Allg. Chem.*, 2015, 641 (15), 2637-2640.

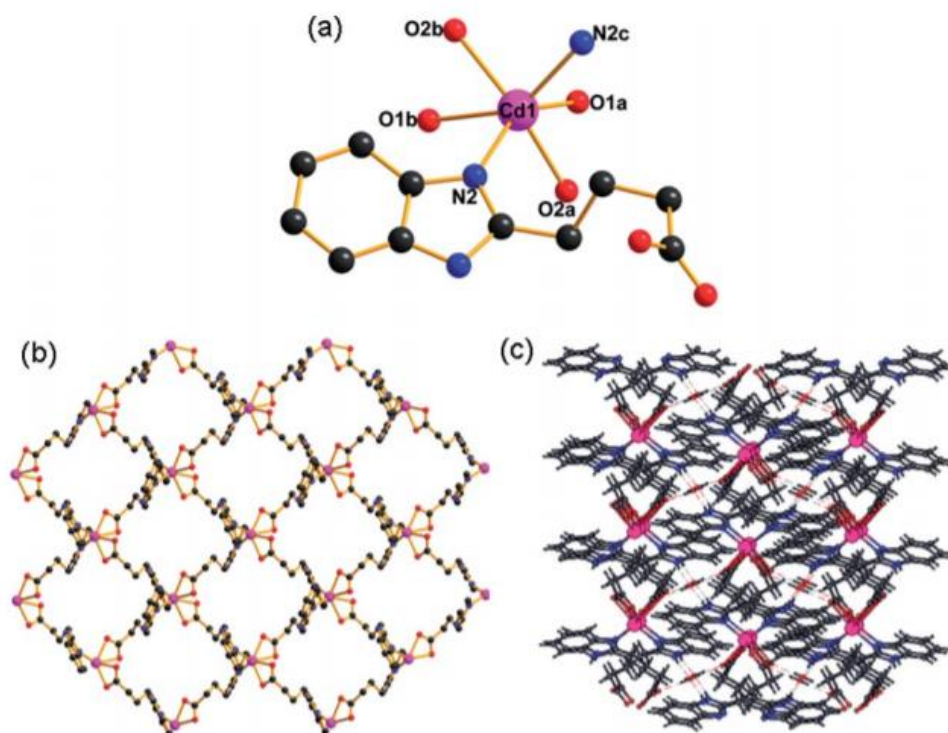


Figure 2.6.1. (a) The coordination environment of Cd^{2+} (b) The 2D-layer structure of $[\text{Cd}(\text{HL})_2]_n \cdot n\text{H}_2\text{O}$ (c) The supramolecular framework of $[\text{Cd}(\text{HL})_2]_n \cdot n\text{H}_2\text{O}$ ²⁶

In Figure 2.6.2. the 3D framework of $[\text{Zn}(\text{L})]_n$ is shown. If the Cd^{2+} -ions are replaced by Zn^{2+} -ions the 3D structure is obtained. Single crystal X-ray diffraction analysis shows that a 3D framework with 3-connected etb topology is existing. In this framework each Zn cation is tetrahedrally coordinated by two carboxylate oxygen atoms and two nitrogen atoms from four different L2 – ligands. The measurements result in a Zn–O and Zn–N distance of 1.973 – 1.976 Å and 1.970 – 1.987 Å. As shown in Figure 2.6.2.c. there are small opened hexagonal channels in the 3D-structure, providing it a high surface.²⁶

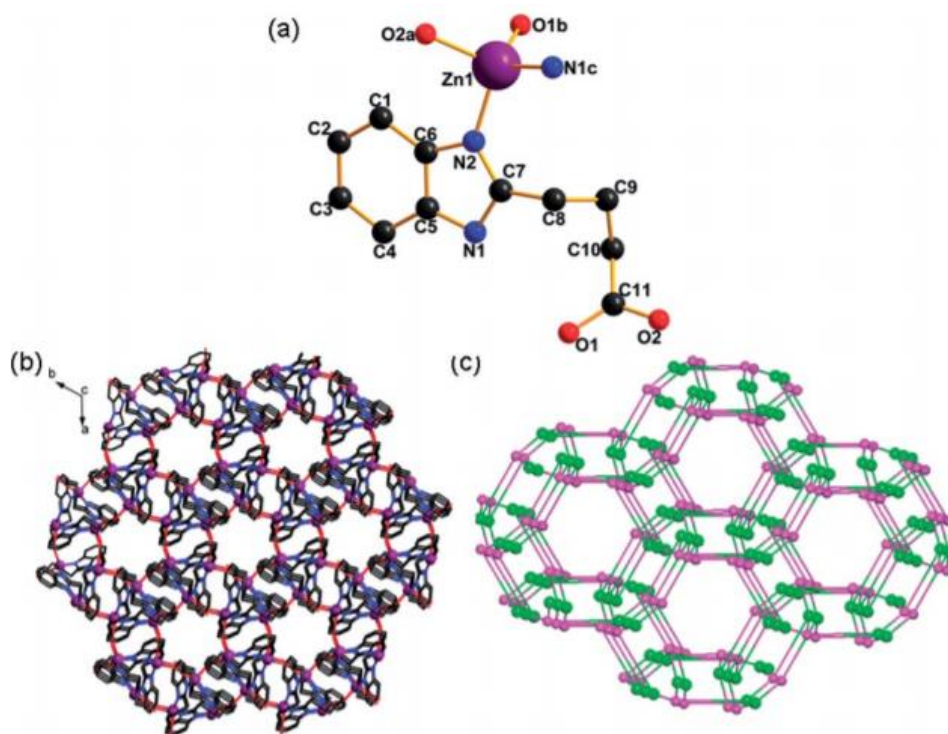


Figure 2.6.2. (a) The coordination environment of Zn^{2+} (b) The 3D framework of $[Zn(L)]_n$ (c) 3- connected etb topological network²⁶

However, a further similar metal-organic framework with a bifunctional organic ligand is reported in Q. Zhai et al. 2013 (27). In this paper imidazole-4,5-dicarboxylic acid (H_3IMDC) ligands and its derivatives were analysed. These ligands were made up of two N and four O atoms and have been elected as multidentate ligands based on their multiple coordination sites for rigid and stable higher dimensional frameworks. The N-X-N angle in the structure is with 144° close to the Si-O-Si angle in for instance zeolites. Another interesting fact is, that the imidazole-4,5-dicarboxylic acid ligand can be partially or completely deprotonated to form different species like H_2IMDC^- , $HIMDC^{2-}$ or $IMDC^{3-}$ at variable pH-values. This could be useful for producing a large diversity of MOF architectures. Lots of MOFs with similar ligand, which only discern in groups on the 2-position of the imidazole ring, have been analysed. The results indicate that the group in the backbone changes its coordination mode. By using ligands with varying alkyl groups at the 2-position some influences on the structure occur. These influences could be the reason why a one-dimensional chain, two dimensional layer or three-dimensional framework is achieved.

The preparation of $[Zn(H_2EIMDC)_2(H_2O)_2] \cdot 2.25H_2O$ was done by dissolving $Zn(NO_3)_2 \cdot 6H_2O$, H_3EIMDC in deionized water. Then the mixture was put in a Teflon-lined reactor at $180^\circ C$ for

five days. By cooling the mixture down to room temperature, colourless plate like crystals were received. The Zn^{2+} cation is coordinated with two nitrogen and two carboxylate oxygen atoms from the individual H_2EIMDC in the equatorial plane, and two oxygen atoms of the water in axial position. So, this structure has an octahedral coordination geometry. As in Figure 2.6.3. shown the hydrogen bonds interact with the molecules to form a 1D chain along the b-axis. This is further connected by crystallized H_2O molecules via hydrogen bonds yielding a 2D layered structure and finally a 3D supramolecular framework.²⁷

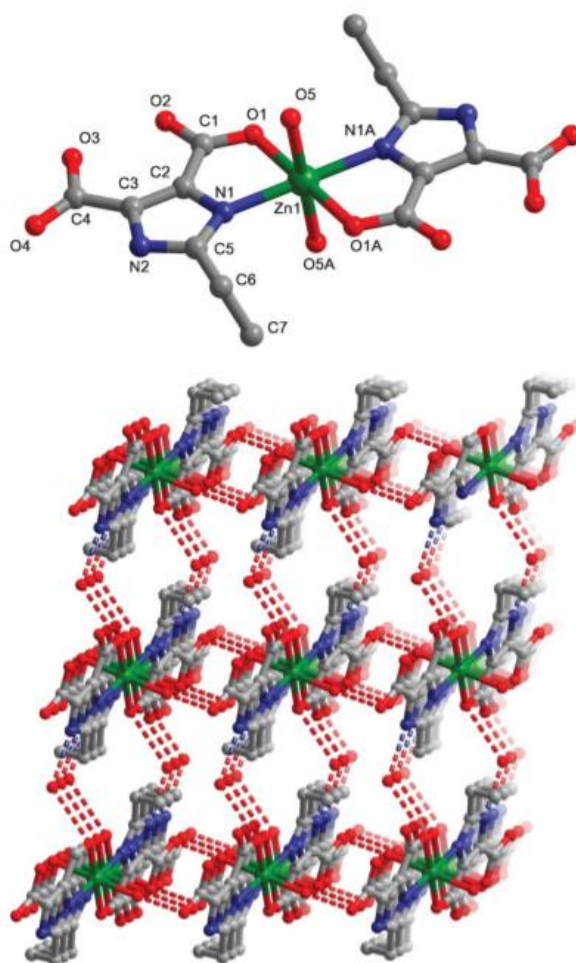


Figure 2.6.3. The basic coordination environment and the 3D supramolecular framework assembled by hydrogen bonds²⁷

²⁷ Q. Zhai, R. Zeng, S. Li, Y. Jiang, M. Hu, Alkyl substituents introduced into novel d10-metalimidazole-4,4-dicarboxylate frameworks: synthesis, structure diversities and photoluminescence properties, *CrystEngComm*, 2013, 15, 965-976.

2.7. Coordination polymers and MOFs based on 1,1'-Bis(propionic acid)-2,2'-biimidazole

The preparation and geometry of functional coordination polymers made up of metal ions and organic linkers have earned considerable attention in the last years due to their structural diversities and potential useful applications.¹

Compounds based upon the 2,2'-biimidazole moiety have been the focus of many studies because of their biological activity as cardiotonics, antiprotozoals, and enzyme active-site models.²⁸ Moreover, 2,2'-biimidazole has been often utilized as a bridging ligand in oligometallic chemistry for catalysis, antitumor medicaments, a biomimetic ligand in bioinorganic chemistry and building blocks of supermolecular frameworks. 2,2'-Biimidazole can build a range of different helical coordination polymers in either cis or trans coordinating mode. The behaviour of for instance a N,N'-dimethylated derivative (Me₂biim) of biimidazole is very different. So, the coordination of the 2,2'-biimidazole derivative coordinated with metal ions yields to a one-dimensional helical structure. Furthermore, polycarboxylate groups are one of the most successful multifunctional ligands in the preparation of MOFs, due to their strong coordination ability, structural rigidity and chemical stability. For that reason a multifunctional ligand like Na₂Pra₂biim = 1,1'-di(propionic acid)-2,2'-biimidazole disodium salt is mentioned.²⁹

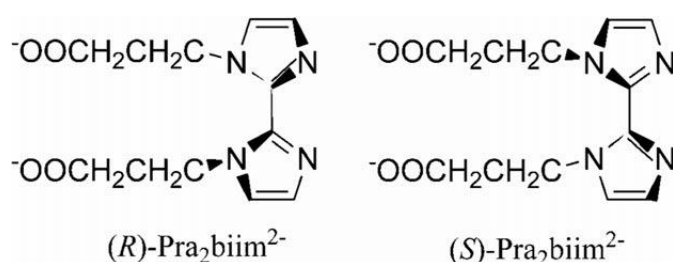


Figure 2.7.1. Isomeric structures of the Pra₂biim²⁻ ligand¹

²⁸ Y. Dong, L. Hou, H. Liang, D. Wei, Solubilities of 1,1'-Di(2-carboxyethyl)-2,2'-biimidazole in Water + Acetic Acid from (292.3 to 355.1) K, J. Chem. Eng. Data, 2008, 53, 2449-2450.

²⁹ R-L. Sang, L. Xu, Unprecedented helix-based microporous metal-organic frameworks constructed from a single ligand, Chem. Commun., 2008, 6143-6145.

Me₂biim favours a bridging rather than a chelating coordination mode, due to the noncoplanarity of the two imidazole rings as suggested by the large dihedral angle (67-89°), which might be caused by repulsion between the methyl substituents.

To obtain the optimum environment for resonance delocalisation and the minimal repulsion between the substituents, the two imidazole rings are coplanar with the two carboxylic arms trans to each other. This planar anti conformation prefers the formation of the CO₂H...N hydrogen bonds [O1...N2A 2.7613(17) Å], yielding to a 2D supramolecular sheet in the ac plane with the H₂Pra₂biim ligand acting as four-connected branch point (Figure 2.7.2.).

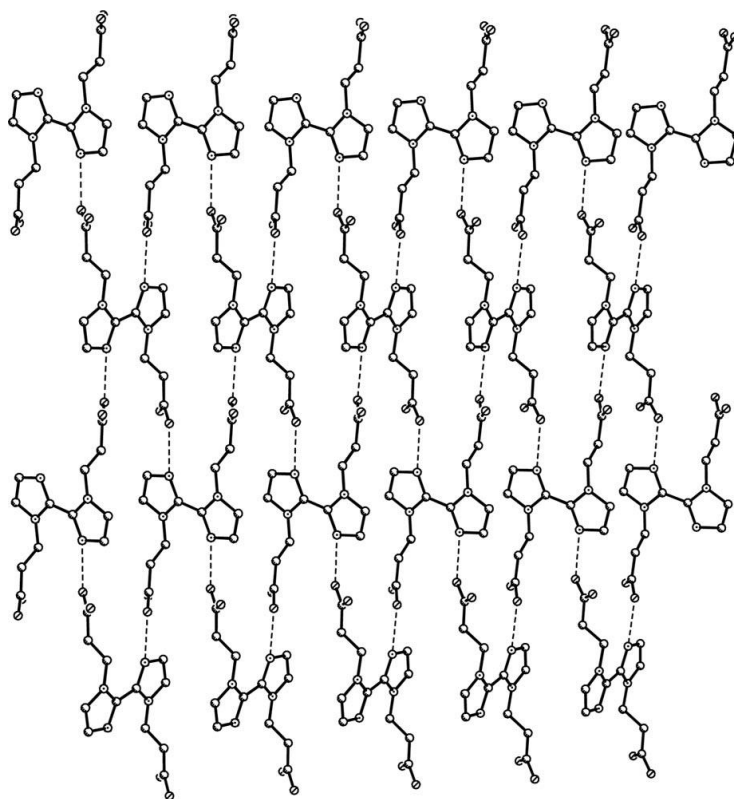


Figure 2.7.2. 2D supramolecular hydrogen-bonded sheet of the H₂Pra₂biim ligand¹

The [Zn(HPra₂biim)Cl]_n polymer shows the *N,N'*-bridged [Zn₂(μ₂-HPra₂biim)₂]²⁺ unit reminding of [Zn₂(μ₂-Me₂biim)₂]⁴⁺. They feature a centrosymmetric structure with tetrahedrally coordinated Zn metal ions. The geometric structure of [Zn(HPra₂biim)Cl]_n is very close to that of [Zn₂Cl₄(μ₂-Me₂biim)₂]. So, the dihedral angle of the imidazole rings in [Zn(HPra₂biim)Cl]_n (85.8°) is very similar to that in [Zn₂Cl₄(μ₂-Me₂biim)₂]. The Zn-Cl and Zn-N bond lengths between those structures are further not significantly different. The reason for the structural development from the discrete [Zn₂Cl₄(μ₂-Me₂biim)₂] complex to the 2D

polymer sheet happens as a consequence of the substitution of one chloride anion in $[\text{Zn}_2\text{Cl}_4(\mu_2\text{-Me}_2\text{biim})_2]$ with one deprotonated propionate arm in $[\text{Zn}(\text{HPra}_2\text{biim})\text{Cl}]_n$. The deprotonated arm operates as a monodentate ligand and probably caused by the lower coordination number of the zinc ion, to interconnect the $[\text{Zn}_2(\mu_2\text{-N,N}'\text{-biim})_2]$ secondary building blocks into a 2D-layered sheet. A 3D supramolecular framework is formed because of the strong hydrogen bonding interaction between the layers (Figure 2.7.3.).¹

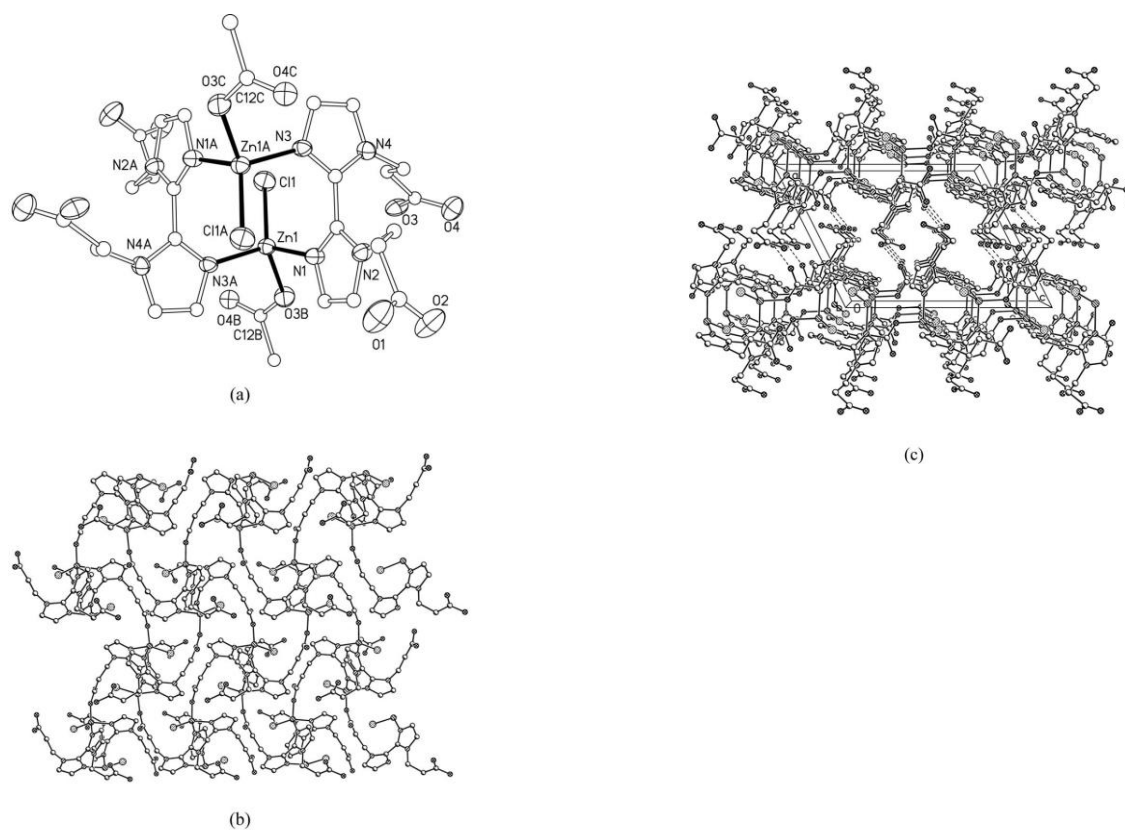


Figure 2.7.3. (a) structure of the $[\text{Zn}_2(\mu_2\text{-HPra}_2\text{biim})_2]^{2+}$; (b) the 2D sheet of $[\text{Zn}(\text{HPra}_2\text{biim})\text{Cl}]_n$; (c) the 3D framework of $[\text{Zn}(\text{HPra}_2\text{biim})\text{Cl}]_n$.¹

Microporous metal-organic frameworks (MMOFs)

The design and the synthesis of microporous metal-organic frameworks (MMOFs) are of great current interest in view of their interesting structural topologies and potential applications in gas storage, separation, catalysis etc.³⁰ These compounds are featuring polyfunctional organic ligands as linkers and metal centres as branch point.³¹ Important factors for practical applications are for example: high porosity and structural kinetic stability.

However, two interesting helix-based MMOF samples were discussed in this thesis. $[M(\text{Pra}_2\text{biim})(\text{H}_2\text{O})]n \cdot x\text{nH}_2\text{O}$ [$M = \text{Cd}$, $x = 2$ (1), $M = \text{Pb}$, $x = 1$ (2)], which were made by the diffusion reaction of $M(\text{NO}_3)_2 \cdot 4\text{H}_2\text{O}$ and $\text{Na}_2\text{Pra}_2\text{biim}$. The Cd^{2+} ion lying on the crystallographic two-fold rotation axis shows a distorted pentagonal bipyramidal coordination geometry. The two apical places are occupied by the free N and the equatorial ones are taken up by the two carboxyl groups and one water molecule. The ligand utilizes all six coordinating atoms available involving four chelating carboxylate oxygen atoms and two nitrogen atoms in a coordination mode.²⁹

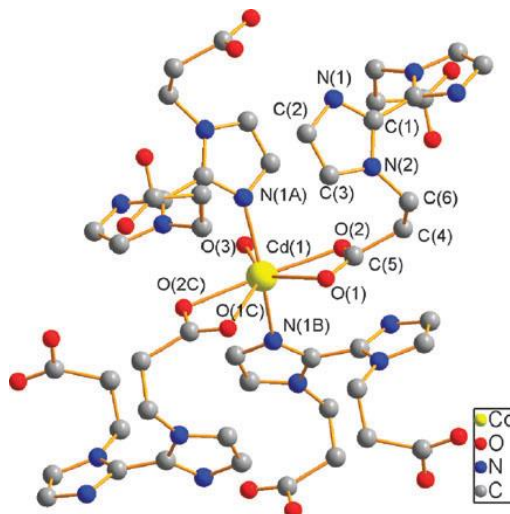


Figure 2.7.4. Compound $[M(\text{Pra}_2\text{biim})(\text{H}_2\text{O})]n \cdot x\text{nH}_2\text{O}$ [$M = \text{Cd}$, $x = 2$ (1)]²⁹

³⁰ (a) O. M. Yaghi, M. O'Keeffe, N. W. Ockwig, H. K. Chae, M. Eddaoudi and J. Kim, *Nature*, 2003, 423, 705; (b) S. Kitagawa, R. Kitaura and S. Noro, *Angew. Chem., Int. Ed.*, 2004, 43, 2334; (c) J. L. C. Rowsell and O. M. Yaghi, *Angew. Chem., Int. Ed.*, 2005, 44, 4670; (d) C. N. R. Rao, S. Natarajan and R. Vaidyanathan, *Angew. Chem., Int. Ed.*, 2004, 43, 1466; (e) M. O'Keeffe and O. M. Yaghi (Editors), *Special Issue on Reticular Chemistry*, *J. Solid State Chem.*, 2005, 178, 2409; (f) H. Li, M. Eddaoudi, M. O'Keeffe and O. M. Yaghi, *Nature*, 1999, 402, 276.

³¹ J. Y. Sun, L. H. Weng, Y. M. Zhou, J. X. Chen, Z. X. Chen, Z. C. Liu and D. Y. Zhao, *Angew. Chem., Int. Ed.*, 2002, 41, 4471.

Moreover, worth mentioning is the microporous structure having hexagonal channels constructed from left- and right-handed helical chains. The metal ions are singly connected by the biim moieties into helical structures of crystallographically imposed C_3 symmetry.

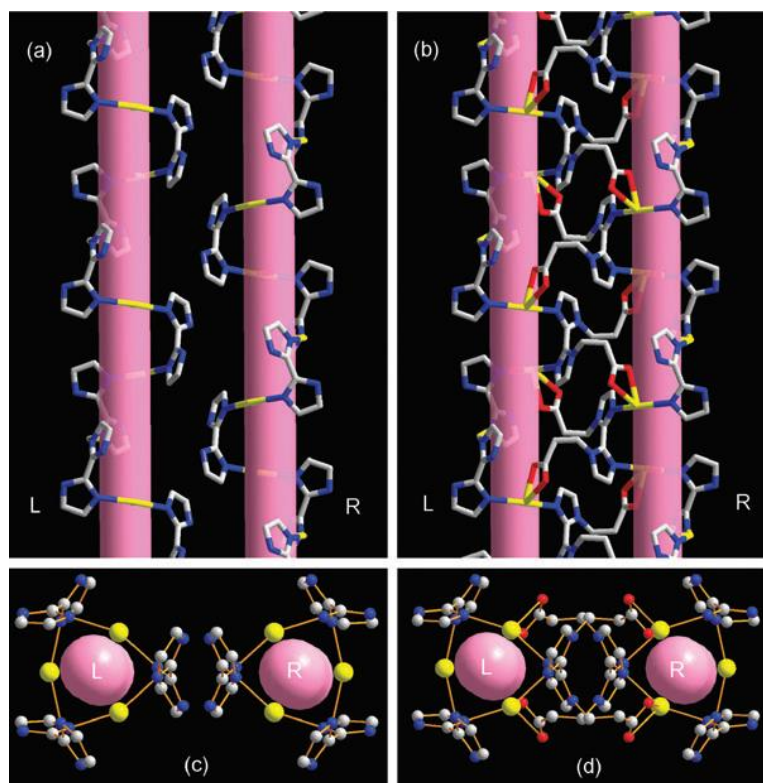


Figure 2.7.5. (a) The helical chain structure along b -axis. (b) The helical chain structure along c -axis. (c,d) Interconnection by carboxyl arms of Pra_2biim ²⁹

In this helical structure occur strong hydrogen bonds between the coordinated water molecules and the carbonyl groups with a O...O bond length of 2.691 Å. Because of the centred space group, the two types R and L of helical tubes, alternately ordered around the hexagonal channels, result. The diameter of the cylindrical structure is about 10.5015 (4) Å, wherein a water hexamer is placed.²⁹

Metal-organic frameworks (MOFs) containing Pra_2biim are of great current interest due to their fascinating structural topologies and potential applications. The preparation of such compounds is also a great challenge because of the difficulty in predicting the overall metal-organic connectivity for a ligand caused by supramolecular isomerism of MOFs. Usually this kind of isomerism is caused by the modified metal coordination geometry and flexible

coordination modes and conformation of the ligands. But this liability offers also a great chance for controlling the formation of the framework by tuning some parameters like reaction temperature, pH-values and counter ions. As mentioned above one generated helix-based microporous MOF with a cylindrical channel built from a single multifunctional ligand $\text{Na}_2\text{Pra}_2\text{biim}$, which are made up of alternately ordered left- and right-handed helical $\text{N,N}'\text{-biim-M}$ tubes interconnected by the carboxyl arms of the ligand, is $[\text{Cd}(\text{Pra}_2\text{biim})(\text{H}_2\text{O})_n] \cdot 2(\text{H}_2\text{O})$. Another interesting aspect is that there are other helix-based supramolecular isomers from $[\text{Cd}(\text{Pra}_2\text{biim})(\text{H}_2\text{O})_n] \cdot 2(\text{H}_2\text{O})$ like $[\text{Cd}(\text{Pra}_2\text{biim})]_n \cdot \text{H}_2\text{O}$, $[\text{Cd}(\text{Pra}_2\text{biim})]_n \cdot 2n\text{H}_2\text{O}$ and $[\text{Cd}(\text{H}_{0.5}\text{Pra}_2\text{biim})(\text{H}_2\text{O})_2]_{2n} \cdot (\text{ClO}_4)_n$ available. These isomers were obtained only by changing the synthesis reaction conditions.³²

³² R-L. Sang, L. Xu, Helix-based supramolecular isomerism of metal-organic framework, *CrystEngComm*, 2010, 12, 3579-3586.

3. Results and Discussion

3.1. The synthesis of 2,2'-Biimidazole

For producing 2,2'-biimidazole-carboxylate containing ligands the synthesis of 2,2'-biimidazole out of glyoxal and ammonia, especially ammonium acetate, must be done first. The condensation reactions of carbonyl compounds with ammonia, amines and derivatives are important for gaining nitrogen-containing heterocyclic substances like pyridines, azoles and so on. These products were for instance used in drugs, insecticides, various dyes and polymers. In the current work the 2,2'-biimidazole was the precursor for further reactions like the aza-Michael addition and finally the synthesis of potentially useful coordination polymers.

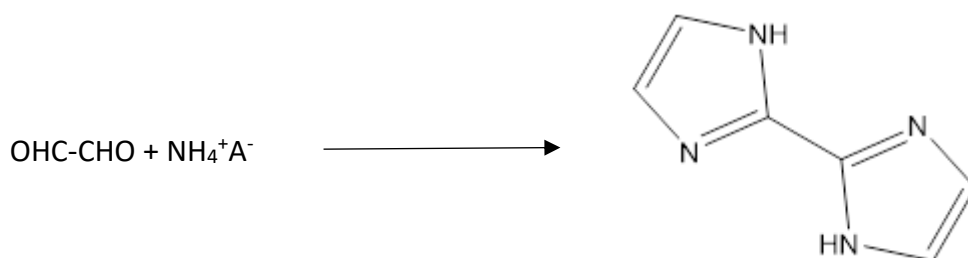


Figure 3.1.1. Synthesis of 2,2'-biimidazole by combining glyoxal and ammonium acetate

The reaction was performed by combining ammonium acetate, which was dissolved in distilled water, and aqueous glyoxal at 40°C. In the theoretical part 2.1. are many possible different products of this reaction listed, so the conditions and the ratio of the educts for the synthesis of a volitional product, like 2,2'-biimidazole, is necessary. To gain particularly 2,2'-biimidazole a ratio of aqueous glyoxal and ammonium acetate 1:2.7 was utilized. For purification a hot filtration with ethylene glycol and decolourizing carbon was performed yielding a white crystalline solid product. The yield of the dried substance was about 25.9 %. This is about the half compared to the used patent-literature. A ¹H-NMR and ¹³C-NMR spectrum of the purified compound are shown in the Figures 3.1.2. and 3.1.3. below.

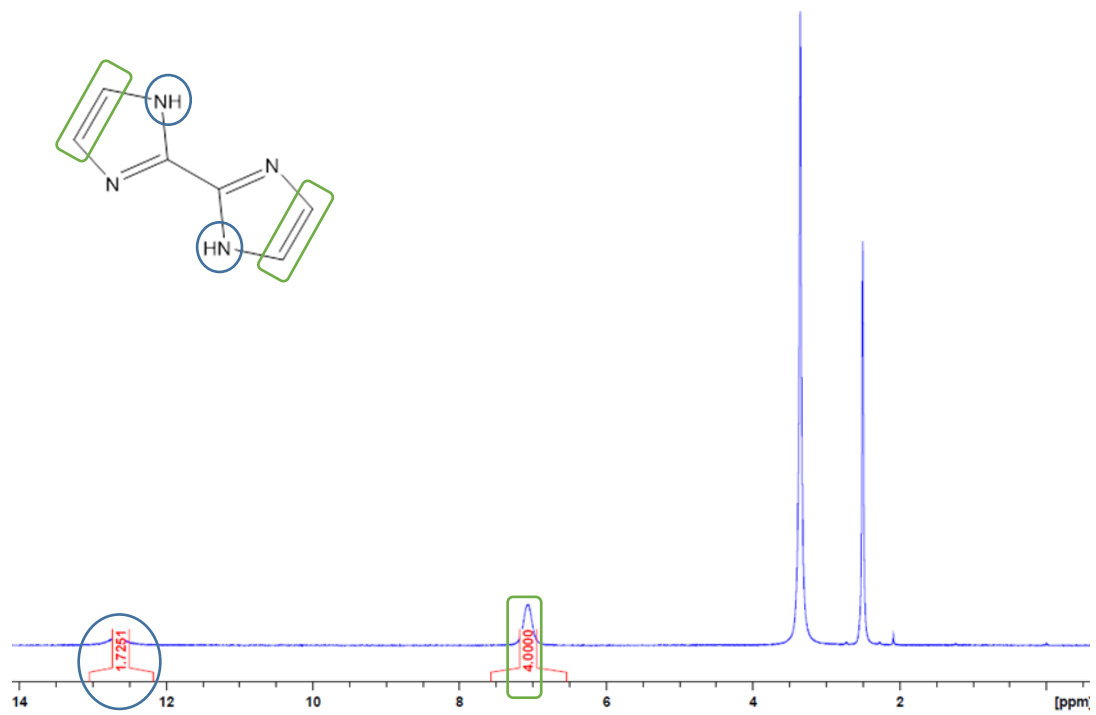


Figure 3.1.2. ¹H-NMR spectrum from the synthesized 2,2'-biimidazole

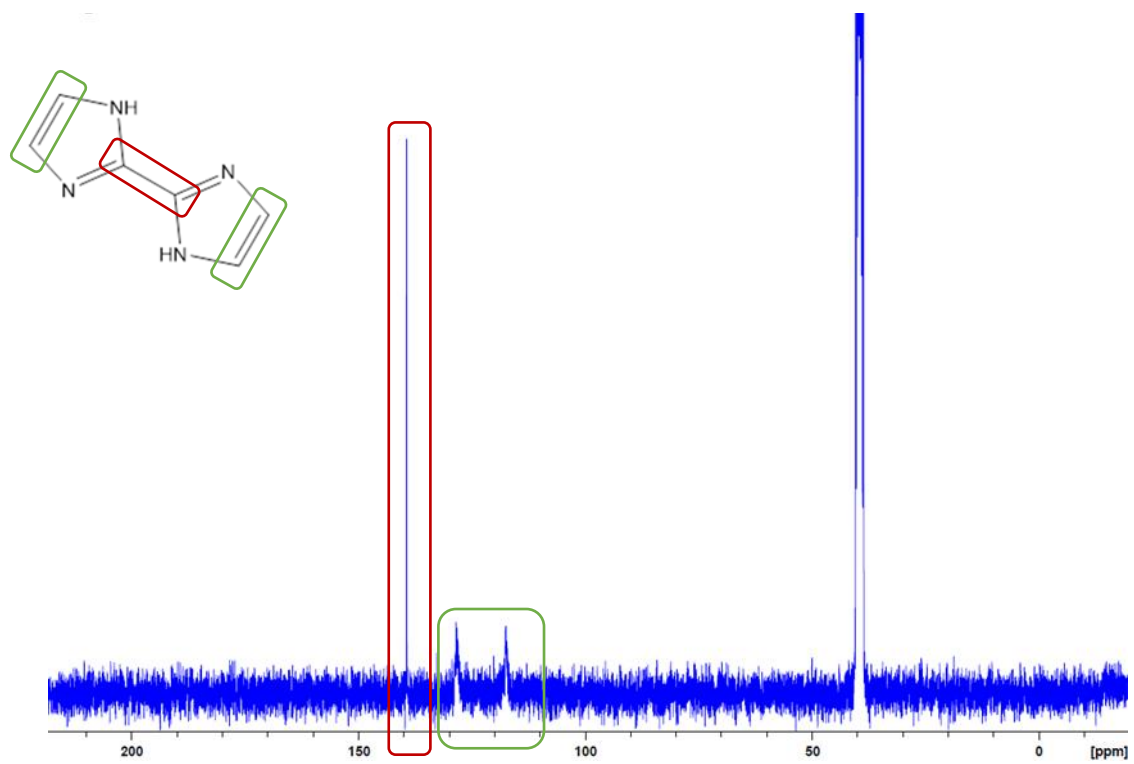


Figure 3.1.3. ¹³C-NMR spectrum from the synthesized 2,2'-biimidazole

3.2. The aza-Michael addition

The aza-Michael addition is due to its simplicity and easy manageability an extensively used preparation method for the synthesis of β -amino carbonyl compounds. This reaction type is usually done at moderate temperature and with the addition of a catalyst and solvent.

Furthermore, an electron rich species, a so-called Michael donor, more specifically an amine as nucleophile, and an electron deficient alkene molecule, a Michael acceptor, like acrylates or acrylamides are needed.

In the current master's thesis, a variety of acceptors (**1-6**) are combined with the donor substance of 2,2'-biimidazole (**A**). In order to generate coordination polymers or MOFs, as Michael donor always the nitrogen heterocyclic educt of 2,2'-biimidazole was used, because of the resulting N,O-coordinating properties. In Figure 3.2.1. the donor and acceptor substances were shown.

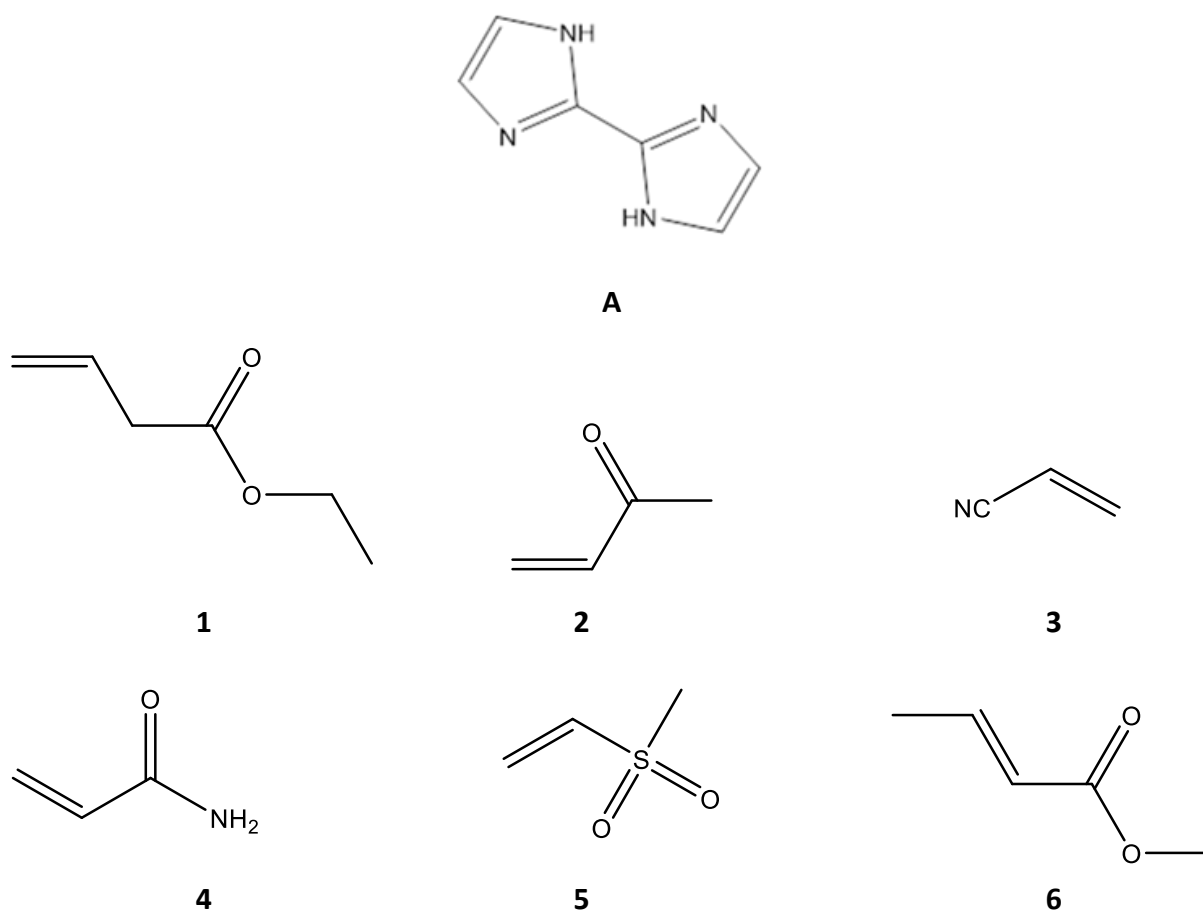
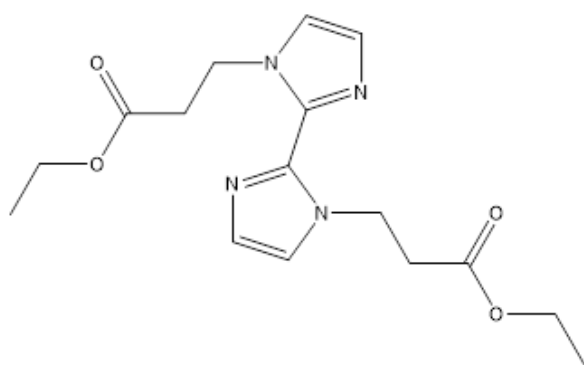
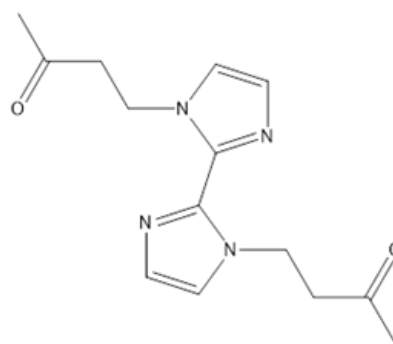


Figure 3.2.1. Structures of the Michael donor (**A**) and acceptor (**1-6**) substances

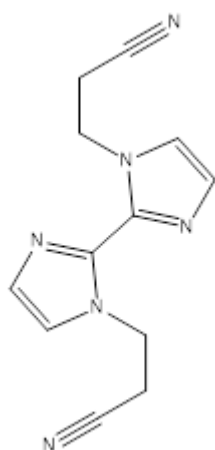
The reaction was performed by combining the acceptor and the donor in the solvent of N,N'-dimethylformamide at 50°C. Only in the case of acceptor 4 the mixture was heated up to 100°C. To accelerate the reactions a solution of 1 N NaOH as catalyst was utilized. In most cases there was an excess of the acceptor from 2.7 equivalents, but in one case, like acceptor 2, there was an excess of 7.2 equivalents necessary to get acceptable yields. In between the reaction ¹H-NMR measurements were taken to show the conversion. After full conversion the heat was removed, the substance was neutralized with 3 M HCl, and the purification step was started. The purification for achieving the final solid products were in each case slightly different, which is shown in the experimental part 5.2. To sum up it was possible to get rid of the solvent and the excess of the acceptor substance resulting in relative clean products in each addition reaction. An exception was acceptor 1, where no product was obtained. All the formed products were given in Figure 3.2.2. in a special colour framed. The product **P1** was further used for the saponification reaction, the products **P2-P5** also showed a good product formation, but were not further studied in this work, and the product **P6** did not show any product formation at all.



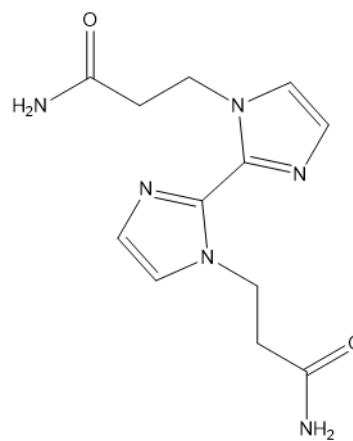
Product **P1** [Yield: 56.4 %]



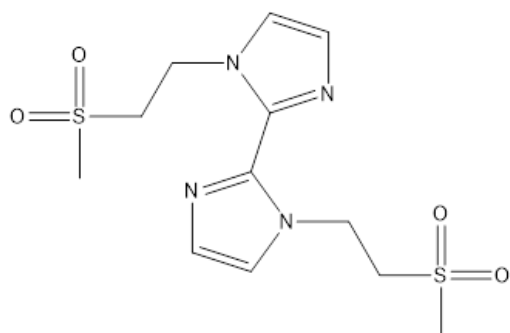
Product **P2** [Yield: 24.0 %]



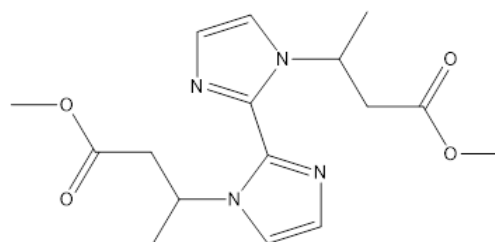
Product **P3** [Yield: 80.4 %]



Product **P4** [Yield: 21.2 %]



Product **P5** [Yield: 48.8 %]



Product **P6** [Yield: 0.0 %]

Figure 3.2.2. Products of the aza-Michael addition

The aza-Michael addition is exemplarily specified for the donor of 2,2'-biimidazole **A** and the acceptor of ethyl acrylate **1** (Figure 3.2.3.). For determining total conversion, a $^1\text{H-NMR}$ measurement after purifying and drying (Figure 3.2.4.) was made. The missing of peaks corresponding to **A** indicates full conversion.

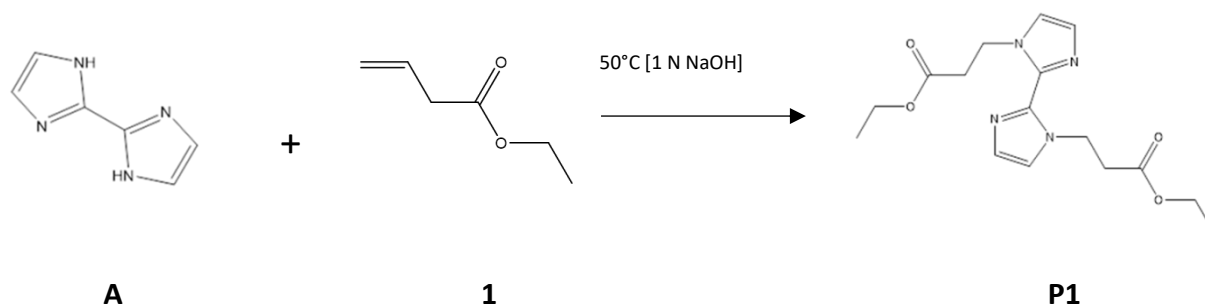


Figure 3.2.3. The aza-Michael reaction of 2,2'-biimidazole **A** and the acceptor of ethyl acrylate **1** yielding to **P1**

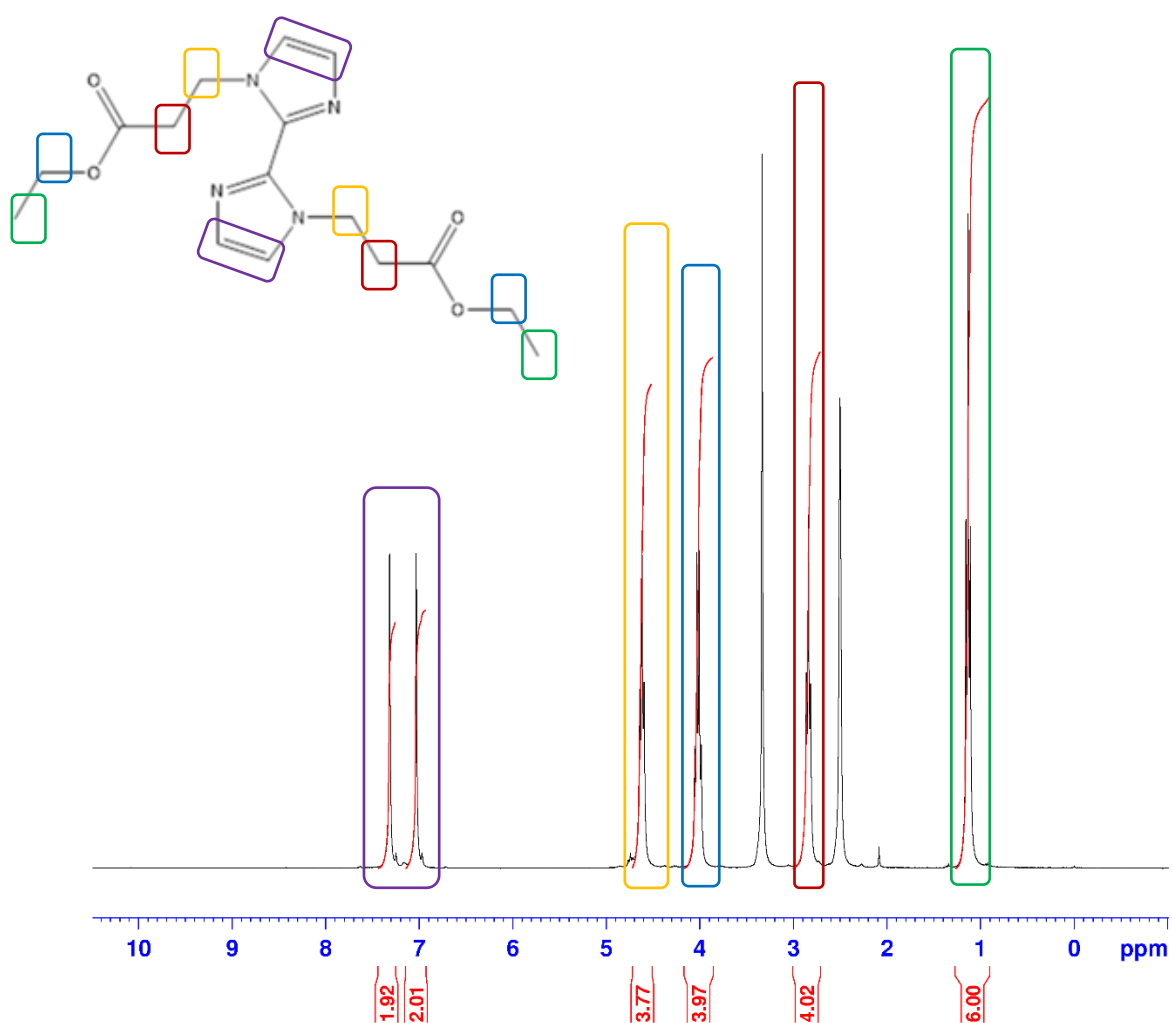


Figure 3.2.4. $^1\text{H-NMR}$ spectrum of the purified and dried **P1** after full conversion

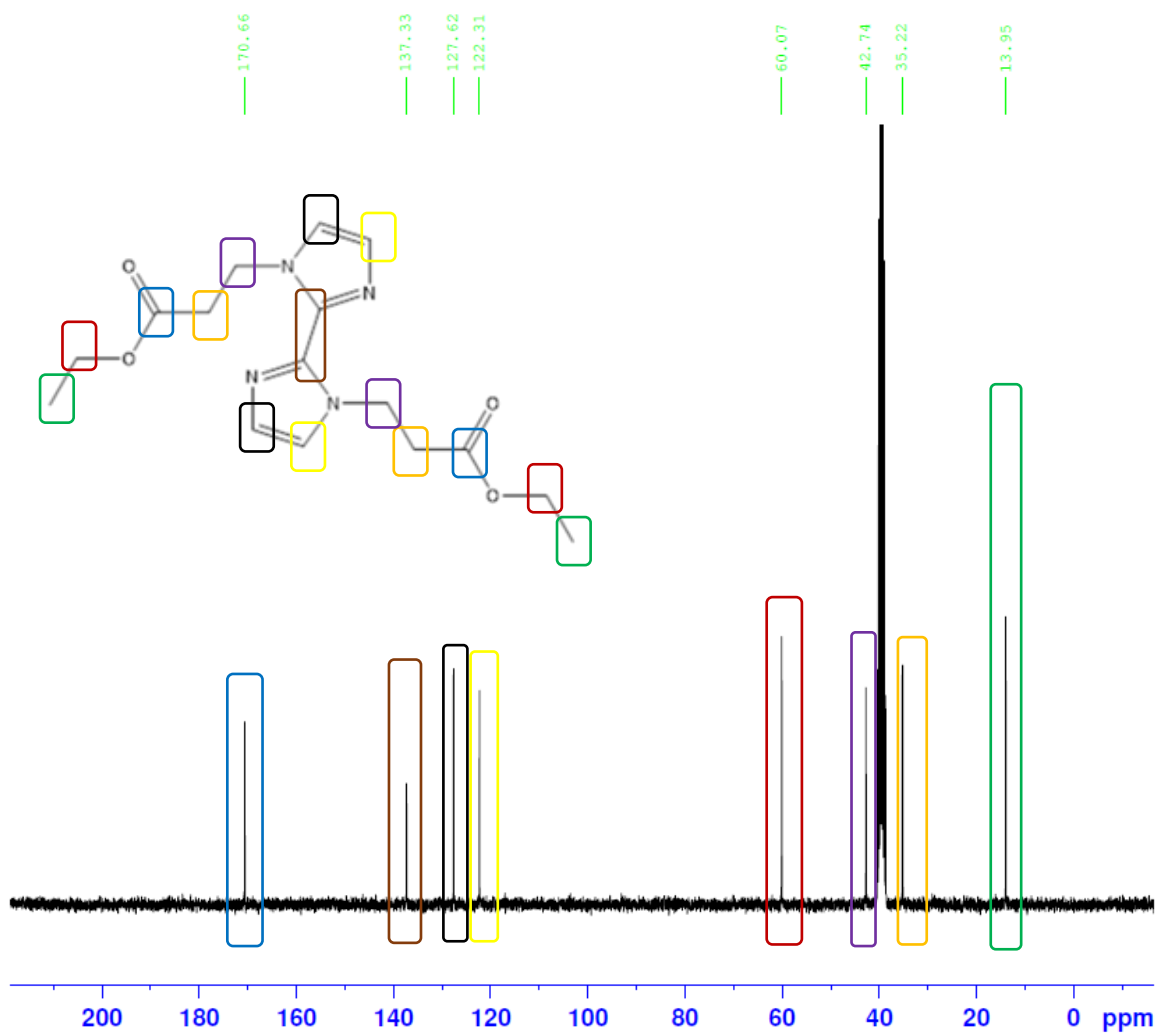


Figure 3.2.5. ^{13}C -NMR spectrum of the purified and dried P1 after full conversion

ATR-IR spectroscopy

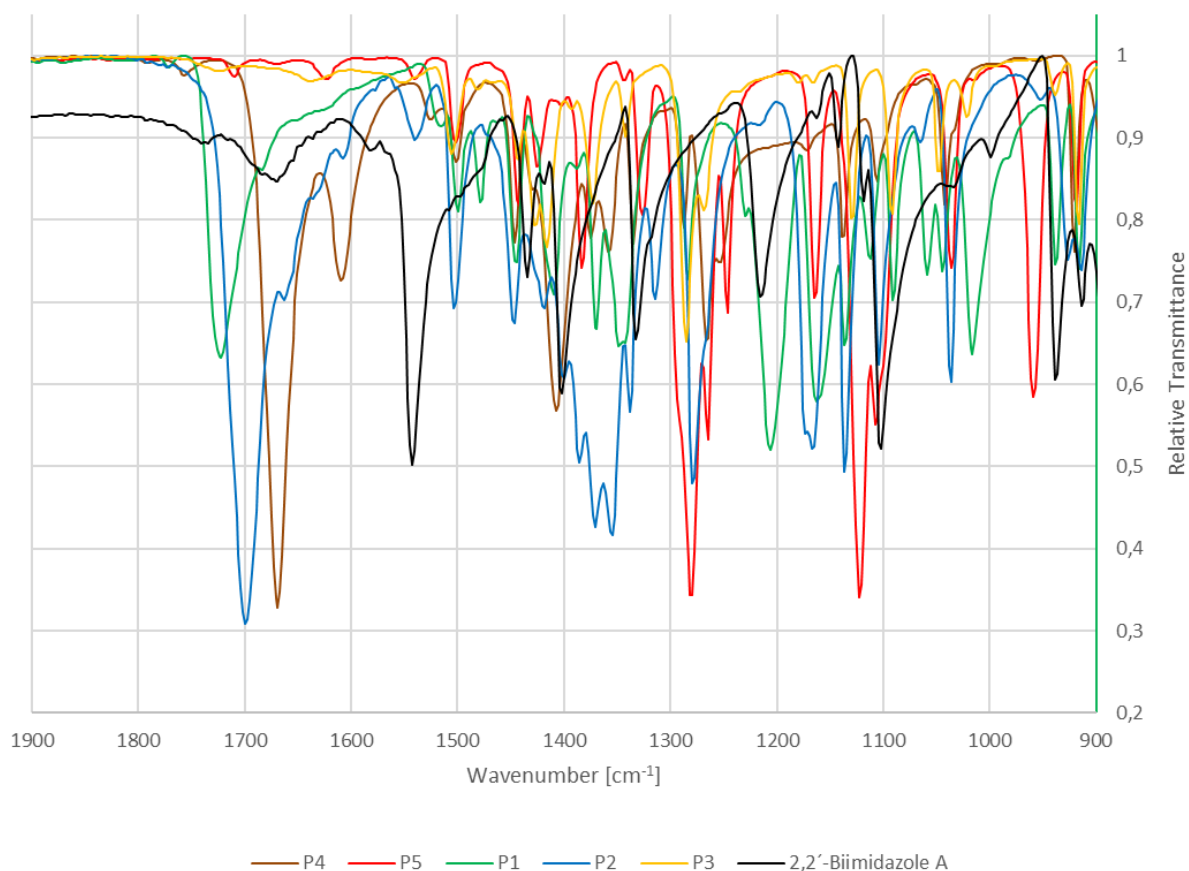


Figure 3.2.6. ATR-IR comparison of 2,2'-Biimidazole **A** with **P1**, **P2**, **P3**, **P4** and **P5**

In Figure 3.2.6. an ATR-IR comparison of the educt 2,2'-Biimidazole **A** (black curve) and the resulting products (**P1-P5**) is represented. Before the measurements were performed the compounds were dried under reduced pressure. One of the biggest differences between the 2,2'-Biimidazole and the product spectrum is the missing of the strong band at around in **P1-P5**. That might be caused by an N-H bending appearance in **A**. The ATR-IR spectrum exhibits the characteristic bands for the corresponding functionalities. In **P1** the ester group occurs for instance around 1721 cm⁻¹, which is in the expected range according to literature.³³ The other characteristic bands and suggested corresponding functionalities are shown in Table 3.2.1.

³³ <https://www.sigmaaldrich.com/technical-documents/articles/biology/ir-spectrum-table.html>, (16.7.2020)

Table 3.2.1. Characteristic bands and suggested corresponding functionalities for P1-P5

	Wavenumber cm^{-1}		Appearance	Functionalities
	Measured [cm^{-1}]	Literature [cm^{-1}] ³³		
P1	1721	1730-1715	(C=O) stretching	Ester
P2	1699	1725-1705	(C=O) stretching	Ketone
P3	2248	2260-2222	(C≡N) stretching	Nitrile
P4	1669	1690	(C=O) stretching	Primary amide
P5	1279	1350-1300	(S=O) stretching	Sulfone

3.3. Saponification reaction

For the saponification reaction a 5,55 M NaOH solution was utilized in an excess of 2.0 equivalents compared to the aza-Michael addition product **P1**. By combining those compounds a mixture resulted, which was heated up to 80°C under reflux and was stirred continuously. 15 minutes later the mixture was completely dissolved, and a colourless solution was formed. After 4 h a full conversion was detected via ¹H-NMR measurement. Finally, the heat was removed, and the product was dried under reduced pressure. A solid white powder, called sodium 3,3-(1H,1'H-[2,2'-biimidazole]-1,1'-diyl)dipropionate (**S1**), was received (Figure 3.3.1.).

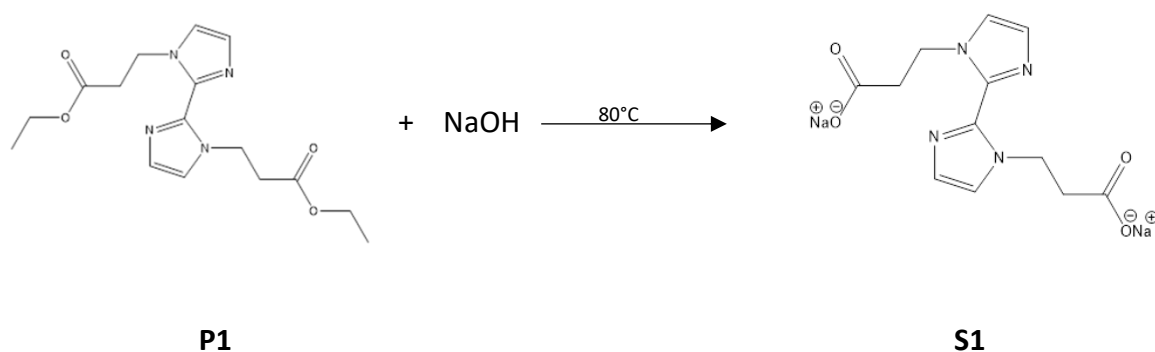


Figure 3.3.1. The received white solid product (**S1**) after the saponification reaction

For the saponification reaction a well-known mechanism is shown in the Figure 3.3.2. below.

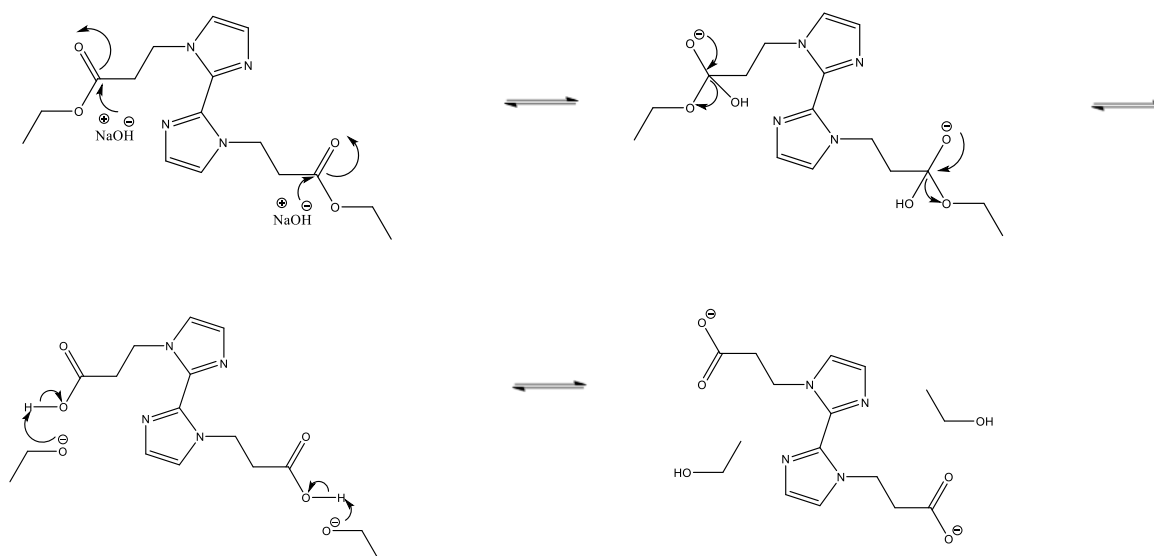


Figure 3.3.2. Suggested mechanism of the saponification reaction from **P1** to **S1** ³⁴

Saponification is a reaction that involves a conversion of an ester with a base, like NaOH by the action of heat into a soap and a corresponding alcohol. In the first step the hydroxide anion reacts with the carbonyl group of the ester. An orthoester is the resulting immediate product. Expulsion of the alkoxide forms a carboxylic acid. The generated alkoxide ion is a very strong base so that the proton is transferred from the carboxylic acid to the alkoxide ion generating an alcohol, as shown in Figure 3.3.2.³⁴

The conversion of the saponification process was measured via ATR-IR spectroscopy. The extinction of the ester group at approximately 1721 cm⁻¹ and the corresponding formation of the carboxylate group at about 1593 cm⁻¹ proofed full conversion (Figure 3.3.3.). This data is expected compared to literature.

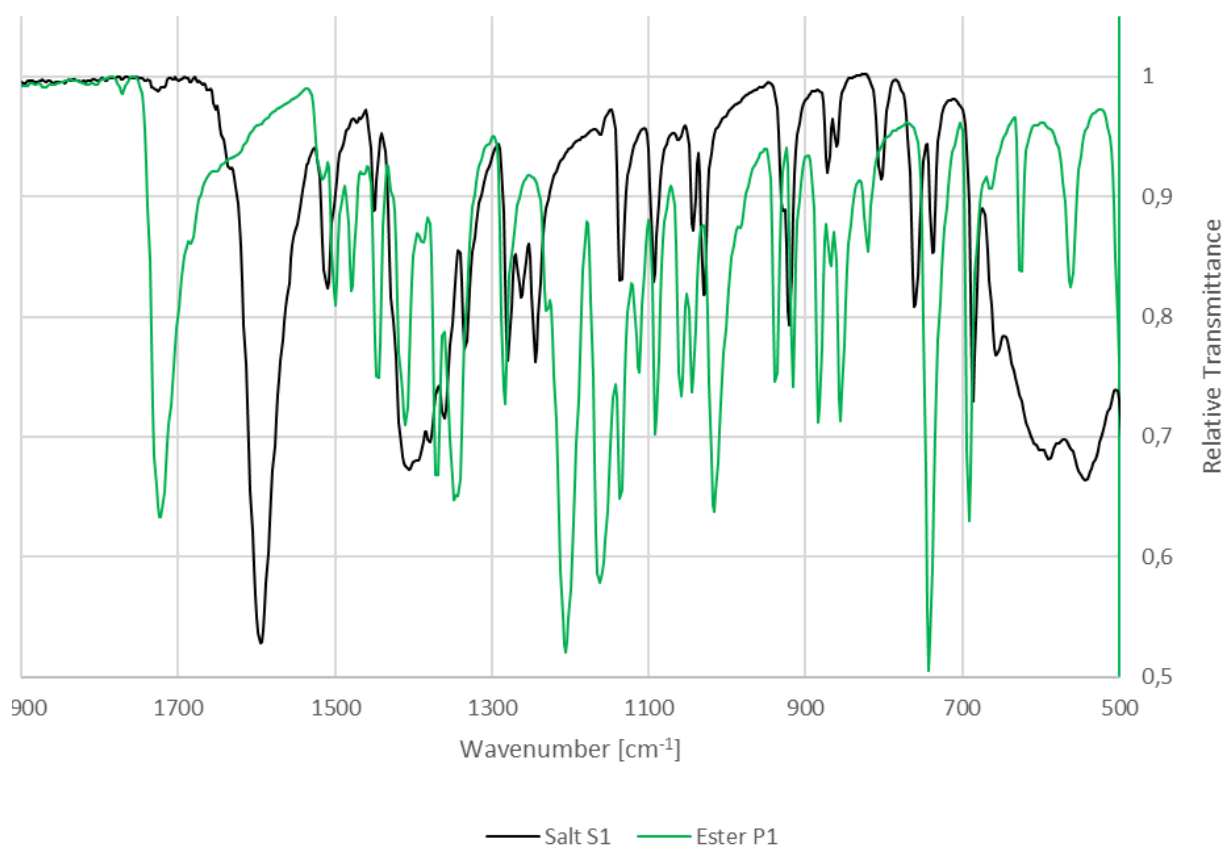


Figure 3.3.3. ATR-IR analysis of the ester and the salt

³⁴ Organikum, Wiley-VCH Verlag GmbH, 23. Auflage, 2009, 494-495.

To detect full conversion also a ^1H -NMR and a ^{13}C -NMR-measurement of **S1** in D_2O after drying was done. The missing of peaks corresponding to **P1** indicates full conversion (Figure 3.3.4. and Figure 3.3.5.).

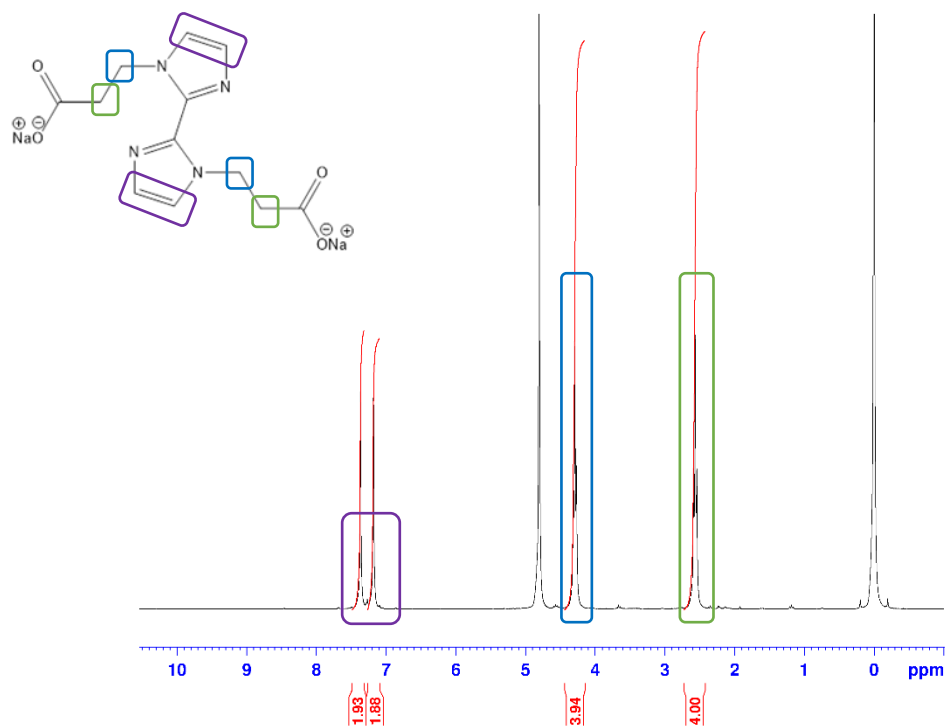


Figure 3.3.4. ^1H -NMR spectrum of the dried **S1** after full conversion

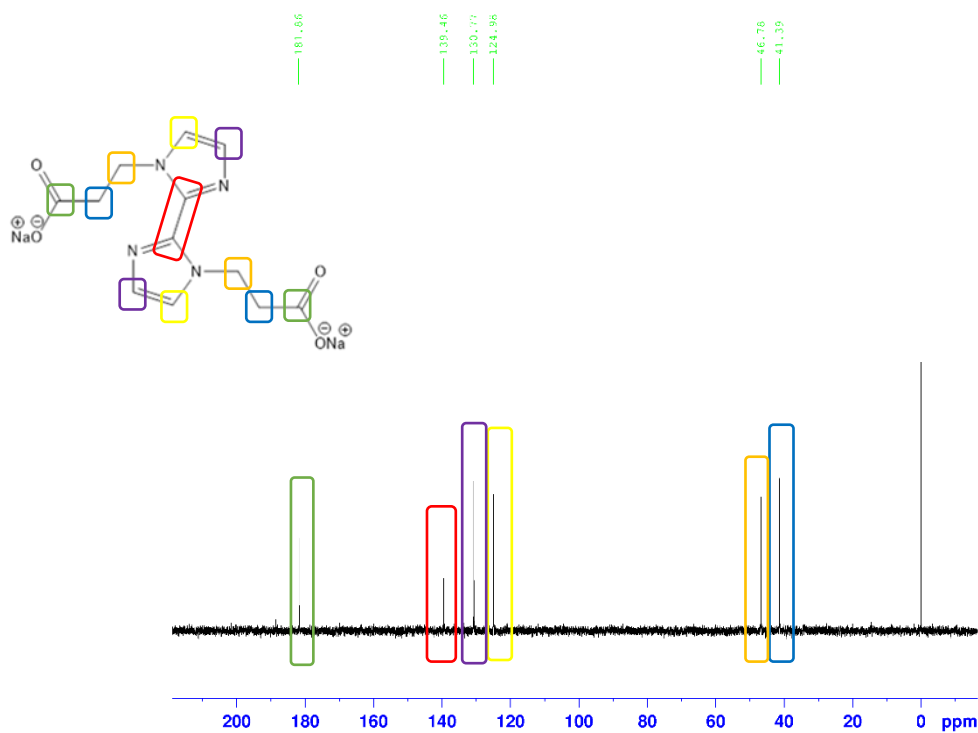
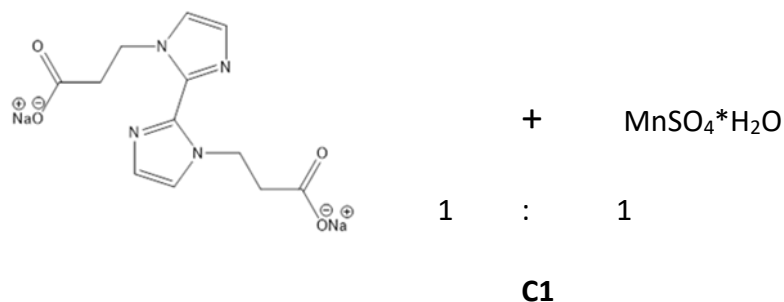


Figure 3.3.5. ^{13}C -NMR spectrum of the dried **S1** after full conversion

3.4. Metal-organic frameworks and coordination polymers

3.4.1. Manganese-organic coordination polymer (Compound C1)

3.4.1.1. $\text{Na}_2\text{Pra}_2\text{biim} + \text{MnSO}_4 \cdot \text{H}_2\text{O}$



0.591 mmol $\text{MnSO}_4 \cdot \text{H}_2\text{O}$ were dissolved in 5 mL water. The same equivalent of the ligand $\text{Na}_2\text{Pra}_2\text{biim}$ were solubilized separately in 5 ml deionized water in a 20 mL glass vial. The manganese sulphate solution was added to the ligand solution generating a colourless solution immediately. Afterwards the vial was closed and heated up to 80°C . Some hours later colourless crystals at the bottom of the vial were formed. The water and Na_2SO_4 was removed and the crystals were washed, filtered and dried under reduced pressure. Finally, the crystals were analysed with different measurements like XRD, SC-XRD, IR and TGA.

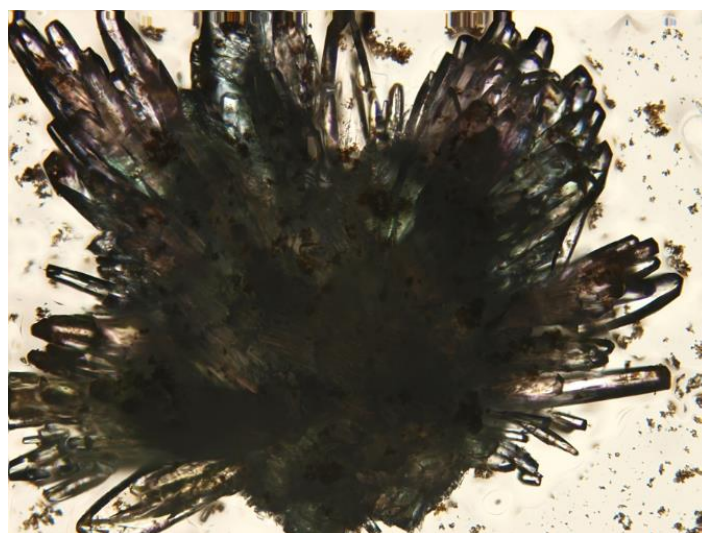


Figure 3.4.1.1. Picture of the manganese crystal (C1)

Single crystal X-ray diffraction (SC-XRD)

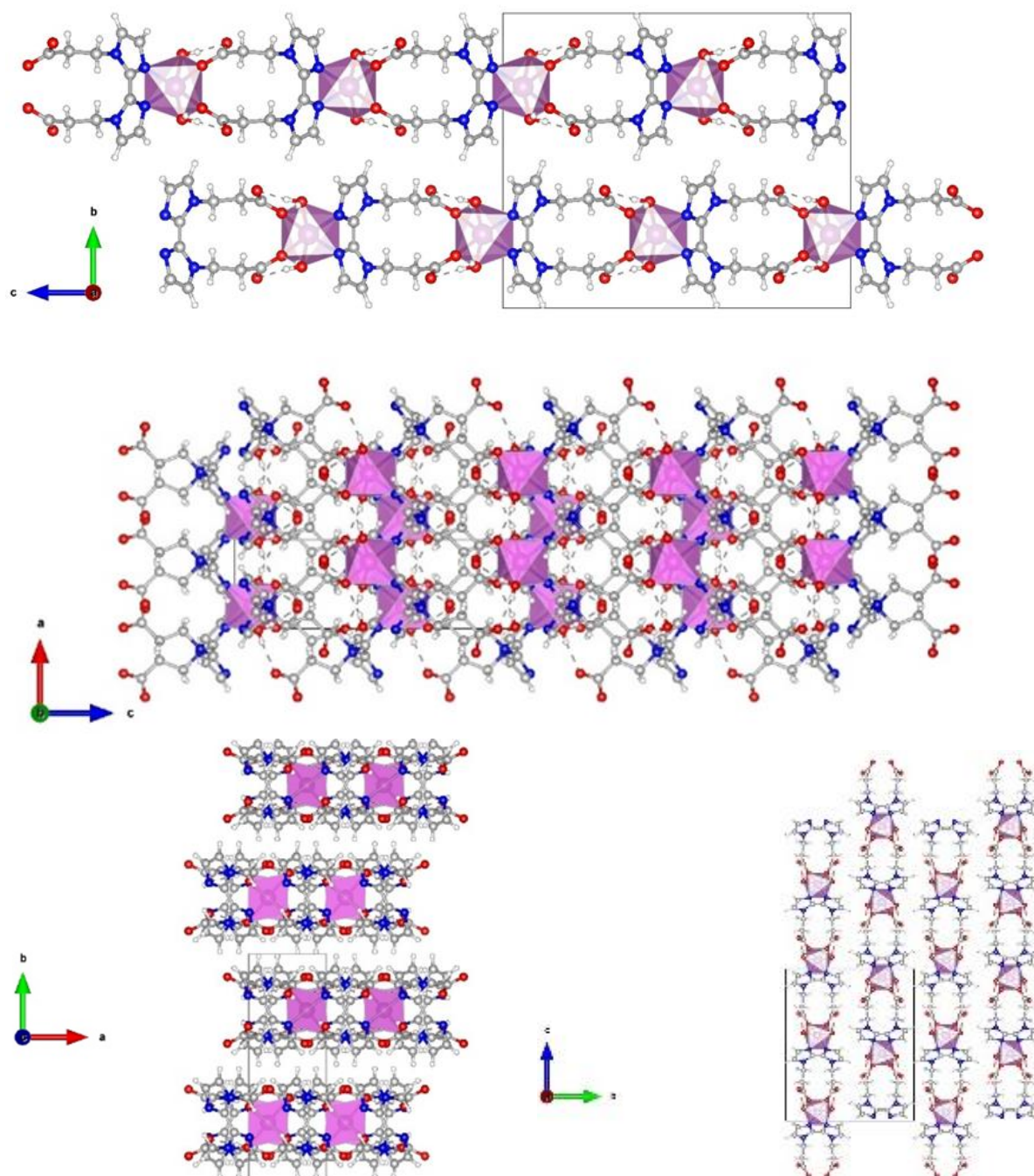


Figure 3.4.1.2. SC-XRD analysis of the manganese-organic crystal structure (C1)

The SC-XRD analysis shows an orthorhombic crystal system and a Pccn space group. The manganese atom is six coordinated and forms a distorted octahedron. The diagonally arranged bond angles range between $(161.62 \text{ O1W}^i\text{—Mn1—O1W})$ and $174 \text{ (O9—Mn1—N1}^{ii})$

and O9—Mn1—N1ⁱⁱⁱ). One of the reasons for this distortion might be the hydrogen bond formation listed in Table 3.4.1.2 and shown in Figure 3.4.1.2. The angles at the equatorial plane range between 83.35 (O9—Mn1—O1W) and 101.04 ° (O9ⁱ—Mn1—O9). The manganese atom in the centre is coordinated with the two nitrogen atoms (N1ⁱⁱ and N1ⁱⁱⁱ) on the one side and two oxygen atoms of the carboxy group (O9ⁱ and O9) on the other side. On axial position the manganese atom is coordinated with the oxygen atoms of two water molecules (O1Wⁱ and O1W). The Mn-O9 and Mn-N bond lengths are in the range of 2.1836 and 2.257 Å. The Mn—O1W bond distance is with 2.222 Å about 0.038 Å larger than the Mn-O bond length of the polymer. The SC-XRD analysis also represents, that the compound crystallizes as 2D coordination polymer sheets.

Table 3.4.1.1. Coordination geometry around Mn¹

Coordination facility around Mn ¹			
Bond lengths (Å)		Bond angles (°)	
Mn1—O9 ⁱ	2.1836 (19) Å	O9 ⁱ —Mn1—O9	101.04 (10) deg
Mn1—O9	2.1836 (19) Å	O9 ⁱ —Mn1—O1W ⁱ	83.36 (8) deg
Mn1—O1W ⁱ	2.222 (2) Å	O9—Mn1—O1W ⁱ	84.99 (8) deg
Mn1—O1W	2.222 (2) Å	O9 ⁱ —Mn1—O1W	84.99 (8) deg
Mn1—N1 ⁱⁱ	2.257 (2) Å	O9—Mn1—O1W	83.35 (8) deg
Mn1—N1 ⁱⁱⁱ	2.257 (2) Å	O1W ⁱ —Mn1—O1W	161.62 (11) deg
		O9 ⁱ —Mn1—N1 ⁱⁱ	84.19 (8) deg
		O9—Mn1—N1 ⁱⁱ	174.51 (8) deg
		O1W ⁱ —Mn1—N1 ⁱⁱ	97.38 (8) deg
		O1W—Mn1—N1 ⁱⁱ	95.51 (9) deg
		O9 ⁱ —Mn1—N1 ⁱⁱⁱ	174.51 (8) deg
		O9—Mn1—N1 ⁱⁱⁱ	84.19 (8) deg
		O1W ⁱ —Mn1—N1 ⁱⁱⁱ	95.51 (9) deg
		O1W—Mn1—N1 ⁱⁱⁱ	97.38 (8) deg
		N1 ⁱⁱ —Mn1—N1 ⁱⁱⁱ	90.64 (12) deg

Table 3.4.1.2. Hydrogen-bond geometry of the manganese-organic coordination polymer (**C1**)

Hydrogen-bond geometry (Å, °)				
<i>D</i> —H... <i>A</i>	<i>D</i> —H	H... <i>A</i>	<i>D</i> ... <i>A</i>	<i>D</i> —H... <i>A</i>
O1 <i>W</i> —H1 <i>WA</i> ...O9	0.87 (4) Å	2.45 (4) Å	2.929 (3) Å	115 (3) deg
O1 <i>W</i> —H1 <i>WA</i> ...O10	0.87 (4) Å	1.85 (4) Å	2.709 (3) Å	169 (4) deg
O1 <i>W</i> —H1 <i>WB</i> ...O9 ^{vi}	0.77 (4) Å	2.06 (4) Å	2.829 (3) Å	171 (4) deg
C4—H4...O10 ^{vii}	0.95 Å	2.50 Å	3.384 (3) Å	154 deg

In Table 3.4.1.2. the hydrogen bond geometry is represented. The hydrogen bridges distance varies from 1.85 Å (O1*W*—H1*WB*...O9^{vi}) to 3.84 Å (C4—H4...O10^{vii}) and the bond angles range from 115° (O1*W*—H1*WA*...O9) to 171° (O1*W*—H1*WB*...O9^{vi}).

In Figure 3.4.1.3. the sphere-packing of the manganese coordination-polymer is illustrated, which indicates almost no porosity.

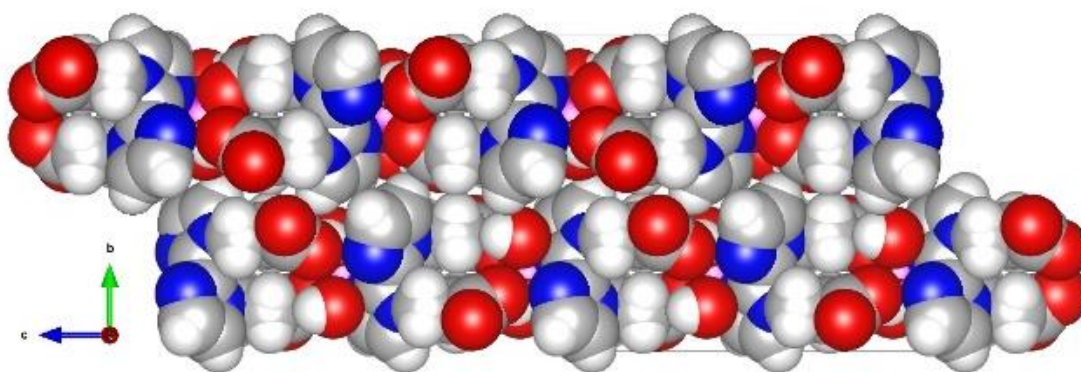


Figure 3.4.1.3. Sphere-packing of the manganese coordination polymer (**C1**)

In Table 3.4.1.3. the crystal data of the manganese-organic coordination polymer is shown. Further crystallographic data and details of measurements are listed in the appendix.

Table 3.4.1.3. Crystal data of the manganese coordination polymer (C1)

$C_{12}H_{16}MnN_4O_6$	$D_x = 1.687 \text{ mg} \cdot \text{m}^{-3}$
$M_r = 367.23$	Space group = Pccn
Crystal system: Orthorhombic	Crystal size (mm) = $0.03 \times 0.03 \times 0.03$
$a = 5.2489 (9) \text{ \AA}$	$\alpha, \beta, \gamma (^\circ) = 90$
$b = 15.273 (3) \text{ \AA}$	$m = 0.95 \text{ mm}^{-1}$
$c = 18.039 (3) \text{ \AA}$	$Z = 4$
$V = 1446.1 (4) \text{ \AA}^3$	Crystal habit: Block, colourless

X-Ray diffraction – XRD:

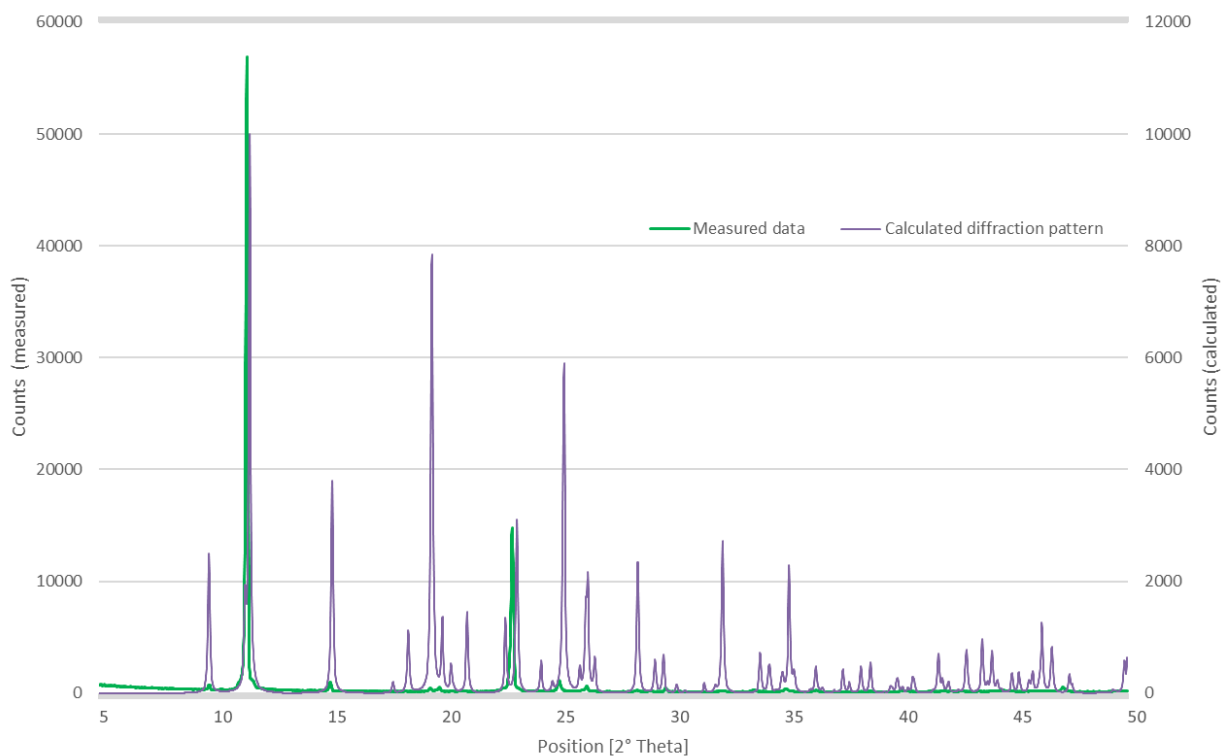


Figure 3.4.1.4. Powder XRD pattern of the manganese-organic coordination polymer C1

In Figure 3.4.1.4. the measured and the calculated ideal XRD-diffractogram of the manganese coordination polymer are compared. The ideal XRD-diffractogram was calculated from the data of the SC-XRD for the crystalline solid state in Mercury program. The crystals have been dried under reduced pressure, before the measurement was done, resulting to a loss of the clearness and to a deterioration of the crystal structure. The violet curve represents the calculated XRD pattern of the compound compared to the measured green one. The pattern shows that the structure of the coordination polymer had lost some of its crystallinity during the drying process. However, some of the resulting reflexes are on similar positions, but not that intense, compared to the calculated ones. There are for instance reflexes at 9.8, 11.5, 15.2, 19.6, 20.3 and 23.3, which are observed at the measured one as well.

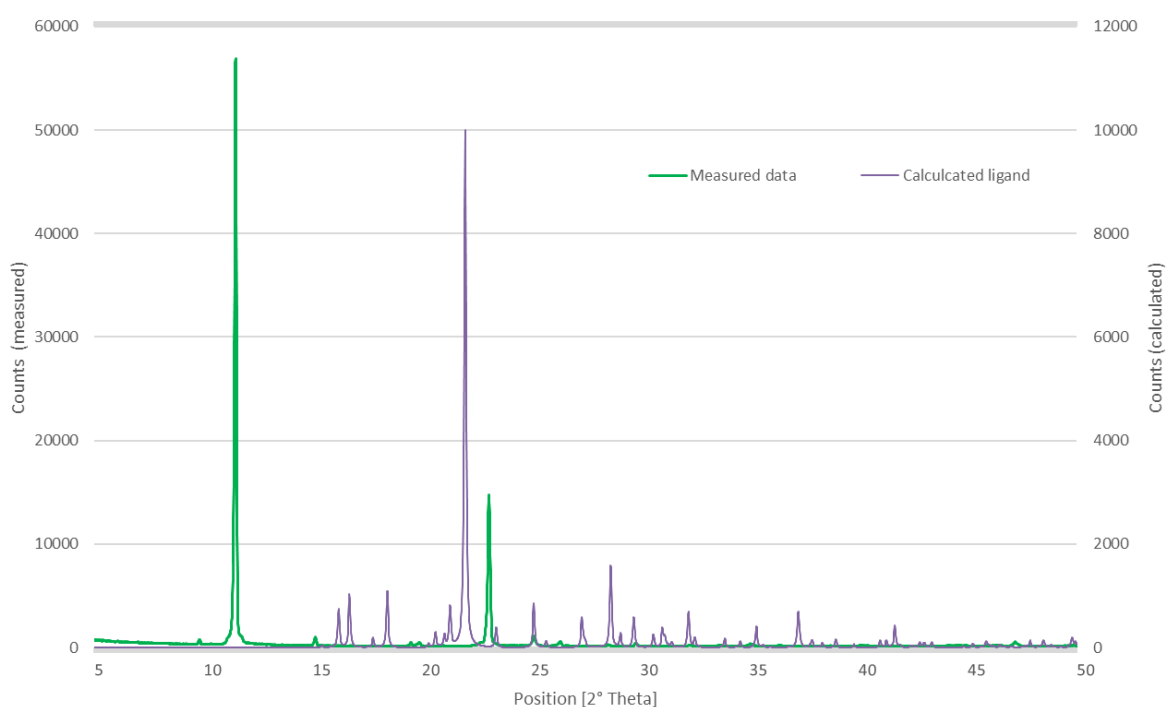


Figure 3.4.1.5. Comparison of the XRD pattern from the manganese-organic coordination sample **C1** with the calculated ligand (literature)

In Figure 3.4.1.5. the XRD pattern comparison between the calculated ligand and the coordination polymer is illustrated. The reflexes from the ligand do not occur in the synthesized compound, which indicates that there is not much uncoordinated ligand in the

sample. The XRD values for the calculated ideal ligand are obtained from R-L. Sang and Li Xu and calculated via Mercury software.¹

Thermogravimetric analysis (TGA)

For determining thermal stability and structural changes as a function of temperature, TGA was done (Figure 3.4.1.6.). Before the measurement was performed the crystals were dried under reduced pressure to get rid of the remaining solvent. During the TGA heating process, a two-step weight loss of in total 34,8 % from the compound was measured. There is a significant endothermic step occurring at approximately 180 °C and resulting in a mass loss of nearly 8.4 %. This mass loss might happen because of the separation from the coordinating water molecules on axial position. The second significant endothermic process occurred at 270 °C and showed a mass loss of 26.4 %. It is supposed that the organic ligand decomposes at this temperature range. In literature a similar compound, like $[\text{Cd}(\text{Pra}_2\text{biim})]_n \cdot 2n\text{H}_2\text{O}$, is investigated, and there happens also an initial weight loss of 4.45 % in the temperature range of 170-250 °C, which is assumed to be the removal of the solvent water molecules. Until 330 °C no further weight loss occurs, but further heating results in the decomposition of the compound.²⁹ Usually, the decomposition of metal-organic frameworks and coordination polymers occurs in a temperature range of about 200-350°C, highly depending on the thermal stability of the organic linkers and other factors. But there were also zinc complexes with a thermal stability over 400°C in literature observed. One reason therefore might be the strong interaction between the metal-carboxylate group.³⁵

³⁵ R. Zou, et al, Highly-thermostable metal-organic frameworks (MOFs) of zinc and cadmium 4,49-(hexafluoroisopropylidene)diphthalates with a unique fluorite topology, Chem.Comm.,2007,2467-2469.

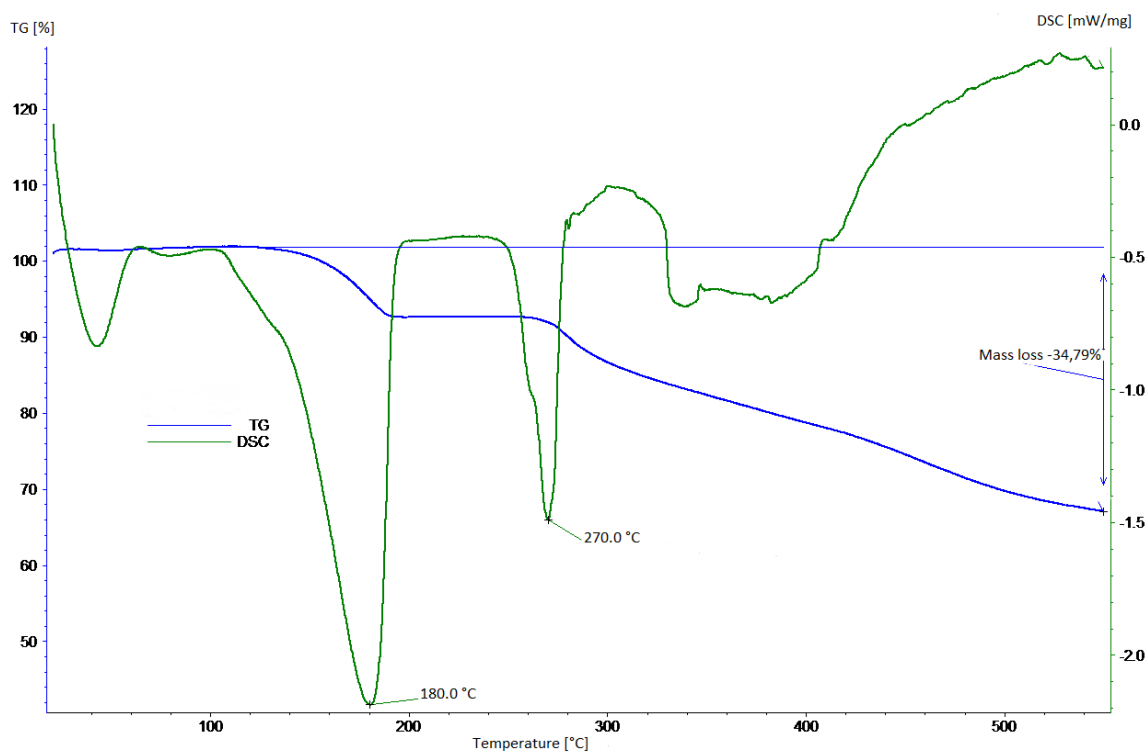


Figure 3.4.1.6. TGA from the manganese-organic coordination polymer **C1**

Infrared-spectroscopy

For further structural analysis an ATR-IR spectroscopy was performed. According to literature³⁶ the bands of the spectrum were dedicated to the functional groups of the sample.

Table 3.4.1.4. Wavenumbers and the suggested according functionalities **C1**

Wavenumber [cm ⁻¹]		
< 1000	Fingerprint area	Aromatic (CH)
1350	Stretching vibration	C-N
1401, 1256	Deformation vibration	Alkane (CH ₃ , CH ₂)
1469	Stretching vibration	Ring C=C and N=C-N
1560	Stretching vibration	Carboxylate (C=O)
3121	Stretching vibration	Alkane (CH ₂)

³⁶ M. Hesse, H. Meier, B. Zech, Spektroskopische Methoden in der organischen Chemie, Thieme, 7. Auflage.

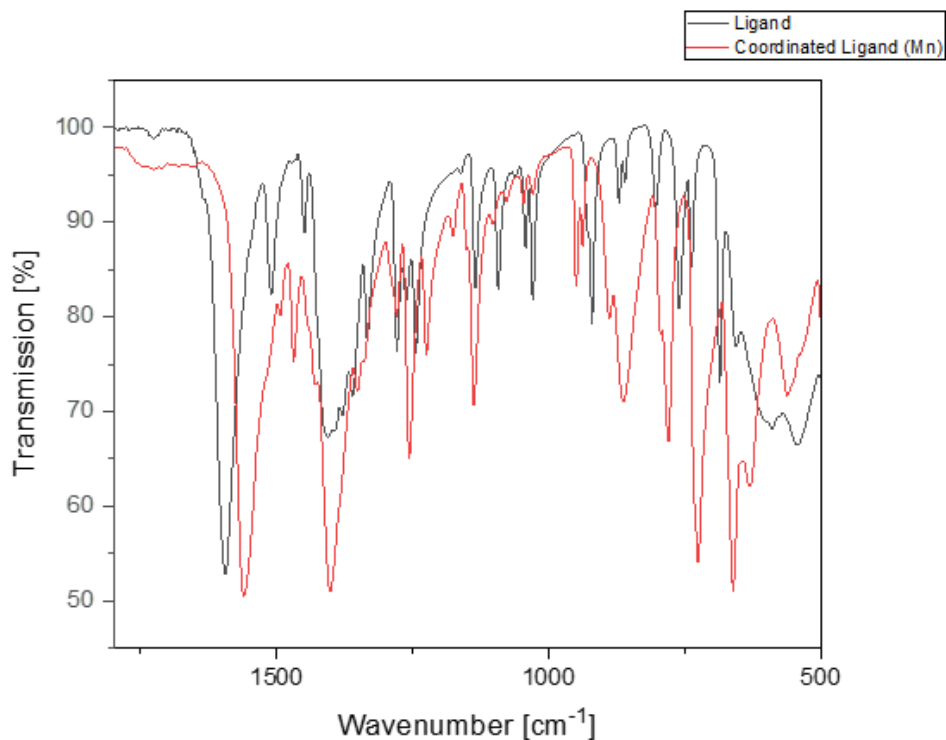
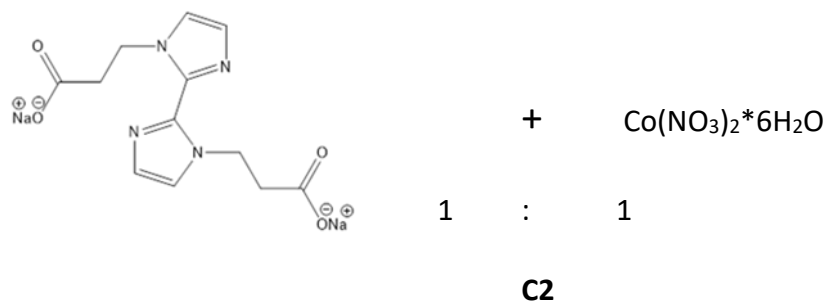


Figure 3.4.1.4. Compared ATR-IR spectrum of the non-coordinated ligand and the manganese coordinated ligand **C1**

In Figure 3.4.1.4. a cut-out of the ATR-IR spectra is represented. In the spectrum the bands of the lonely ligand (black curve) and coordinated ligand (red curve) are highlighted. As mentioned in literature the stretching vibration of the non-coordinated ligand carboxylate group occurs at 1595 cm⁻¹. In the case of the coordinated ligand the carboxylate band was determined at 1560 cm⁻¹, which is a significant lower wavenumber.

3.4.2. Synthesis of a cobalt-organic (C2) and a nickel-organic coordination polymer (C3)

3.4.2.1. $\text{Na}_2\text{Pra}_2\text{biim} + \text{Co}(\text{NO}_3)_2 \cdot 6\text{H}_2\text{O}$



0.546 mmol $\text{Co}(\text{NO}_3)_2 \cdot 6\text{H}_2\text{O}$ were solubilized in 5 mL water. The same equivalent of the ligand $\text{Na}_2\text{Pra}_2\text{biim}$ were dissolved separately in 5 ml deionized water in a 20 mL glass vial. The cobalt nitrate solution was added to the ligand solution generating a violet solution immediately. Afterwards the vial was not closed and heated up to 80°C . Some hours later small violet crystals at the bottom of the vial were observed. The water and NaNO_3 was removed and the crystals were washed, filtered and dried under reduced pressure. Finally, the crystals were analysed with different measurements like XRD, TGA and IR.

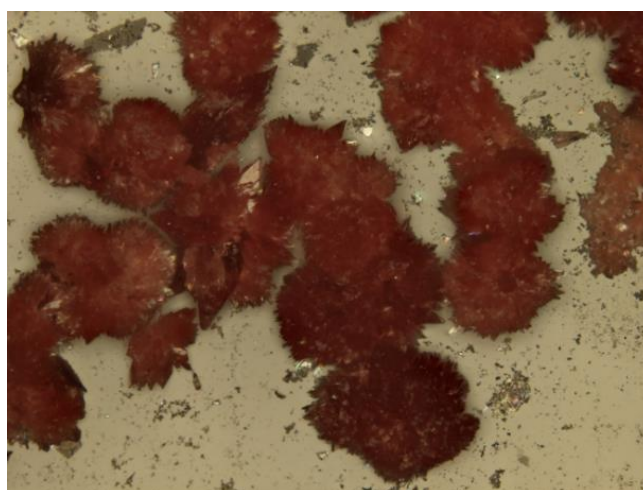
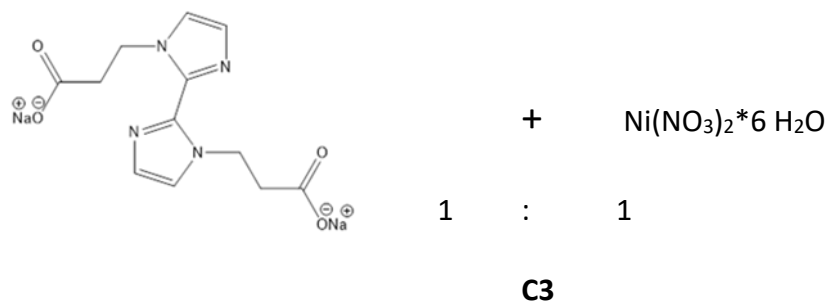


Figure 3.4.2.1. Picture of the cobalt crystals (C2)

3.4.2.2. $\text{Na}_2\text{Pra}_2\text{biim} + \text{Ni}(\text{NO}_3)_2 \cdot 6 \text{H}_2\text{O}$



0.344 mmol $\text{Ni}(\text{NO}_3)_2 \cdot 6\text{H}_2\text{O}$ were solubilized in 5 mL water. The same equivalent of the ligand $\text{Na}_2\text{Pra}_2\text{biim}$ were dissolved separately in 5 ml deionized water in a 20 mL glass vial. The nickel nitrate solution was added to the ligand solution generating a green solution immediately. Afterwards the vial was closed and heated up to 80°C . Some hours later small green crystals at the bottom of the vial were observed. The water and NaNO_3 was removed and the crystals were washed, filtered and dried under reduced pressure. Finally, the crystals were analysed with different measurements like XRD, TGA and IR.

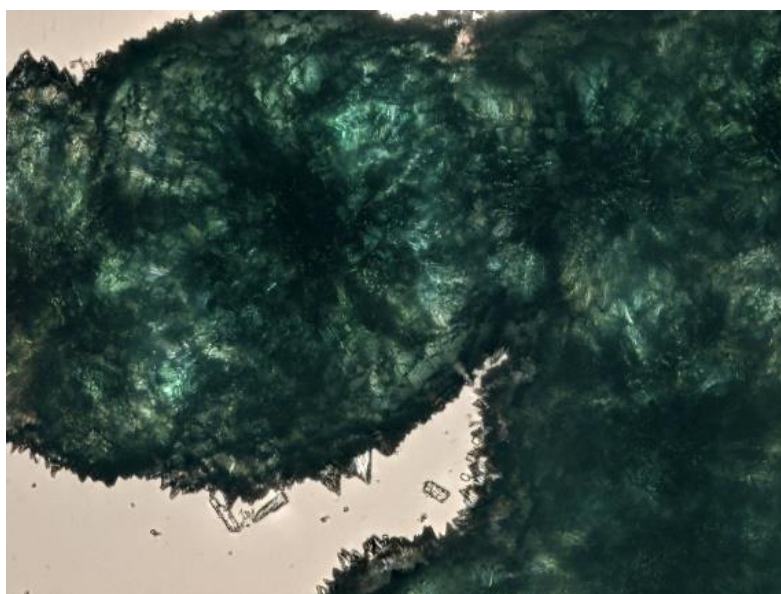


Figure 3.4.3.1. Picture of the nickel crystals (C3)

X-Ray diffraction – XRD:

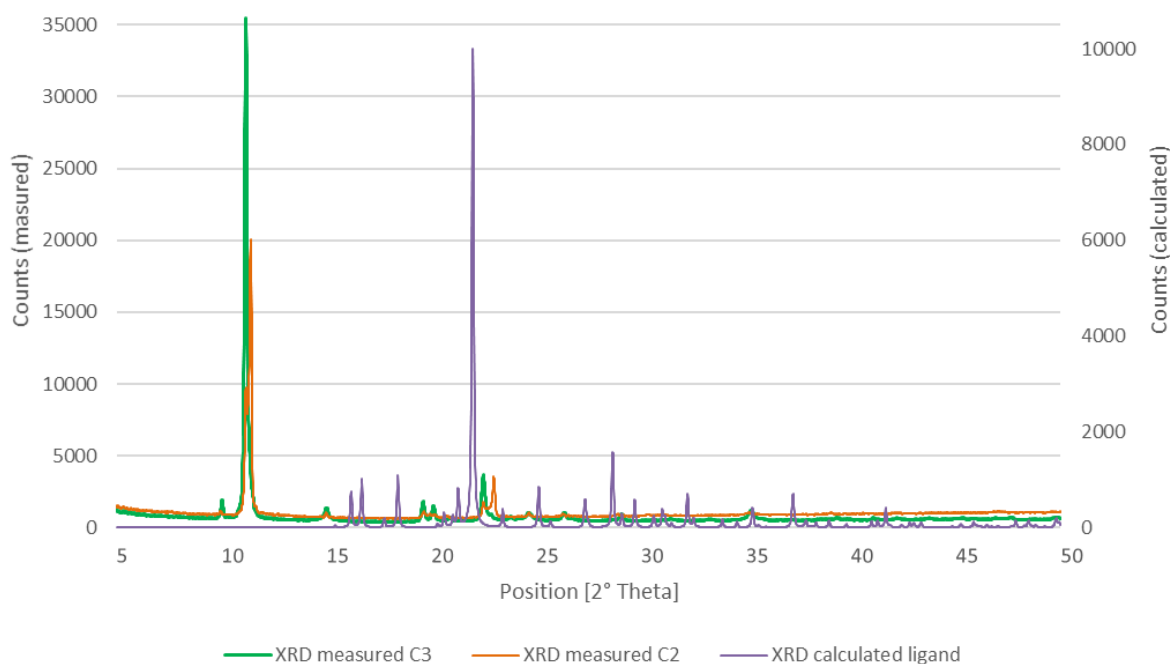


Figure 3.4.2.3. Powder XRD pattern of the measured cobalt sample (**C2**), the nickel sample (**C3**) and the calculated ligand

For the Figure 3.4.2.3. three XRD patterns are matched. The violet curve represents the calculated ideal XRD diffractogram of the ligand, done via Mercury software, and illustrates that the reflexes to the uncoordinated ligand are different to the measured and synthesised compounds. The data for the ligand was obtained from R-L. Sang and Li Xu¹. For the green and blue curves, two samples have been prepared. Before the measurement was done, the crystals have been dried under reduced pressure. The reflexes of both samples are quite similar to each other. In the performed XRD measurement, also some small reflexes, which could be caused by the loss of some crystallinity during the drying process, are detectable. Furthermore, the XRD diffractogram of **C2** and **C3** shows some commonalities with the XRD powder pattern of **C1**, which has a 2D coordination polymer structure. So, it could be suggested that **C2** and **C3** are also potentially coordination polymers.

Thermogravimetric analysis (TGA)

Thermogravimetric analysis was performed on the polycrystalline example to examine the thermal stability as a function of temperature. Before the measurement was done the crystals have been dried under reduced pressure. The TGA graph is given in Figure 3.4.2.3. The sample **C2** underwent a three-step weight loss of in total 46.63 %. The first weight loss step occurs at 185 °C with 7.3 %. According to literature this step can be dedicated to the release of the coordination water molecules. The other two endothermic steps at 276 °C and 312 °C might happen because of the decomposition of the ligand. So, a similar ligand in literature began to decompose at around 265 °C.²⁹ The TGA measurements of compound **C3** showed a similar thermal stability to **C1**. There was also a two-step weight loss at 217.0 °C and at 312.0 °C happening.

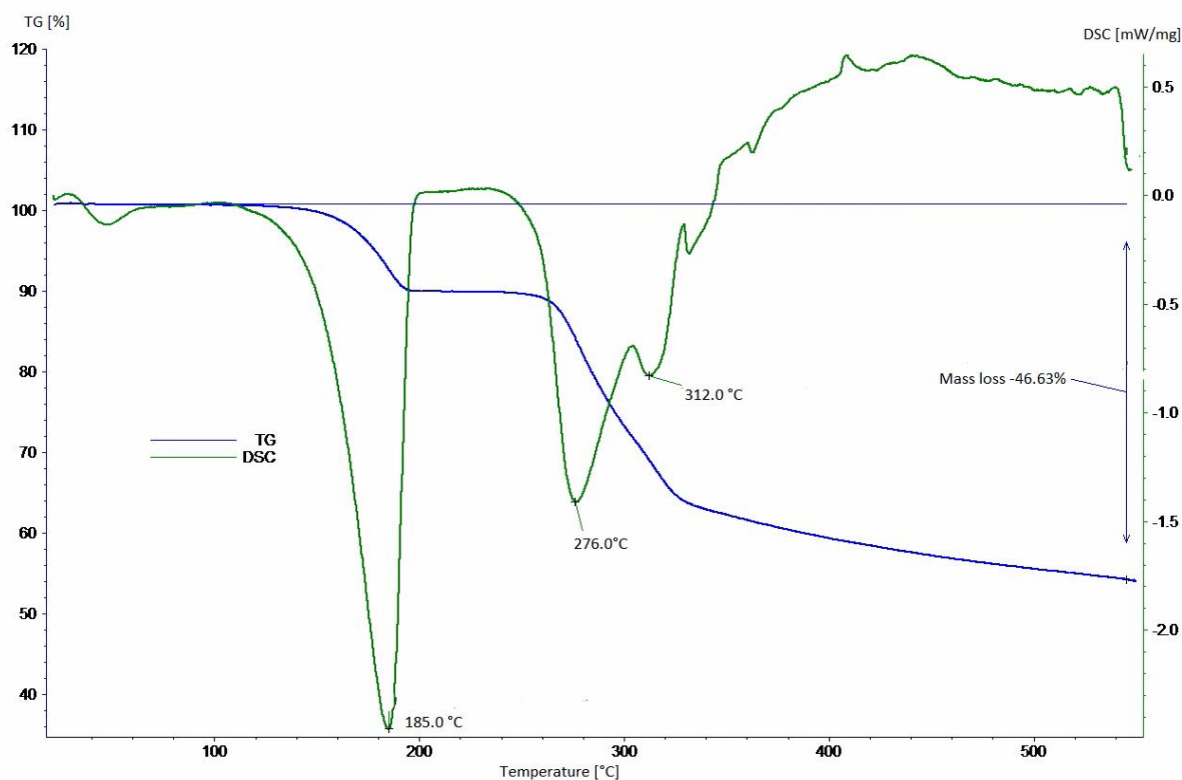


Figure 3.4.2.3. TGA from **C2**

ATR-IR spectroscopy

An ATR-IR spectroscopy was performed. According to literature³⁷ the bands of the spectrum were dedicated to the functional groups of the sample.

Table 3.4.2.1. Wavenumbers and the suggested according functionalities of **C2** and **C3**

Wavenumber [cm ⁻¹]			
C2	C3		
< 1000	< 1000	Fingerprint area	Aromatic (CH)
1333	1332	Stretching vibration	C-N
1405, 1258	1405,1259	Deformation vibration	Alkane (CH ₃ , CH ₂)
1468	1468	Stretching vibration	Ring C=C and N=C-N
1560	1556	Stretching vibration	Carboxylate (C=O)
3125	3127	Stretching vibration	Alkane (CH ₂)

In Figure 3.4.2.4. a comparison between the non-coordinated ligand and the compounds **C1** (blue curve), **C2** (red curve) and **C3** (green curve) is illustrated. The black curve represents the bands of the free ligand. There are some noticeable differences in the curve, although the spectrum is ligand dominated. A significant difference is observable in the carboxylate band, which occurs, with 1593 cm⁻¹ in the uncoordinated case. In **C1**, **C2** and **C3** this band is shifted to lower ranges at about 1560 cm⁻¹, which might be caused by a probably coordination to the metal ion. Other perceivable differences between are for example recognisable at much lower wavenumbers. So, the ligand curve **S1** showed for instance almost no bands at 700 cm⁻¹ and 785 cm⁻¹, but **C1**, **C2** and **C3** did. One of the reasons for these signals might result from the vibration of possible coordination bonds metal to ligand.

³⁷ M. Hesse, H. Meier, B. Zech, Spektroskopische Methoden in der organischen Chemie, Thieme, 7. Auflage.

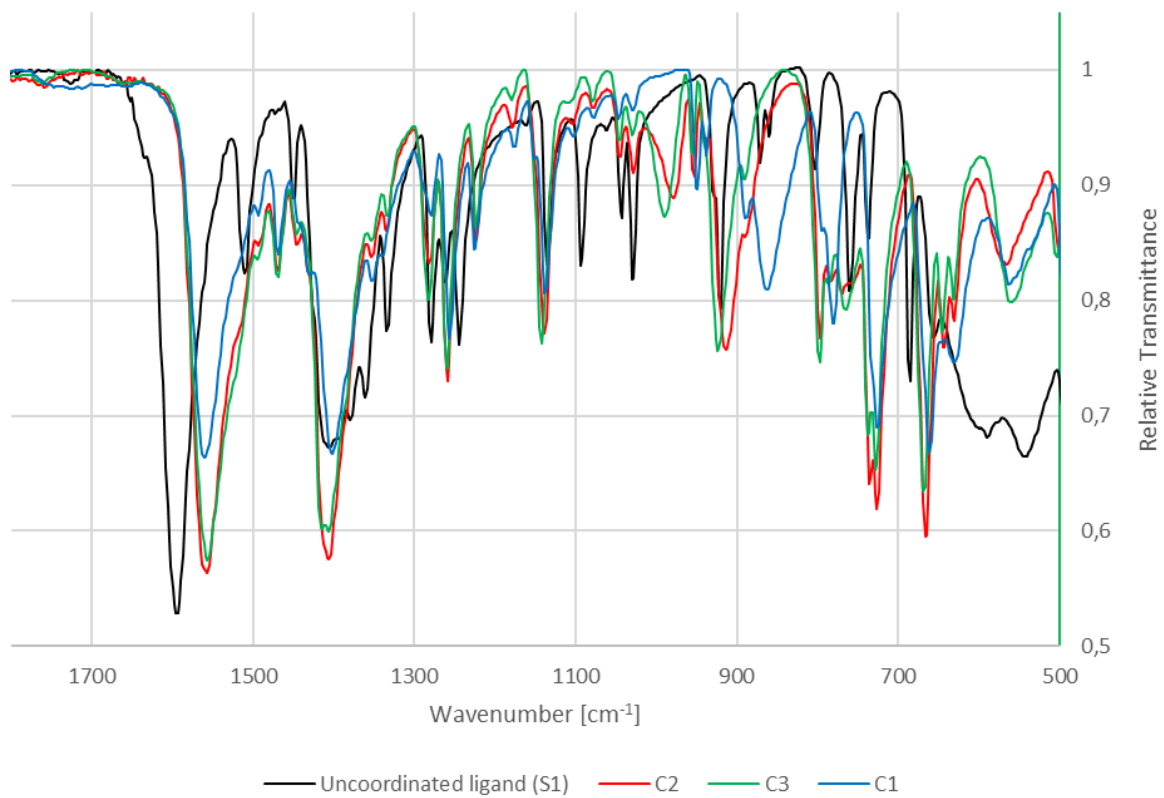


Figure 3.4.2.4. Compared ATR-IR spectrum of **S1**, **C1**, **C2** and **C3**

4. Conclusion and Outlook

Different metal-organic compounds have been prepared. The preparation focused the use of $\text{Pra}_2\text{biim}^{2-}$ as a nitrogen and carboxylate containing multifunctional ligand and different metal ions like Mn^{2+} , Co^{2+} and Ni^{2+} . The ligand precursor (H_2biim) has been prepared out of ammonium acetate and aqueous glyoxal. After purification and drying an aza-Michael addition with different acceptor substances was done. This study was focused on the ethyl acrylate product. The received product has been saponified to yield a pure salt as the ligand. With this multifunctional linker and metal salts metal-organic substances have been assembled. It was possible to determine the crystal structure from the manganese-organic coordination polymer. The most products have been characterized with different measurements like $^1\text{H-NMR}$, $^{13}\text{C-NMR}$, SC-XRD, XRD, AT-IR and TGA.

The $^1\text{H-NMR}$ and $^{13}\text{C-NMR}$ measurements have been done to characterize and identify the ligand compounds. Therefore, this method has been chosen to analyse the ligand precursor H_2biim and the aza-Michael products and the saponified linker. Furthermore, an ATR-IR spectrum of all compounds was recorded and analysed.

The SC-XRD measurement was only done with the manganese sample, because the other crystal compounds have been too small for the instrumentation. The result of this measurement showed that the manganese transparent crystals form a two-dimensional polymer sheet with almost no porosity. Before the XRD measurement the crystals have been dried under reduced pressure and unfortunately some lost their clearness and a bit of their crystalline structure, which was shown in the XRD measurement. So, it is suggested that the water molecules are an important factor for the formation of the crystal structure. In addition, the same tendency was obtained in the other metal-organic structures. Finally, the TGA analysis showed that the manganese-organic coordination polymer underwent a two-step weight loss, where the first one at $180.0\text{ }^\circ\text{C}$ might be corresponded to the loss of the coordinated water and the second at $270\text{ }^\circ\text{C}$ to the decomposition of the ligand. Similar results have been obtained with the other crystals.

5. Experimental

5.1. Reagents

5.1.1. Chemical reaction products

All chemical products have been bought from Sigma-Aldrich, TCI or ABCR, and were, unless mentioned otherwise, used as preserved. The solvents for synthesis reactions, workup, and purification were of analytical grade and used as preserved.

5.2. Instruments

5.2.1. NMR-spectroscopy

For recording the ^1H and ^{13}C NMR-spectra a Bruker Ultrashield 300 was used. The spectra were received in deuterated solvents, CDCl_3 , D_2O and DMSO ($\text{C}_2\text{D}_6\text{OS}$) at 300.46 MHz for ^1H and 75.53 for ^{13}C . The Chemical shifts for the ^1H spectra are referred in points per million (ppm) relative to the singlet of CDCl_3 at 7.26 ppm and relative to the signal of D_2O at 4.79 ppm and DMSO ($\text{C}_2\text{D}_6\text{OS}$) at 2.50 ppm. Moreover, the Chemical shifts for the ^{13}C spectra are referred in points per million (ppm) relative to the singlet of CDCl_3 at 77.16 ppm and relative to the signal of D_2O at 0 ppm and DMSO ($\text{C}_2\text{D}_6\text{OS}$) at 39.52 ppm. The other occurring peaks in the graph were analysed according to literature. The shape is mentioned as follows: s (singlet), d (doublet), t (triplet), m (multiplet).

5.2.2. Single Crystal – X-ray diffraction (SC-XRD)

The SC-XRD measurements were done by Ana Torvisco, Ph.D., Institute for Inorganic Chemistry, on an APEX II diffractometer from Bruker with $\text{Mo-K}\alpha$ radiation.

5.2.3. X-ray diffraction (XRD)

X-ray powder diffraction patterns were measured with a Siemens D-5005 powder diffractometer with Bragg-Brentano θ/θ geometry, operated at 40 kV and 15 mA, using $\text{Cu K}\alpha$ radiation, a graphite monochromator and a scintillation counter. The step width constituted 0.01° with constant counting times of $10^\circ/\text{min}$.

5.2.4. Infrared-spectroscopy (IR)

The IR-spectroscopy measurements were performed on an Alpha FT-IR spectrometer from Bruker with Platinum ATR single reflection diamond ATR module and the outcomes are shown in cm^{-1} .

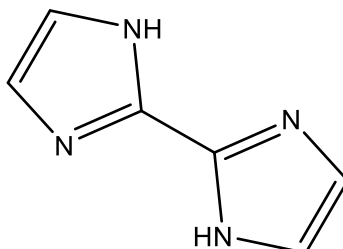
5.2.5. Thermogravimetric analysis (TGA)

The TGA analysis were taken on a Netzsch STA 449 C. For purging and protection in this measurements helium with a flow rate of 50 ml/min was used. The material of the crucible was aluminium oxide and the temperature range of the realized experiments ranged from 20 to 550 with a heating rate of 10 K/min.

5.3. Synthesis reactions

5.3.1. Synthesis of 2,2'-Biimidazole

5.3.1.1. 2,2'-Biimidazole



13 mL of distilled water were added to 70.8 g (0.9185 mol) ammonium acetate. Then 100 g (0.3446 mol) of 20 wt. percent of aqueous glyoxal were added dropwise with vigorous stirring at 40 °C over a period of 3h. The mixture could stir for an additional 17 h at room temperature. The obtained slurry was washed alternately with 3x40 ml acetone and 3x40 ml distilled water. A brown substance was received. 260 mL ethylene glycol was heated up to 135 °C and a hot filtration with the brown substance and decolorizing carbon was performed yielding to a white 2,2'-Biimidazole product. This product was washed with methanol and then dried under vacuum (Schlenk line) at room temperature.

Yield: 4.1 g, (0.0305 mol), (25.9 %), white solid.

$C_6H_6N_4$ [134.14 g/mol]

1H -NMR (300 MHz, DMSO- d_6) δ = 7,06 (s, 4H, C₄-H, C₅-H), 12,67 (s, 2H, N₁-H) ppm.

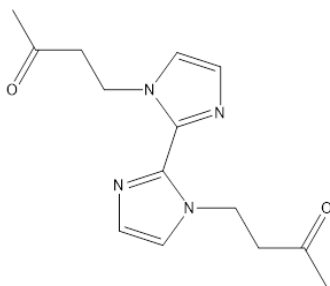
^{13}C - NMR (75 MHz, DMSO- d_6) δ = 139,1 (Im²), 128,3 (Im⁴-H), 116,8 (Im⁵-H) ppm.

Literature:

- Cho Jin-rae, A preparation method of 2,2'-bi-1h-imidazole using an ammonium salt and glyoxal, KR Patent KR100456092B1, 8.11.2004.
- Z. Huiming, Y. Xiaogang, Z. Jiang et al., Synthesis of 2,2'-biimidazole-based platinum(ii) polymetallaynes and tuning their fluorescent response behaviors to Cu²⁺ ions through optimizing the configuration of the organic spacers and steric effect, RSC Adv., 2015,5, 88758-88766.

5.3.2. Aza-Michael reaction

5.3.2.1. 4,4'-(1H,1'H-[2,2'-biimidazole]-1,1'-diyl)bis(butan-2-one)



In a Schlenk-tube was combined 0.250 g (1.8637 mmol, 1.0 eq.) of 2,2'-Biimidazole, 20 mL N,N'-dimethylformamide (DMF) and 200 μ l of 1 N NaOH. The mixture was stirred and heated to 50°C. A solution composed of 0.958 g (13.6681 mmol, 7.2 eq.) Methyl vinyl ketone dissolved in 1,4 ml DMF was added dropwise to the Schlenk-tube over a period of 10 minutes. Within 20 min after the addition, all the 2,2'-Biimidazole solubilized in a golden solution. After 2 h, the gold solution was neutralized with 66,6 μ L of 3M HCl (aq) and heating stopped. The solvent was removed via vacuum distillation in a hot water bath, generating a viscous red oil which crystallized upon cooling. To this red oil was added 50 mL of distilled water and 5 mL of 0,3M HCl. The solution was extracted twice with 5 mL of DCM. Afterwards the solution was neutralized with 3.2 mL of 0,5 M NaOH and extracted four times with 5 mL of DCM. The solvent was removed via rotoevaporation in a hot water bath, yielding a white crystalline solid product. The solid product was dried under reduced pressure to get rid of the remaining solvent.

Yield: 0.123 g [24.0 %]

$C_{14}H_{18}N_4O_2$ [274.14 g/mol]

IR: 1699 cm^{-1} ; 1725-1705 cm^{-1} ³³

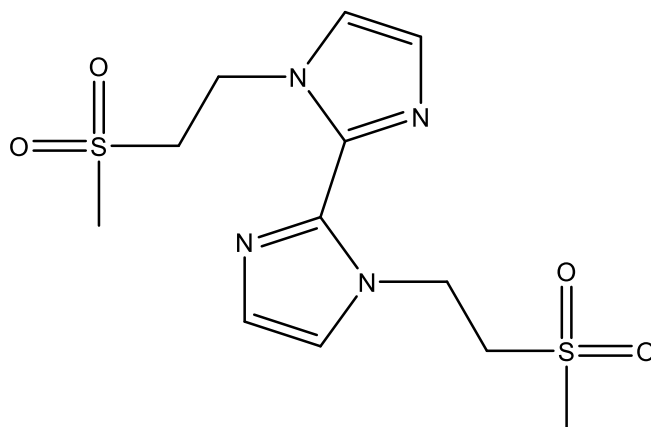
1H -NMR (300 MHz, DMSO- d_6) δ = 2,04 (s, 6H, CH₃), 2,95 (t, 4H, CH₂-C=O), 4,51 (t, 4H, Ar-CH₂), 7,01 (d, 2H, Ar-CH), 7,32 (d, 2H, Ar-CH) ppm.

^{13}C - NMR (75 MHz, DMSO- d_6) δ = 29,8 (CH₃), 41,9 (CH₂-C=O), 44,1 (Ar-CH₂), 122,2 (Im⁵-H), 127,6 (Im⁴-H), 137,4 (Im²), 206,5 (C=O) ppm.

Literature:

- W. Barnett, R. Baughman, P. Secondo, C. Hermansen, 1,1'-Di(hydrazinocarbonylmethyl)-2,2'-biimidazole monohydrate and 1,1'-di[2-(hydrazinocarbonyl)ethyl]-2,2'-biimidazole, Acta crystallographica Section C, Crystal structure communications, 2002, 58. o565-7.

5.3.2.2. 1,1'-bis(2-(methylsulfonyl)ethyl)-1H,1'H-2,2'-biimidazole



In a Schlenk-tube was combined 0.05g (0.3727 mmol, 1.0 eq.) of 2,2'-Biimidazole, 4 mL N,N'-dimethylformamide (DMF) and 40 μ l of 1 N NaOH. The mixture was stirred and heated to 50°C. A solution composed of 0.106 g (0.9987 mmol, 2.7 eq.) Methyl vinyl sulfone dissolved in 1,4 ml DMF was added dropwise to the Schlenk-tube over a period of 10 minutes. Within 10 min after the addition, a white suspension was produced. After 2 h, the gold solution was neutralized with 13,3 μ l of 3M HCl (aq) and heating stopped. The solid product was filtered and washed with DCM. The white solid was dried under reduced pressure to get rid of the remaining solvent.

Yield: 0.063 g [48.8 %]

C₁₂H₁₈N₄O₄S₂ [346.08 g/mol]

IR: 1279 cm⁻¹; 1350-1300 cm⁻¹³³

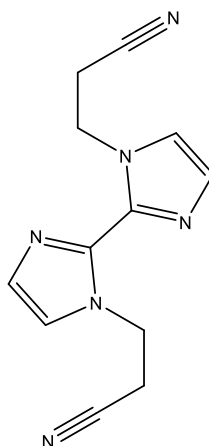
¹H-NMR (300 MHz, DMSO-d₆) δ = 2,96 (s, 6H, CH₃), 3,71 (t, 4H, CH₂-S=O), 4,84 (t, 4H, Ar-CH₂), 7,11 (d, 2H, Ar-CH), 7,42 (d, 2H, Ar-CH) ppm.

¹³C- NMR (75 MHz, DMSO-d₆) δ = 40,8 (Ar-CH₂), 41,0 (CH₃), 53,9 (CH₂-S=O), 122,8 (Im⁵-H), 127,8 (Im⁴-H), 137,3 (Im²) ppm.

Literature:

- W. Barnett, R. Baughman, P. Secondo, C. Hermansen, 1,1'-Di(hydrazinocarbonylmethyl)-2,2'-biimidazole monohydrate and 1,1'-di[2-(hydrazinocarbonyl)ethyl]-2,2'-biimidazole, Acta crystallographica Section C, Crystal structure communications, 2002, 58. o565-7.

5.3.2.3. 3,3'-(1H,1'H-[2,2'-biimidazole]-1,1'-diyl)dipropanenitrile



In a 50-mL round bottom flask, equipped with an oil bath and magnetic stirring bar, was combined 0.400 g (2.9820 mmol, 1.0 eq.) of 2,2'-Biimidazole, 6 mL DMSO and 400 μ L of 1 N NaOH. The mixture was stirred and heated to 80°C. Then 6.318 g (119.1 mmol, 40.0 eq.) Acrylonitrile was added dropwise to the round bottom over a period of 10 minutes. Within 30 min after the addition, all the 2,2'-Biimidazole solubilized in a red solution. After 2 h, the red solution was neutralized with 133 μ L of 3M HCl (aq) and heating stopped. The solvent and the remaining educts were removed via vacuum distillation in a hot oil bath, generating a viscous red oil. To the red oil 40 mL distilled water was added yielding to a light-yellow solid product. The product was dried under reduced pressure to get rid of the remaining solvent.

Yield: 0.576 g [80.5 %]

$C_{12}H_{12}N_6$ [240,11 g/mol]

IR: 2248 cm^{-1} ; 2260-2222 cm^{-1} ³³

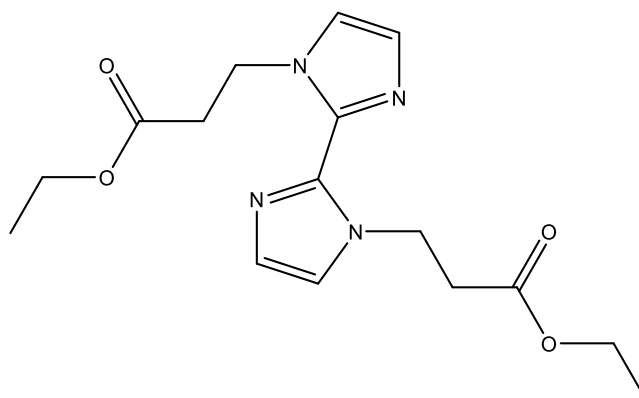
1H -NMR (300 MHz, DMSO- d_6) δ = 3,12 (t, 4H, CH_2 -CN), 4,69 (t, 4H, Ar- CH_2), 7,09 (d, 2H, Ar-CH), 7,41 (d, 2H, Ar-CH) ppm.

^{13}C - NMR (75 MHz, DMSO- d_6) δ = 19,1 (CH_2 -CN), 42,6 (Ar- CH_2), 118,4 (CN), 122,7 (Im⁵-H), 127,9 (Im⁴-H), 137,1 (Im²) ppm.

Literature:

- W. Barnett, R. Baughman, P. Secondo, C. Hermansen, 1,1'-Di(hydrazinocarbonylmethyl)-2,2'-biimidazole monohydrate and 1,1'-di[2-(hydrazinocarbonyl)ethyl]-2,2'-biimidazole, Acta crystallographica Section C, Crystal structure communications, 2002, 58. o565-7.

5.3.2.4. Diethyl 3,3-(1H,1'H-[2,2'-biimidazole]-1,1'-diyl)dipropionate



In a 250-mL round bottom flask, equipped with an oil bath and magnetic stirring bar, was combined 2.0 g (14.91 mmol, 1.0 eq.) of 2,2'-Biimidazole, 160 mL N,N'-dimethylformamide (DMF) and 1.6 mL of 1 N NaOH. The mixture was stirred and heated to 50°C. A solution composed of 4 g (40.0 mmol, 2.7 eq.) ethyl acrylate dissolved in 8 mL DMF was added dropwise to the Schlenk-tube over a period of 10 minutes. Within 20 min after the addition, all the 2,2'-Biimidazole solubilized in a golden solution. After 2 h, the golden solution was neutralized with 0.53 mL of 3M HCl (aq) and heating stopped. The solvent was removed via vacuum distillation in a hot water bath, generating a viscous red oil which crystallized upon cooling. To this red oil was added 200 mL of distilled water and a white solid product precipitated. The solid white crystalline product was filtered and dried under reduced pressure to get rid of the remaining solvent.

Yield: 2.81 g [56.4 %]

C₁₆H₂₂N₄O₄ [334,16 g/mol]

IR: 1721 cm⁻¹; 1730-1715 cm⁻¹ ³³

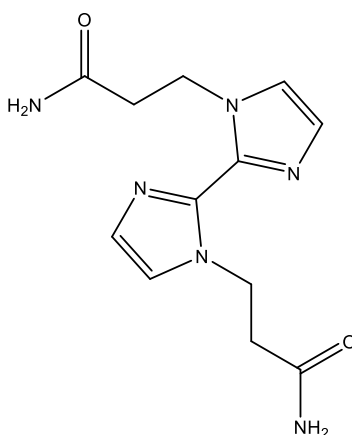
¹H-NMR (300 MHz, DMSO-d₆) δ = 1,12 (s, 6H, CH₃), 2,85 (t, 4H, CH₂-C=O), 4,02 (t, 4H, CH₂-CH₃) 4,62 (t, 4H, Ar-CH₂), 7,07 (d, 2H, Ar-CH), 7,33 (d, 2H, Ar-CH) ppm.

¹³C- NMR (75 MHz, DMSO-d₆) δ = 14,0 (CH₃), 35,2 (CH₂-C=O), 42,7 (Ar-CH₂), 60,1 (CH₂-CH₃) 122.3 (Im⁵-H), 127,6 (Im⁴-H), 137,3 (Im²), 170,6 (C=O) ppm.

Literature:

- W. Barnett, R. Baughman, P. Secondo, C. Hermansen, 1,1'-Di(hydrazinocarbonylmethyl)-2,2'-biimidazole monohydrate and 1,1'-di[2-(hydrazinocarbonyl)ethyl]-2,2'-biimidazole, Acta crystallographica Section C, Crystal structure communications, 2002, 58. o565-7.

5.3.2.5. 3,3-(1H,1'H-[2,2'-biimidazole]-1,1'-diyl)dipropanamide



In a Schlenk-tube was combined 0.250 g (1.8637 mmol, 1.0 eq.) of 2,2'-Biimidazole, 20 mL N,N'-dimethylformamide (DMF) and 200 μ l of 1 N NaOH. The mixture was stirred and heated to 50°C. A solution composed of 0.353g (4.9662 mmol, 2.7 eq.) Acrylamide dissolved in 0.7 mL DMF was added dropwise to the Schlenk-tube over a period of 10 minutes. After 2 h no solution was formed. Therefore, the suspension was heated up to 100 °C. Within 25 min after reaching 100°C, all the 2,2'-Biimidazole solubilized in a light-green solution. After 2 h, the light-green solution was neutralized with 66,6 μ l of 3M HCl (aq) and heating stopped. The solvent was removed via vacuum distillation in a hot water bath, generating a white solid substance., which was washed with DCM and methanol. The solid product was dried under reduced pressure to get rid of the remaining solvent.

Yield: 0.109 g [21.2 %]

$C_{12}H_{16}N_6O_2$ [276,13 g/mol]

IR: 1669 cm^{-1} ; 1690 cm^{-1} ³³

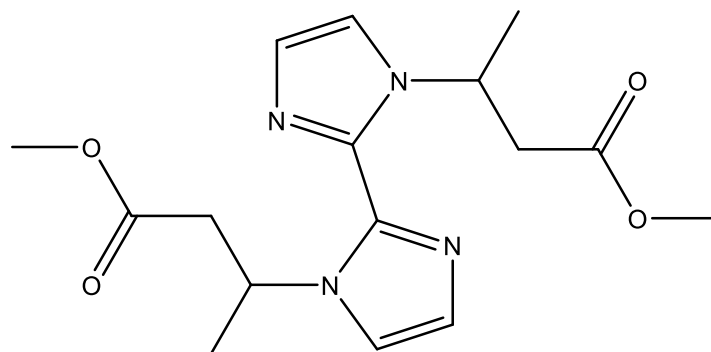
1H -NMR (300 MHz, DMSO- d_6) δ = 2,58 (t, 4H, CH_2 -C=O), 4,55 (t, 4H, Ar- CH_2), 6,86 (d, 2H, Ar-CH), 7,02 (s, 2H, NH_2), 7,24 (s, 2H, NH_2), 7,35 (d, 2H, Ar-CH) ppm.

^{13}C - NMR (75 MHz, DMSO- d_6) δ = 36,4 (CH_2 -C=O), 43,2 (Ar- CH_2), 122,2 (Im^5 -H), 127,5 (Im^4 -H), 137,3 (Im^2), 171,8 (C=O) ppm.

Literature:

- W. Barnett, R. Baughman, P. Secondo, C. Hermansen, 1,1'-Di(hydrazinocarbonylmethyl)-2,2'-biimidazole monohydrate and 1,1'-di[2-(hydrazinocarbonyl)ethyl]-2,2'-biimidazole, Acta crystallographica Section C, Crystal structure communications, 2002, 58. o565-7.
- ²⁷<https://www.sigmaaldrich.com/technical-documents/articles/biology/ir-spectrum-table.html> (16.7.2020)

5.3.2.6. Dimethyl 3,3-(1H,1'H-[2,2'-biimidazole]-1,1'-diyl)dibutyrate



In a Schlenk-tube was combined 0.250 g (1.8637 mmol, 1.0 eq.) of 2,2'-Biimidazole, 20 mL N,N'-dimethylformamide (DMF) and 200 μ l of 1 N NaOH. The mixture was stirred and heated to 50°C. A solution composed of 0.497g (4.9640 mmol, 2.7 eq.) trans-Methyl crotonate dissolved in 0.8 mL DMF was added dropwise to the Schlenk-tube over a period of 10 minutes. After 2 h no solution was formed. Therefore, the suspension was heated up to 100 °C. After 2 h, the mixture was neutralized with 66,6 μ l of 3M HCl (aq) and heating stopped. A $^1\text{H-NMR}$ measurement was made but did not show any product formation.

Yield: 0,0g [0,0 %]

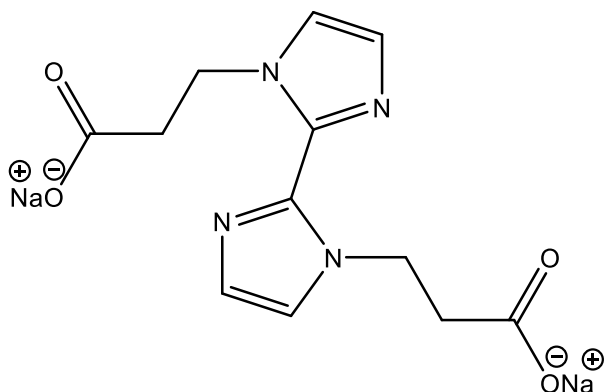
$\text{C}_{16}\text{H}_{22}\text{N}_4\text{O}_4$ [334,16 g/mol]

Literature:

- W. Barnett, R. Baughman, P. Secondo, C. Hermansen, 1,1'-Di(hydrazinocarbonylmethyl)-2,2'-biimidazole monohydrate and 1,1'-di[2-(hydrazinocarbonyl)ethyl]-2,2'-biimidazole, Acta crystallographica Section C, Crystal structure communications, 2002, 58. o565-7.

5.3.3. Saponification reaction

5.3.3.1. $\text{Na}_2\text{Pra}_2\text{biim}$ = 1,1'-di(propionic acid)-2,2'-biimidazole disodium salt



3.03 mL of a 5.55 M NaOH solution (0.0168 mol, 2.0 eq.) were added to 2.8114 g of Diethyl 3,3-(1H,1'H-[2,2'-biimidazole]-1,1'-diyl)dipropionate in a Schlenk tube. The mixture was heated up to 80°C under reflux and was stirred continuously. After 15 minutes a completely dissolved colourless solution was noticed and 4 h later a full conversion was detected via ^1H -NMR. The heat was removed, and the liquid became a white solid under drying with reduced pressure.

Yiel: 2.70 g [$> 99\%$]

$\text{Na}_2\text{C}_{12}\text{H}_{12}\text{N}_4\text{O}_4$ [322,07 g/mol]

IR: 1593 cm^{-1}

^1H -NMR (300 MHz, D_2O) δ = 2,58 (t, 4H, $\text{CH}_2\text{-C=O}$), 4,30 (t, 4H, Ar- CH_2), 7,19 (d, 2H, Ar-CH), 7,38 (d, 2H, Ar-CH) ppm.

^{13}C - NMR (75 MHz, D_2O) δ = 41,4 ($\text{CH}_2\text{-C=O}$), 46,8 (Ar- CH_2), 125,0 ($\text{Im}^5\text{-H}$), 130,8 ($\text{Im}^4\text{-H}$), 139,5 (Im^2), 181,9 (C=O) ppm.

5.3.4. Metal-organic frameworks and coordination polymers

5.3.4.1. Zink-organic coordination polymer



100.0 mg $\text{Zn}(\text{NO}_3)_2 \cdot 6\text{H}_2\text{O}$ (0.336 mmol, 1.0 eq.) were solubilized in 5 mL water. 108.0 mg (0.336 mmol, 1.0 eq.) of the ligand $\text{Na}_2\text{Pra}_2\text{biim}$ were dissolved separately in 5 ml deionized water in a 20 mL glass vial. The zinc nitrate solution was added dropwise to the ligand solution with a syringe. A white crystalline precipitation happened instantly. Afterwards the vial was closed and heated up to 80°C for 2 hours. After 24 h the vial was opened, and the water was skimmed, filled with another 9 ml of deionized water and heated up to 80°C . This procedure was done twice after every 2 hours. 24 hours later the white precipitate was unchanged and filtered. The white solid component was dried under reduced pressure.

5.3.4.2. Copper-organic coordination polymer



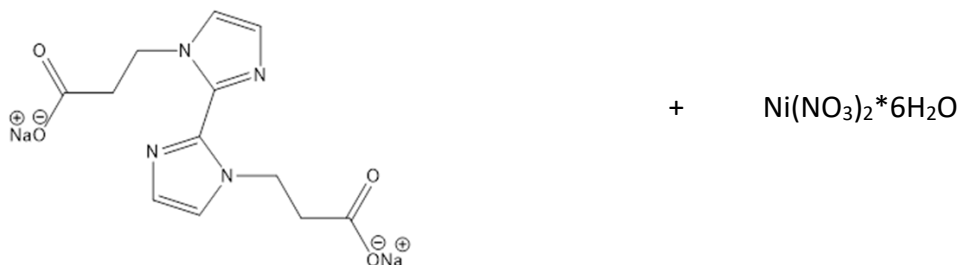
100.0 mg $\text{Cu}(\text{NO}_3)_2 \cdot 3\text{H}_2\text{O}$ (0.414 mmol, 1.0 eq.) were solubilized in 5 mL water. 133.0 mg (0.414 mmol, 1.0 eq.) of the ligand $\text{Na}_2\text{Pra}_2\text{biim}$ were dissolved separately in 5 ml deionized water in a 20 mL glass vial. The copper nitrate solution was added dropwise to the ligand solution with a syringe. A blue solution was generated immediately. Afterwards the vial was closed and heated up to 80°C for 2 hours. After two hours very small blue crystals were observed at the bottom of the glass vial. 21 h later the heat was removed, and the vial was exposed to room temperature for another 72 h, but the crystals did not grow enough for further analysis.

5.3.4.3. Cobalt-organic coordination polymer (C2)



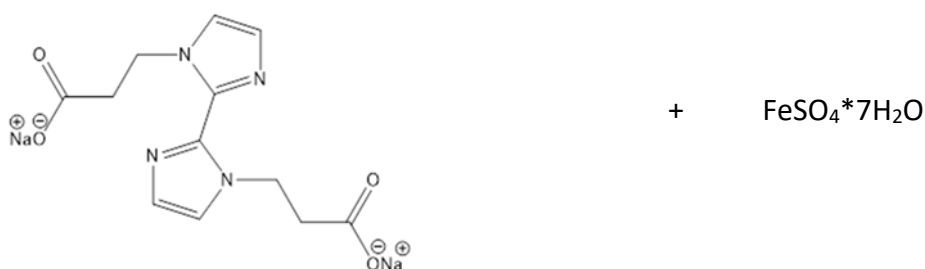
100.0 mg $\text{Co}(\text{NO}_3)_2 \cdot 6\text{H}_2\text{O}$ (0.546 mmol, 1.0 eq.) were solubilized in 5 mL water. 176.0 mg (0.546 mmol, 1.0 eq.) of the ligand $\text{Na}_2\text{Pra}_2\text{biim}$ were dissolved separately in 5 ml deionized water in a 20 mL glass vial. The cobalt nitrate solution was added dropwise to the ligand solution with a syringe. A violet solution was generated immediately. Afterwards the vial was not closed and heated up to 80°C for 2 hours. After 1h small violet crystals were observed at the bottom of the glass vial. After 20 h the solution was colourless, the water was skimmed, filled with another 9 ml of deionized water and heated up to 80°C . This procedure was done twice after every 2 hours. The violet crystals were filtered and dried under reduced pressure.

5.3.4.4. Nickel-organic coordination polymer (C3)



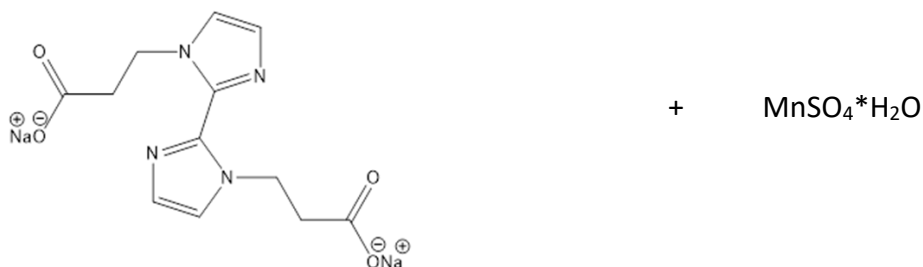
100.0 mg $\text{Ni}(\text{NO}_3)_2 \cdot 6\text{H}_2\text{O}$ (0.344 mmol, 1.0 eq.) were solubilized in 5 mL water. 111.0 mg (0.344 mmol, 1.0 eq.) of the ligand $\text{Na}_2\text{Pra}_2\text{biim}$ were dissolved separately in 5 ml deionized water in a 20 mL glass vial. The nickel nitrate solution was added dropwise to the ligand solution with a syringe. A light green solution was generated immediately. Afterwards the vial was closed and heated up to 80°C for 2 hours. After 1h small greenish crystals were observed at the bottom of the glass vial. After 24 h the solution was colourless, the water was skimmed, filled with another 9 ml of deionized water and heated up to 80°C . This procedure was done twice after every 2 hours. The green crystals were filtered and dried under reduced pressure.

5.3.4.5. Iron-organic coordination polymer



100.0 mg $\text{FeSO}_4 \cdot 7\text{H}_2\text{O}$ (0.360 mmol, 1.0 eq.) were solubilized in 5 mL water. 116.0 mg (0.360 mmol, 1.0 eq.) of the ligand $\text{Na}_2\text{Pra}_2\text{biim}$ were dissolved separately in 5 ml deionized water in a 20 mL glass vial. The iron sulphate solution was added dropwise to the ligand solution with a syringe. A rubiginous solution was generated immediately. Afterwards the vial was closed and heated up to 80°C for 17 hours. A brown precipitate was formed. Half an hour later the water was skimmed, filled with another 9 ml of deionized water and heated up to 80°C . This procedure was done twice after every 2 hours. The brown solid was filtered and dried under reduced pressure, but it was only iron oxide.

5.3.4.6. Manganese-organic coordination polymer (C1)



100.0 mg $\text{MnSO}_4 \cdot \text{H}_2\text{O}$ (0.591 mmol, 1.0 eq.) were solubilized in 5 mL water. 190.0 mg (0.591 mmol, 1.0 eq.) of the ligand $\text{Na}_2\text{Pra}_2\text{biim}$ were dissolved separately in 5 ml deionized water in a 20 mL glass vial. The manganese sulphate solution was added dropwise to the ligand solution with a syringe. A colourless solution was generated. Afterwards the vial was closed and heated up to 80°C for 20 hours. A brown precipitate and colourless crystals were formed. Two hours later the water was skimmed, filled with another 9 ml of deionized water and heated up to 80°C . This procedure was done twice after every 2 hours. The colourless crystals and the brown solid were filtered and dried under reduced pressure.

6. List of Abbreviations

Analytical methods

TGA	Thermogravimetric analysis
XRD	X-ray powder diffraction
SC-XRD	Single-crystal-X-ray diffraction
NMR	Nuclear Magnetic Resonance
Ppm	Parts per million
s	Singlet
d	Doublet
t	Triplet
m	Multiplet
q	Quadruplet
Hz	Hertz
MHz	Megahertz
IR	Infrared

Chemical formula and others

H ₂ Biim (BI)	2,2'-bisimidazole
DMSO-d ₆	Dimethylsulfoxide
CDCl ₃	Deuterated chloroform
NaOH	Sodium hydroxide
Na ₂ Pra ₂ biim	1,1'-di(propionic acid)-2,2'-biimidazole disodium salt
MOF	Metal-organic framework
ZIF	Zeolitic imidazolate framework

7. List of Figures

Fig. 2.2.1. The formation of ethanediimine ⁹	6
Fig. 2.3.1. Different synthesis mechanisms of hydrated imidazole-2-carboxaldehyde ⁹	8
Fig. 2.4.1. Structure of 1,1'-diethyl-2,2'-biimidazole	10
Fig. 2.4.2. Structure of $[\text{Rh}_2(\text{R}_2\text{bim})\text{Cl}_2(\text{CO})_4]$ (R = Et, Pr) ¹²	11
Fig. 2.4.3. Synthesis of disubstituted 2,2'-bi-1H-biimidazoles ¹³	12
Fig. 2.4.4.1. "Basic unit" of the two-dimensional hydrogen-bonded network. The dashed lines show the intermolecular interactions. ¹⁴	14
Fig. 2.4.4.2. Structure of the two-dimensional hydrogen-bonded network. The dashed lines show the O—H...O interactions. ¹⁴	14
Fig. 2.4.5.1. Structure of the robust heteromeric hydrogen-bonded synthons ¹⁵	15
Fig. 2.4.5.2. The structure of $[\text{Zn}(\text{H}_2\text{biim})_2(\text{H}_2\text{O})_2]^{2+}$ ¹⁵	16
Fig. 2.4.5.3. 2-D network made by hydrogen bonds ¹⁵	17
Fig. 2.4.5.4. 3-D network made by hydrogen bonds ¹⁵	17
Figure 2.4.6.1. Reactivity of the N-heterocycles in the Aza-Michael reaction ¹¹	19
Figure 2.4.6.2. Nucleophile catalysed mechanism of the Aza-Michael addition ¹⁹	19
Figure 2.5.1. Crystal structures of ZIFs ²⁰	21
Figure 2.5.2. (a,b) Zeolitic imidazolate framework-8 (c) micrograph of the high surface structure of ZIF-8 ²⁵	22
Figure 2.6.1. (a) The coordination environment of Cd^{2+} (b) The 2D-layer structure of $[\text{Cd}(\text{HL})_2]_n \cdot n\text{H}_2\text{O}$ (c) The supramolecular framework of $[\text{Cd}(\text{HL})_2]_n \cdot n\text{H}_2\text{O}$ ²⁶	24
Figure 2.6.2. (a) The coordination environment of Zn^{2+} (b) The 3D framework of $[\text{Zn}(\text{L})]_n$ (c) 3- connected etb topological network ²⁶	25
Figure 2.6.3. The basic coordination environment and the 3D supramolecular framework assembled by hydrogen bonds ²⁷	26
Figure 2.7.1. Isomeric structures of the $\text{Pra}_2\text{biim}^{2-}$ ligand ¹	27
Figure 2.7.2. 2D supramolecular hydrogen-bonded sheet of the $\text{H}_2\text{Pra}_2\text{biim}$ ligand ¹	28
Figure 2.7.3. (a) structure of the $[\text{Zn}_2(\mu_2\text{-HPra}_2\text{biim})_2]^{2+}$; (b) the 2D sheet of $[\text{Zn}(\text{HPra}_2\text{biim})\text{Cl}]_n$; (c) the 3D framework of $[\text{Zn}(\text{HPra}_2\text{biim})\text{Cl}]_n$ ¹	29
Figure 2.7.4. Compound $[\text{M}(\text{Pra}_2\text{biim})(\text{H}_2\text{O})]_n \cdot x\text{nH}_2\text{O}$ [M = Cd, x = 2 (1)] ²⁹	30
	75

Figure 2.7.5. (a) The helical chain structure along b-axis. (b) The helical chain structure along c-axis. (c,d) Interconnection by carboxyl arms of Pra ₂ biim ²⁹	31
Figure 3.1.1. Synthesis of 2,2'-biimidazole by combining glyoxal and ammonium acetate	33
Figure 3.1.2. ¹ H-NMR spectrum from the synthesized 2,2'-biimidazole	34
Figure 3.1.3. ¹³ C-NMR spectrum from the synthesized 2,2'-biimidazole	34
Figure 3.2.1. Structures of the Michael donor (A) and acceptor (1-6) substances	35
Figure 3.2.2. Products of the aza-Michael addition	37
Figure 3.2.3. The aza-Michael reaction of 2,2'-biimidazole A and the acceptor of ethyl acrylate 1 yielding to P1	38
Figure 3.2.4. ¹ H-NMR spectrum of the purified and dried P1 after full conversion	38
Figure 3.2.5. ¹³ C-NMR spectrum of the purified and dried P1 after full conversion	39
Figure 3.2.6. ATR-IR comparison of 2,2'-Biimidazole A with P1, P2, P3, P4 and P5	40
Figure 3.3.1. The received white solid product (S1) after the saponification reaction	42
Figure 3.3.2. Suggested mechanism of the saponification reaction from P1 to S1 ³⁴	42
Figure 3.3.3. ATR-IR analysis of the ester and the salt	43
Figure 3.3.4. ¹ H-NMR spectrum of the dried S1 after full conversion	44
Figure 3.3.5. ¹³ C-NMR spectrum of the dried S1 after full conversion	44
Figure 3.4.1.1. Picture of the manganese crystal (C1)	45
Figure 3.4.1.2. SC-XRD analysis of the manganese-organic crystal structure (C1)	46
Figure 3.4.1.3. Sphere-packing of the manganese coordination polymer (C1)	47
Figure 3.4.1.4. Powder XRD pattern of the manganese-organic coordination polymer C1	49
Figure 3.4.1.5. Comparison of the XRD pattern from the manganese-organic coordination sample C1 with the calculated ligand (literature)	50
Figure 3.4.1.6. TGA from the manganese-organic coordination polymer C1	52
Figure 3.4.1.4. Compared ATR-IR spectrum of the non-coordinated ligand and the manganese coordinated ligand C1	53
Figure 3.4.2.1. Picture of the cobalt crystals (C2)	54
Figure 3.4.3.1. Picture of the nickel crystals (C3)	55
Figure 3.4.2.3. Powder XRD pattern of the measured cobalt sample (C2), the nickel sample (C3) and the calculated ligand	56

Figure 3.4.2.3. TGA from C2	57
Figure 3.4.2.4. Compared ATR-IR spectrum of S1, C1, C2 and C3	59

8. List of Tables

Table 2.2.1. Possible products of the reaction of glyoxal with ammonium salts in an aqueous solution ⁹	2
Table 3.2.1. Characteristic bands and suggested corresponding functionalities for P1-P5	41
Table 3.4.1.1. Coordination geometry around Mn ¹	47
Table 3.4.1.2. Hydrogen-bond geometry of the manganese-organic coordination polymer (C1)	48
Table 3.4.1.3. Crystal data of the manganese coordination polymer (C1)	49
Table 3.4.1.4. Wavenumbers and the suggested according functionalities C1	52
Table 3.4.2.1. Wavenumbers and the suggested according functionalities of C2 and C3	58

9. Appendix

The ¹H- and ¹³C-NMR spectra of all synthesized compounds from the 2,2'-bisimidazole synthesis, the aza-Michael addition reaction and saponification can be found in the ICTM file ANYONE listed below. The same is valid for the IR-spectra from the metal organic compounds and the corresponding free ligands. The TGA, SC-XRD and XRD data are also listed and well-regulated in the same file.

M:\ICTM\ANYONE\Josef Hoedl\Master Thesis_Data